Analysis of TEMPO-adducts of Protein-based Radicals by Mass Spectrometry

P. John Wright

A Thesis

In

The Department

Of

Chemistry and Biochemistry

Presented in Partial Fulfillment of the Requirements

For the Degree of Doctor of Philosophy at

Concordia University, Montreal, Quebec, Canada

August 2003

Abstract

Analysis of TEMPO-adducts of Protein-based Radicals by Mass Spectrometry

P. John Wright, Ph.D.
Concordia University 2003

Heme peroxidases catalyze the one-electron oxidation of a wide variety of organic and inorganic substrates using hydrogen peroxide (H_2O_2) as an oxidant. Use of these enzymes in environmentally sound biotechnological and industrial applications is limited by their stability under harsh conditions such as high H_2O_2 concentrations and extremes in pH.

In of this thesis, a detailed study on the characterization of the low-pH heme-pocket stability of horseradish peroxidase isozyme c (HRPC) is reported. FTIR ν(CO) and Soret-CD spectra of HRPC-CO, and Soret absorption of ferric HRPC from two commercial sources were recorded to probe time-dependent heme-pocket changes at pH 3.0 in phosphate, citrate and formate buffers. Both HRPC-CO samples exhibit identical pH 7.0 ν(CO) bands at 1934 and 1905cm^{-1}. However, in the pH 3.0 spectrum of sample A, the 1934cm^{-1} band was dominant while a broad 1969cm^{-1} band appeared in sample B, which was assigned to solvent-exposed heme. The intensity of this band was greater in citrate than phosphate buffer, but in formate the 1934cm^{-1} band remained dominant. In the presence of 1mM $CaCl_2$, no time- or buffer-anion-dependent conformation changes were detected, revealing that buffer-anion-dependent leaching of the stabilizing-Ca^{2+} from HRPC occurs at pH 3.0. Since the N-glycans present in HRPC are of the flexible-

protein-surface-shielding type, the variation in low-pH conformational stability of the HRPC samples could be attributed to heterogeneous glycosylation which was detected by SDS-PAGE.

The second focus of this thesis is the reactive intermediates generated in the HRPC, cytochrome c peroxidase (CCP), and myoglobin (Mb) polypeptides upon their reaction with H_2O_2 in the absence of donor substrate. The use of the stable nitroxide radical, 2,2,6,6-tetramethylpiperidinyl-N-oxy (TEMPO$^{\bullet}$) as a tool in the mass spectrometric (MS) detection of protein-based radicals was explored. The HRPC/H_2O_2 reaction was used to generate radicals in low-molecular-weight derivatives of tyrosine, tryptophan and phenylalanine. TEMPO$^{\bullet}$ was added as a radical scavenger and the products analyzed by electrospray ionization mass spectrometry (ESI-MS). Dramatically higher mass-adduct yields were obtained using radical scavenging vs radical trapping with the spin trap 3,5-dibromo-4-nitrosobenzenesulfonate (DBNBS). To examine the efficiency of TEMPO$^{\bullet}$ scavenging of protein-based radicals, horse heart Mb and CCP were incubated with a 10-fold molar excess of H_2O_2 and TEMPO$^{\bullet}$ and MS analysis of the tryptic peptides derived from the proteins revealed that 1 and 9 TEMPO-adducts of Mb and CCP, respectively, were formed.

The thermal lability of the carboxylamine bond (C-ON) formed between TEMPO$^{\bullet}$ and the Mb polypeptide was exploited to confirm spin scavenging by electron paramagnetic resonance (EPR) and visible spectroscopy. Release of TEMPO$^{\bullet}$ from singly TEMPO-labeled intact (Mb_{TL}) and digested Mb was observed at 37°C and above 67°C, respectively, and incubation of excess DBNBS with intact Mb_{TL} at 37°C revealed the

exchange of the TEMPO label for a DBNBS label by ESI-MS. Intact TEMPO-labeled CCP (CCP_{TL}) did not oxidize ferrocytochrome c [cytc(Fe^{II})] at 25°C, but 7.0 and 9.5 equivalents of cyt c(Fe^{II}) were oxidized per mole CCP_{TL} on 10s incubation at 37 and 47°C, respectively. Capping of protein-based radicals may contribute to peroxidase stability and lead to their use in cosmetic and industrial applications.

Operating in the positive-ion mode of the ESI source, molecular ions were observed at m/z 156 ($TEMPO^+$), 157 ($TEMPO^{\bullet}$) and 158 ($TEMPOH_2^+$) in the mass spectrum of $TEMPO^{\bullet}$. This revealed that $TEMPO^{\bullet}$ is converted to $TEMPO^+$ and TEMPOH due to the electrolytic processes that occur in the metal ES capillary to maintain charge balance in the charged droplets. The formation of $TEMPO^+$ in solution promotes the subsequent oxidation of the solvent through an Anelli-like reaction, which generates TEMPOH. Since the electrochemical reduction of $TEMPO^+$ to TEMPOH is irreversible, the TEMPOH formed, which is detected as $TEMPOH_2^+$, acts as an electron sink in the ESI source.

Acknowledgements

First of all, I would like to thank Dr. Ann English for her guidance, support and research ideas during my Ph.D.

I wish to thank the members of my committee, Drs. Justin Powlowski and Paul Joyce. I would especially like to thank Drs. Angelo Filosa (AstraZeneca R&D Montreal), Tito Scaiano (University of Ottawa) and Scott Bohle (McGill University) for taking the time to help me out.

I would also like to thank the people at Agilent Technologies, AstraZeneca R&D (Montreal), Merck Frosst Centre for Therapeutic Research, MDS Pharma Services, ThermoFinnigan, Micromass, McGill University and the University of Ottawa, who allowed me to use their equipment and resources.

It goes without saying that I would like to acknowledge everyone at Concordia who has played some part in my development as a scientist. It is important that I mention Iolie Bakas, Andrea Romeo, Luca Maretti (University of Ottawa), Limei Tao, Heng Jiang, Mengwei Ye, Biao Shen, Jacqueline Montalibet, Vira Patel, and Drs. Lucille Serfass and Farida Mohamed. I would like to make a special thank you to Pascal Turcotte and Marika Dochia.

I am grateful to my brother Scott and sister Lindsay for their support.

Contributions of Colleagues

Chapters 2 and 3 are published manuscripts, while Chapters 4 and 5 are currently being prepared for publication. All abbreviation, citation, figure and table numbering systems in the published works were changed to the format of this thesis.

Chapter 2 was published in the *Journal of Biological Inorganic Chemistry* [Wright, P.J. and English A.M. (2001) *J Biol Inorg Chem* 6, 348-358] and is reproduced here with the permission of the journal. I carried out all of the work reported in this publication and prepared the manuscript. A.M. English provided intellectual support and edited the manuscript.

Chapter 3 was published in the *Journal of the American Chemical Society* [Wright, P.J. and English A.M. (2003) *J Am Chem Soc 125*, 8655-65] and is reproduced here with the permission of the journal. I carried out all of the work reported in this publication and prepared the manuscript. A.M. English provided intellectual support and edited the manuscript. J.C. Scaiano (Ottawa) is acknowledged for suggesting the use of TEMPO$^{\bullet}$ as a spin scavenger.

Chapter 4 is being prepared for submission to the *Journal of the American Chemical Society*. I carried out all of the work reported in this publication and prepared the manuscript. S. Bohle (McGill) helped with the EPR experiments and together with A.M. English provided intellectual support and edited the manuscript.

Chapter 5 is being prepared for submission to Analytical Chemistry. I carried out all of the MS work reported in this publication and prepared the manuscript. AstraZeneca R&D Montreal, MDS Pharma Services, ThermoFinnigan and Agilent Technologies

provided use of their mass spectrometers. A.M. English proved intellectual support and edited the manuscript.

Dedications

To my parents,

Jane and Peter Wright;

Thanks.

Table of Contents

List of Figures

List of Tables

List of Schemes

List of Abbreviations

ABTS	2,2'-azinobis(3-ethylbenzothiazoline-6-sulfonic acid
A_N	hyperfine coupling constant
CCP	cytochrome c peroxidase
CCP_{TL}	CCP from the $TEMPO^{\bullet}/H_2O_2$ labeling reaction
CD	circular dichroism
CID	collision-induced dissociation
cytc(Fe^{II})	ferrocytochrome c
DBNBS	3,5-dibromo-4-nitrosobenzene sulphonate
DTPA	diethylenetriamine-N,N,N',N'',N'''-pentaacetic acid
EPR	electron paramagnetic resonance
ESI	electrospray ionization
F	phenylalanine
FTIR	Fourier transform infrared
HPLC	high performance liquid chromatography
HRPC	horseradish peroxidase isozyme c
HRPC-CO	ferrous CO adduct of HRPC
$HRPC_{TL}$	HRPC from the $TEMPO^{\bullet}/H_2O_2$ labeling reaction
K_f	formation constant
LFRP	"living" free-radical polymerization
LIP	lignin peroxidase
MALDI-ToF	matrix-assisted laser desorption time-of-flight
Mb	myoglobin
Mb_{TL}	Mb from the $TEMPO^{\bullet}/H_2O_2$ labeling reaction
MNP	2-methyl-2-nitrosopropane
MS	mass spectrometry
NAF	N-acetyl-*l*-phenylalanine
NAWA	N-acetyl-*l*-tryptophanamide
NAYA	N-acetyl-*l*-tyrosinamide
*r*HRPC	recombinant HRPC

RZ	Reinheitzahl value
$R^{\bullet}$	organic free radical
SDS-PAGE	sodium dodecyl sulfate polyacrylamide gel electrophoresis.
SS/LC/MS	spin scavenging coupled with HPLC and ESI-MS
SS/MALDI	spin scavenging coupled with MALDI-ToF
ST	spin trap
ST/LC/MS	spin trapping coupled with HPLC and ESI-MS
ST/LC/MS	spin trapping coupled with HPLC and ESI-MS
$TEMPO^{\bullet}$	2,2,6,6-tetramethylpiperidinyl-1-oxy
TFA	trifluoroacetic acid
W	tryptophan
Y	tyrosine

1. Introduction

1.1 Initial Goals and Thesis Outline

The initial goal of this thesis was to compare the low-pH activities of heme peroxidases, which are of industrial relevance. Due to literature discrepancies, we commenced with a study of the low-pH heme-pocket stability of horseradish peroxidase isozyme c (HRPC) using techniques such as Fourier transform infrared (FTIR) and circular dichroism (CD) spectroscopies. CO is a sensitive probe of the heme pocket and multiple conformers of the FeCO unit in HRPC-CO were detected in the ν(CO) region of its IR spectrum (*1*). Resonance Raman results confirmed the presence of pH-dependent conformational equilibria (*2, 3*); at neutral pH two FeCO stretching modes were observed indicating linear (form I) and tilted FeCO (form II) conformers (*2, 3*). Form I alone was observed at high pH and the conversion of the absorbance intensity to this conformer is coupled to an acid-alkaline transition with a pK_a of 8.8 (*4*).

Smulevich *et al.* (*5*) and Feis *et al. (6)*, reported the formation of a low-pH form of HRPC-CO (form III), which differed dramatically from preliminary observations in our laboratory (*1*). The main difference between the studies was the source of the HRPC used. Hence, in Chapter 2 a systematic time- and pH-dependent investigation of the ν(CO) region of HRPC-CO from two commercial suppliers was undertaken to help clarify the low-pH heme-pocket conformations of HRPC-CO. CD and UV-visible spectroscopies also were used to determine the heme-pocket and secondary structural changes occurring at pH 3.0. SDS-PAGE analysis highlighted differences in glycosylation patterns. The combined results suggest that the glycans stabilize the HRPC

heme pocket under low-pH conditions by shielding the enzyme's surface from the solvent and that heterogeneous glycosylation causes variation in the low-pH stability of HRPC.

This is significant, since much work has been carried out to stabilize peroxidases under considerably harsher conditions (high temperature, extremes in pH and high peroxide concentrations) than those found in the natural environment in order to use peroxidases as alternatives to chemical catalysts in commercial and industrial applications (*7*). Because of the intriguing possibility of varying glycosylation as a way of stabilizing the active site of HRPC at low pH, an interest arose in studying HRPC mutants with altered glycosylation patterns. This line of research was not pursued due to the lack of suitable resources to perform such experiments. For instance, the construction of HRPC mutants with altered glycosylation cannot be carried out in *E. coli* since they do not possess the machinery for glycosylation, and the yields of HRPC produced in fungal cell lines that possess the ability for glycosylation are very low (*8-14*). Therefore, the use of HRPC glycosylation mutants in industrial and commercial processes is not feasible at present. Hence, the focus of this thesis switched to an investigation of the reactions of peroxidases with excess H_2O_2 in the absence of electron donor substrates.

The reaction of heme proteins with H_2O_2 results in the formation of highly reactive Fe^{IV}=O and $P^{\bullet}$ species, where $P^{\bullet}$ is a porphyrin or protein-based radical. Despite the importance of protein-based radicals in physiological processes, the factors and mechanisms that control their formation, localization, delocalization, and propagation remain obscure (*15, 16*). Cytochrome c peroxidase (CCP) from *Saccharomyces cerevisiae* and horse heart myoglobin (Mb) were used here as model heme proteins since they are known to form protein-based radicals via intramolecular electron transfer from

the polypeptide to the heme (*17*). Investigations into the detection and localization of peroxidase-based radicals by mass spectrometry (MS), which is of ongoing interest in our research group (*18, 19*), was undertaken. The development of a novel radical detection method is reported in Chapter 3. Spin scavenging with the stable nitroxide radical, 2,2,6,6-tetramethylpiperidinyl-N-oxy (TEMPO$^{\bullet}$), coupled with enzymatic digestion and electrospray ionization (ESI) MS or matrix assisted laser desorption ionization time of flight (MALDI-ToF) MS analysis provides a new tool for research on protein-based radicals.

In Chapter 4, the lability of the carboxylamine bond created by the scavenging of protein-radicals by TEMPO$^{\bullet}$ was explored. On heating TEMPO-labeled Mb, the regeneration of TEMPO$^{\bullet}$ was confirmed by electron paramagnetic resonance (EPR) spectroscopy. The storage of oxidizing equivalents in TEMPO-adducts of H_2O_2-oxidized Mb and CCP was examined using exogenous donor substrates. While studying TEMPO$^{\bullet}$ by ESI-MS, oxidized and reduced forms of the analyte, which are believed to be due to the inherent electrochemical properties of the ES source, were observed. Hence, in Chapter 5, a systematic analysis of the effects of the solvent, electrolyte and ESI-MS parameters on the oxidation and reduction of TEMPO$^{\bullet}$ in the ESI source is reported.

1.2 Heme Peroxidases

Heme peroxidases are enzymes that catalyze the one-electron oxidation of a wide variety of organic and inorganic substrates using peroxide (ROOH) as an oxidant (eqn 1.1) (*20*).

$$2AH + ROOH \rightleftharpoons 2A^{\bullet} + ROH + H_2O \qquad (1.1)$$

Peroxidases purified thus far from plants, fungi and bacteria all contain a noncovalently bound ferriprotoporphyrin IX (hemin) (Figure 1.1) (*21*).

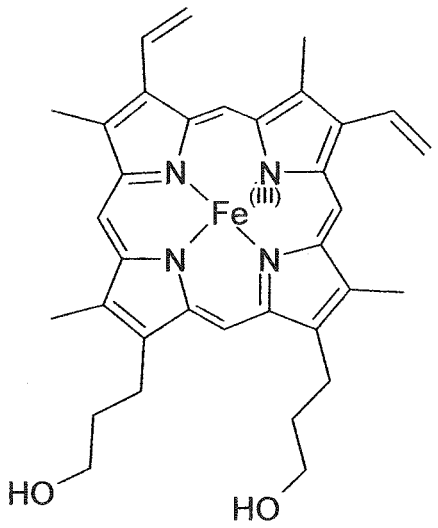

Figure 1.1. Ferriprotoporphyrin IX (1,3,5,8-tetramethyl-2,4-divinylporphine-6,6-dipropionic acid).

1.2.1 Heme Peroxidase Catalysis

Heme peroxidase catalysis proceeds in three distinct steps (*21*). First, the native ferric enzyme reacts with the oxidizing substrate, H_2O_2, or another hydroperoxide, ROOH, to yield compound I (*22*). Compound I is not a classical enzyme–substrate complex, but rather a reactive intermediate with a high formal Fe oxidation state (+5 compared with +3 for the resting enzyme). In the case of extracellular plant peroxidases (class III) such as HRPC, compound I exists as an oxyferryl heme and a porphyrin-based radical. However, intracellular peroxidases (class I) such as CCP undergo intramolecular electron transfer from the polypeptide to form a stable protein-based radical. Compound I is capable of oxidizing a range of donor substrates by a mechanism involving two sequential one-electron steps. The first of the steps leads to the generation of a second

enzyme intermediate, compound II (oxidation state +4), which is subsequently reduced to the native enzyme (E) by a second molecule of donor substrate:

$$E + H_2O_2 \rightarrow \text{Compound I} + H_2O \quad (1.2)$$

$$\text{Compound I} + AH \rightarrow \text{Compound II} + A^{\bullet} \quad (1.3)$$

$$\text{Compound II} + AH \rightarrow E + A^{\bullet} + H_2O \quad (1.4)$$

There are several fates for the free radical product ($A^{\bullet}$). It may dimerize, react with another substrate molecule, or oxidize another species (*23*).

Interestingly, in the absence of electron donor, HRPC exhibits catalase-like (catalatic) turnover ($2H_2O_2 \rightleftharpoons O_2 + 2H_2O$), where yet another spectroscopically distinguishable species, termed compound III is observed and the peroxidase is inactivated leading to the modification of the heme to form a verdohemoprotein (P670) (*24*). The precise inactivation mechanism for HRPC in the absence of substrate has not been elucidated clearly to date (*25*). Interestingly, other peroxidases such as CCP do not undergo catalatic turnover in the absence of donor substrates (*26*). The reduction of additional H_2O_2 molecules by CCP compound I occurs via intramolecular electron transfer to the Fe^{IV}=O heme, and the formation of a new protein-based radical, $P_x^{\bullet+}$ (*27*). The reaction of H_2O_2 with the newly formed Fe^{III} then regenerates Fe^{IV}=O and an additional protein radical $P_y^{\bullet+}$ (eqns 1.5-1.6).

$$Fe^{IV}{=}O,P^{\bullet+} + 2H^+ \rightarrow Fe^{III},P^{\bullet+}, P_x^{\bullet+} \quad (1.5)$$

$$Fe^{III},P^{\bullet+}, P_x^{\bullet+} + H_2O_2 \rightarrow Fe^{IV}{=}O, P^{\bullet+}, P_x^{\bullet+},P_y^{\bullet+} + H_2O \quad (1.6)$$

For many years, CCP was one of a few enzymes known to utilize a tryptophan (W191) radical during catalytic turnover (*27-30*). Although CCP has a similar secondary structure to class II (secretory fungal) and class III peroxidases, it contains an unusually high number of redox-active amino acid residues (seven tryptophans (W) and fourteen tyrosines (Y)) for a protein with a total of 294 residues. These numbers are especially notable when compared with other peroxidases of similar size such as HRPC (one W and five Y) (*31*), ascorbate peroxidase (two W and seven Y) (*32*), lignin peroxidases (LIP) (three W and no Y) (*33*) or manganese peroxidase (one W and no Y) (*34*).

1.2.2 Heme Peroxidase Active Sites

The nature of the active-site residues in peroxidases determines the function carried out by the heme (*35*). From a comparison of the crystal structures of peroxidases and other heme proteins such as Mb, which has been shown to turnover H_2O_2 via intramolecular electron transfer to a tyrosine residue (Y103) (*36, 37*), the increased polarity of the distal heme cavity in peroxidases is apparent and is believed to promote H_2O_2 heterolysis (*22*). Many heme proteins possess distal and proximal histidines, but the H-bonding and acid-base properties of these residues differ significantly (*15, 22, 35, 38*). For example in CCP, the proximal histidine (NE2) is H-bonded to a carboxylate side chain, though it is weakly H-bonded to a backbone carbonyl in Mb (*15, 22, 35, 38*). The imidazole ND1 atom of the distal histidine is partially exposed to solvent in Mb but H-bonded to the carboxamide side chains of an asparagine residue in HRPC (*15, 22, 35, 38*). This ensures that NE2 of the neutral imidazole ring is an H-bond acceptor from Fe-bound ligands in the ferric peroxidases (*15, 22, 35, 38*), where the pK_a of the distal

histidine is depressed to values between 4 and 5, due to the proximity of the δ-guanidinium group of the distal arginine (Figure 1.2) (*39-41*).

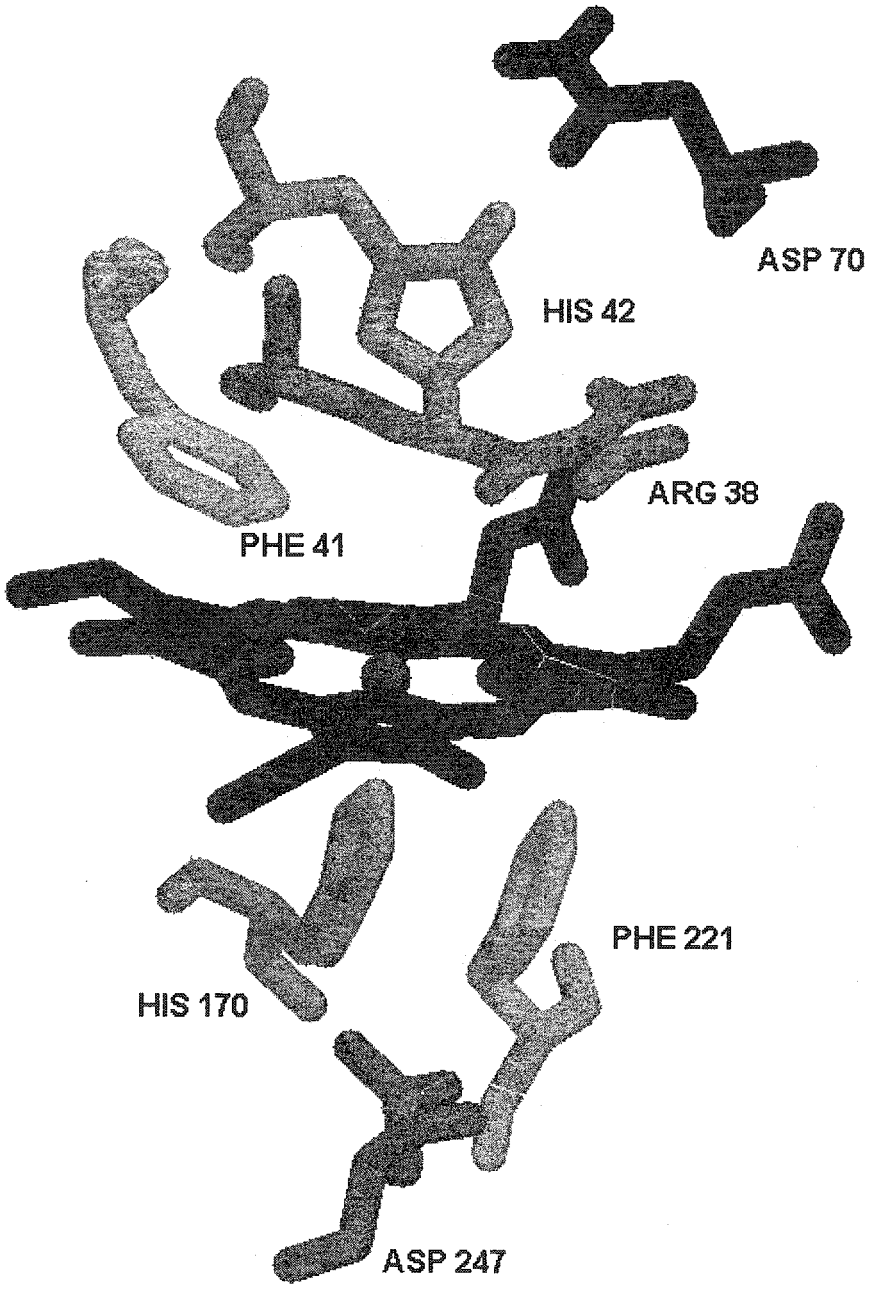

Figure 1.2. Rasmol modeling of the heme and active-site residues of horseradish peroxidase isozyme C (HRPC) using published coordinates (PDB: 1H58) (*31*). The δ-meso heme edge, facing the viewer, lies at the bottom of the substrate access channel that leads into the active site.

A function of CCP is believed to be the elimination of H_2O_2 by using electrons (via cytochrome c) from the electron-transport chain (*22, 38*). It recently was reported that CCP also is involved in conveying an oxidative-stress signal to the transcription factor Pos9 in *Saccharomyces cerevisiae* (*42*). Since the W191F mutant, which has no ferrocytochrome c-oxidizing activity (*42*), also is able to trigger the Pos9 transcriptional activation domain, the signaling function of CCP is independent of the electron flux in the mitochondria. Therefore, identification of the sites of heme-mediated H_2O_2-induced radical formation in CCP (eqns 1.5-1.6) is of interest since radicals are likely involved in oxidative-stress signaling in yeast mitochondria (*42, 43*).

Formation of compound I-type (Fe^{IV}=O) species of Mb has been detected in isolated ischemic-reperfused rat hearts (*44*) and such species are considered important in the development of myocardial reperfusion injuries after a period of ischemia (*45*). Presumably, the excess H_2O_2 produced during repurfusion can react readily with Mb, which is present at millimolar concentrations in cardiac myocytes. Generation of Fe^{IV}=O and $P^{\bullet}$ species leads to cellular damage.

Several amino acids including Y, lysine (K), histidine (H), phenylalanine (F) and W have been proposed as sites of radical formation in Mb, (*18, 46-49*). W and Y are considered the main sites of radical formation in CCP (*37, 50*). Determinination of the actual sites of polypeptide-based radical stabilization would provide insight into the nature of the oxidative-damage and signaling cascades carried out by the heme-mediated oxidation of Mb and CCP.

1.3. Protein-based Radical Detection

1.3.1 Spin Trapping

The direct observation of protein-based radicals in biological systems is often hampered by their low concentration (10^{-7} M) and high rates of self-reaction (10^{-7}-10^{-9} $M^{-1}s^{-1}$) (*51*). To date, EPR spectroscopy has been the most used tool for protein-based radical detection but the assignment of EPR signals to specific amino acid residues remains ambiguous (*16, 52*). Spectroscopic probe molecules such as diamagnetic spin traps (ST), which contain a nitroso function or a nitrone functional group, react with primary radicals to form more stable radical adducts (Figure 1.3) and facilitate their detection by EPR [reviewed in (*53-55*)]. In a typical experiment, the ST is added to a solution containing the radical-generating reactants and the products are monitored by EPR. The appearance in the EPR spectrum of the spin adduct R-ST$^{\bullet}$ is then considered evidence that R$^{\bullet}$ is an intermediate in the reaction (*54*). However, such a conclusion is valid only if the ST reacts directly with R$^{\bullet}$ to form R-ST$^{\bullet}$, which is not always the case since the ST can participate in the reaction under study in a variety of ways (*54*). For example, if the ST is oxidized to its radical cation (ST$^{\bullet+}$) by one of the components of the radical generating reaction, it then can react with a nucleophile (R^-) present to give the spin adduct R-ST$^{\bullet}$ (*54*). It also is difficult to assign protein-based radicals since EPR spectral interpretation does not always allow the unambiguous identification of specific amino-acid residues (*18, 52*). For instance, DeGray *et al.* (*56*) misassigned W14 and W7 as sites of radical formation in H_2O_2-oxidized Mb since they interpreted the EPR signals as arising from W-based rather than Y-based radicals.

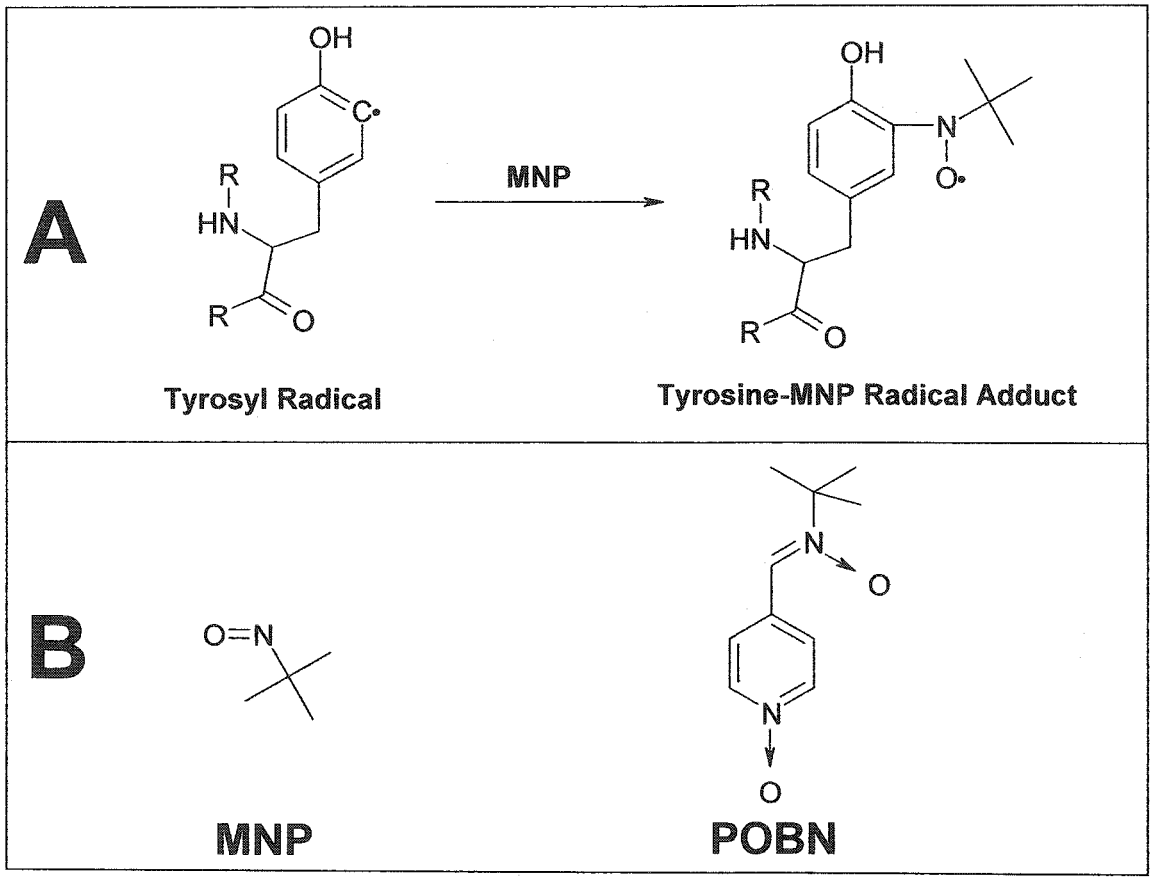

Figure 1.3. (A) A typical spin-trapping reaction in which a tyrosyl radical reacts with 2-mono-nitrosopropane (MNP) to form a more stable tyrosyl radical adduct. (B) STs with a nitroso (MNP) and a nitrone [α-(4-pyridyl 1-oxide)-*N*-*tert*-butylnitrone (POBN)] functional group. Arrows in POBN indicate donation of lone-pair of electrons on N atoms to O atoms (*53*).

To overcome this limitation, the spin trapping technique was adapted for MS in our laboratory (*18, 19, 50*). The ST was added in large excess to the reaction mixture containing the radical generating components, followed by online high performance liquid chromatography (HPLC) and ESI-MS analysis to confirm the presence of a protein-ST mass adduct. The protein-ST adduct then was enzymatically digested and the resulting peptides sequenced using MS/MS to determine the site of radical formation. This novel technique has greatly increased the specificity and sensitivity of protein-based radical identification (*18, 19, 50, 57, 58*).

STs used in previous MS studies to detect $P^{\bullet+}$ generated in H_2O_2-Mb and H_2O_2-cytochrome c reactions were chosen because they are water-soluble and exhibit a reduction potential (~2 V) (*59*) larger than the oxidation state of the H_2O_2-catalyzed reaction (~1.2V) (*16*). Therefore, "inverted spin-trapping" where the H_2O_2-catalyzed reaction oxidizes the ST, which then reacts with an amino acid residue producing the same results as the direct reaction of the ST with a protein radical, can be ruled out. Although MS detection of spin adducts has been successful in unambiguously identifying H_2O_2-induced radical formation on Y103, K42 and H64 in Mb (*18*), it has also led to incorrect interpretations, such as attributing non-covalent adduct formation in cytochrome c to spin adducts (*19*). Hence, the use of spin scavenging (SS) rather than spin trapping is explored in this thesis as discussed next.

1.3.2 Spin Scavenging of Protein-based Radical with TEMPO•

To overcome the inherent limitations of protein-based radical detection by MS using STs (Section 1.3.1), the use of SS as a tool for the detection of protein-based

radicals by MS was investigated. SS should provide two major advantages over spin trapping since 1) a diamagnetic adduct is formed rather than a spin adduct, and 2) SS should be faster than ST or $k_{SS} > k_{ST}$:

$$R^{\bullet} + SS^{\bullet} \xrightarrow{k_{SS}} R\text{-}SS \qquad (1.7)$$

$$R^{\bullet} + ST \xrightarrow{k_{ST}} R\text{-}ST^{\bullet} \qquad (1.8)$$

For carbon-centered radicals ($R^{\bullet}$), the published values of k_{SS} are ~ 10^9 $M^{-1}s^{-1}$ compared to k_{ST} ~ 10^7 $M^{-1}s^{-1}$ (*51, 53*). The development of radical-detection technology combining SS and mass spectrometric analysis of the adducts (R-SS) is discussed in detail in Chapter 3.

1.3.3 Thermal Activation of TEMPO-Capped Protein-based Aromatic Radicals

When $TEMPO^{\bullet}$ binds to the radicals formed in heme proteins (Chapter 3), the resultant carboxylamine bonds are less stable than those formed with primary carbon-centered radicals, such as in polyvinyl radicals. This instability is presumed to be caused by steric hindrance between the $TEMPO^{\bullet}$ methyl groups and the polypeptide. The carboxylamine bond instability is exploited in Chapter 4 to both confirm by EPR the release of $TEMPO^{\bullet}$ from TEMPO-labeled Mb, and to unleash the oxidizing equivalents stored in the CCP polypeptide, which are counted by monitoring the oxidation of the donor substrates, ferrocytochrome c and ABTS.

The thermal instability of the carboxylamine bond is the basis of "living" free radical polymerization (LFRP) mediated by stable nitroxide radicals. LFRP has seen much growth in recent years (*60*) due to the fact that polymeric materials with low dispersity can be prepared easily by heating the neat monomer with a nitroxide-based

initiator to 120-130°C under an inert atmosphere. This process involves the reversible termination of the growing polymeric radical by the stable nitroxide, producing an inactive species, in which the nitroxide is covalently bound to the end of the polymer chain. The carbon-oxygen bond is homolytically unstable at high temperatures (120-130°C) and cleaves to give the nitroxide and polymeric radicals. The latter undergoes chain extension with the monomer to yield a similar polymeric radical in which the degree of polymerization has increased. Recombination of this polymeric radical with the nitroxide then gives a new dormant species, which has the same structure as the original polymer with a one-monomer addition (*60, 61*).

1.4 Overview of Techniques Used in the Thesis

1.4.1 Circular Dichroism Spectroscopy

Circular dichroism (CD) spectroscopy measures the difference in absorbance by a substance of right- and left-circularly polarized light. It has been shown that the far-UV CD absorption (between 260 and 180nm) provides information on the different secondary structural elements in a protein: α-helix, parallel and antiparallel β-sheet, and turns (*62*). CD is used in this thesis to examine the effects of low pH on the conformational stability of HRPC (Section 2.4.3).

1.4.2 Fourier Transform Infrared Spectroscopy

Fourier transform infrared (FTIR) spectroscopy, under a variety of experimental conditions is a highly sensitive probe of protein conformation (*63, 64*). Secondary structural information is obtained from the amide I region, which is composed primarily

of peptide carbonyl stretching vibrations. These vibrations are sensitive to backbone conformation and the degree of H-bonding of the carbonyls (*63*). Fourier self-deconvolution (FSD) can be used to enhance the resolution of spectral data by separating overlapping spectral features that cannot be resolved by collecting data at a higher resolution setting (*63*).

CO ligation to heme proteins has received much attention since the bound CO can act as a sensitive probe of the active site (*5, 39, 65, 66*). The C-O stretching mode ν(CO) is detected easily by FTIR absorption in the 1900-2000cm^{-1} region. The nature of the H-bonding differences at low pH in the heme cavity of commercial preparations of HRPC is discussed in Chapter 2.

1.4.3 Electron Paramagnetic Resonance Spectroscopy

EPR (or electron spin resonance, ESR) is the resonance absorption of microwave radiation by unpaired electrons in a magnetic field. The technique is confined to the study of species with unpaired electron spins. The experiment is based on the fact that in a magnetic field the difference in energies between the two spin states of an unpaired electron is given by:

$$\Delta E = g\mu_B B \qquad (1.9)$$

where g is a parameter (the g-factor of the electron) that depends on structure but is equal to 2.0023 for a free electron, μ_B is the Bohr magneton and B the magnetic field. The resonant absorption of radiation occurs when the magnetic field B is adjusted to satisfy the resonance condition:

$$h\nu = g\mu_B B \qquad (1.10)$$

Typical magnetic fields are 0.3Torr and the microwave frequency used is in the X-band (8-10GHz) (*67*).

Hyperfine structure is seen in EPR signals due to the presence of magnetic nuclei. These give rise to a magnetic field that depends on the orientation of the magnetic nuclei, which results in splitting of the resonance line into components (see Figure 4.3). The hyperfine structure can be used in some cases to identify the radical species (*67*).

EPR is used in Chapter 4 to confirm the thermally induced homolytic cleavage of the Mb-TEMPO carboxylamine bond by detecting the presence of free TEMPO$^{\bullet}$ in the heated solution.

1.4.4 Electrospray Ion Source as a Controlled-Current Electrolytic Cell

ESI-MS analysis of TEMPO-adducts is central to the work discussed in Chapters 3 and 4. However, little attention has been paid to ESI-MS analysis of free TEMPO$^{\bullet}$. The nitrosium ion TEMPO^{+} was the dominant species in the reported ESI mass spectrum (*68*), but TEMPO^{+}, TEMPOH$^{\bullet+}$ and $TEMPOH_2^{+}$ ions are all observed with different intensities in the ESI mass spectra reported in Chapter 5. The ESI source functions as a constant or a controlled-current electrolytic cell (CCE) (*69, 70*). The potential at the metal/solution interface in the ES capillary, which determines whether or not a particular species will undergo a redox reaction in the capillary, is a function of both the ES current (i_{ES}) and the reduction potentials and concentrations of the other species in solution. The extent to which one or more reactions occur also is controlled by the flow rate of the solution through the ES capillary [Figure 1.5] (*69-73*). In positive-ion mode, oxidation of TEMPO$^{\bullet}$ to TEMPO^{+} is assumed to occur at the capillary. TEMPO^{+} generated at the

capillary is a strong oxidant and promotes the oxidation of the solvent to yield the reduced form, TEMPOH. The effects of these chemical and electrochemical reactions on the resulting species observed by the mass analyzer are investigated in Chapter 5.

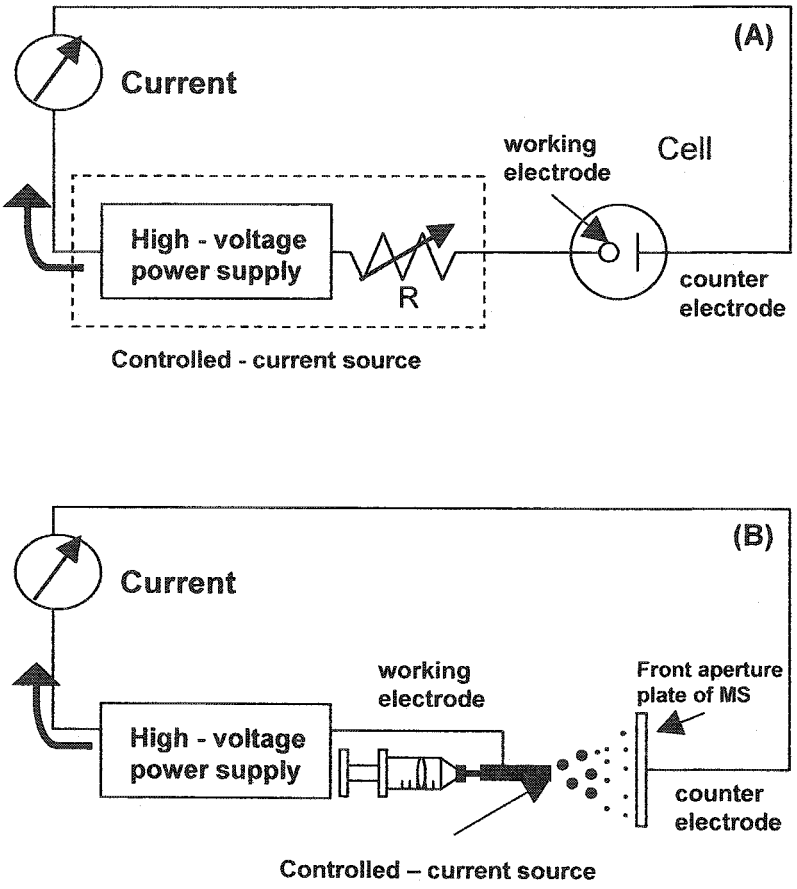

Figure 1.4. Schematic illustration comparing the basic instrumental components of (A) a controlled-current electrolytic (CCE) cell and (B) electrospray (ES) ion source (*69*).

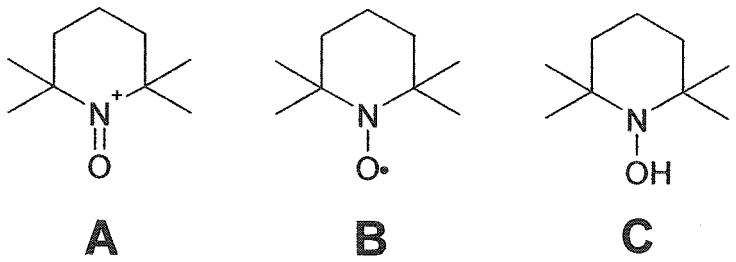

Figure 1.5. (**A**) *N*-oxo-nitrosium ion; (**B**) 2,2,6,6-tetramethylpiperidinyl-1-oxy (TEMPO•) and (**C**) the corresponding hydroxylamine (TEMPOH).

2.0 Buffer-Anion-Dependent Ca^{2+} Leaching from Horseradish Peroxidase at Low pH

2.1 Abstract

Despite highly conserved active-site structures, members of the plant peroxidase superfamily exhibit a wide range of pH optima. Horseradish peroxidase isozyme C (HRPC) is an ideal peroxidase to investigate the structural determinants of pH stability and activity in superfamily members. Conflicting reports exist on the low-pH stability of HRPC and consequently the pK_a of the catalytic distal histidine, which is neutral in active peroxidases. Towards resolving such discrepancies, acid-induced changes in HRPC from two popular commercial suppliers were *systematically* analyzed. Specifically, FTIR ν(CO) and Soret-CD spectra of HRPC-CO, and Soret absorption of ferric HRPC were recorded to probe time-dependent heme-pocket changes at pH 3.0 in phosphate, citrate and formate buffers, while the FTIR amide I' and far-UV CD spectra were examined to probe changes in secondary structure. Both HRPC-CO samples exhibited identical pH 7.0 ν(CO) bands at 1934 and 1905cm^{-1}. In the pH 3.0 spectrum of sample **A**, the 1934cm^{-1} band was dominant while a broad 1969cm^{-1} band appeared in sample **B**. The intensity of this band, which is assigned to solvent-exposed heme, was greater in citrate than phosphate buffer, but in formate the 1934cm^{-1} band remained dominant. Other spectral changes mirrored the ν(CO) trends. No time- or buffer-anion-dependent conformation changes were detected in 1mM $CaCl_2$ revealing that buffer-anion-dependent leaching of stabilizing-Ca^{2+} from HRPC occurs at pH 3.0. Since the N-glycans present in HRPC are of the flexible-protein-surface-shielding type, the variation in low-pH conformational

stability of the HRPC samples could be attributed to heterogeneous glycosylation, which was detected by SDS-PAGE. It is further proposed that glycosylation patterns may affect the low-pH stability of class II and III plant peroxidases.

2.2 Introduction

Heme peroxidases are ubiquitous enzymes that catalyze the one-electron oxidation of a wide variety of organic and inorganic substrates using H_2O_2 as an oxidant (*20*). Plant, fungal and bacterial peroxidases are members of the plant peroxidase superfamily, which can be subdivided into three classes based on structural differences and sequence alignment (*74, 75*). The intracellular peroxidases such as cytochrome *c* peroxidase (CCP) are placed in class I, secretory fungal peroxidases such as lignin peroxidase (LIP) in class II, while extracellular plant peroxidases like horseradish peroxidase (HRPC) are in class III (*20*). Within the plant peroxidase superfamily, there are nine invariable residues, five of which are located at the active site. In addition to prominent α-helices, class II and III plant peroxidases possess common structural features such as disulfide bridges, glycosylation sites and both proximal and distal Ca^{2+} binding sites (*20, 39, 76*). Despite the conservation of structural features and active-site residues, the pH optima and pIs differ dramatically within this superfamily. For instance, LIP has a pI of 3-5 and exhibits a narrow pH optimum of 2-3 (*76, 77*), whereas HRPC has a pI of 8-9 and pH optimum of 6-7 (*20*).

Given its stability over a broad pH range, HRPC is an ideal model peroxidase to investigate factors that control low-pH stability and activity within the plant peroxidase superfamily. A neutral distal histidine is required for peroxidase activity (*76, 78*), and the

pK_a of the distal His42 of ferric HRPC is depressed to ~ 4 (*22, 35*) by the presence of Arg38 in the heme pocket (*39-41*). Nonetheless, heme-linked ionizations with considerably higher pK_as have been assigned to His42 in other oxidation and ligation states of HRPC such as compound II (pK_a = 8.5) (*78*), ferric HRPC-CN (pK_a = 10.6) (*78, 79*) and ferrous HRPC-CO (pK_a = 8.7) (*6*). pH titrations of the catalytic residues have been studied extensively in the CO adduct of HRPC since CO is a sensitive probe of the heme pocket (*80-83*). The FTIR ν(CO) spectra of HRPC-CO reveal two FeCO conformers at pH 7.0: form I (1934cm^{-1}) has a linear, non-H-bonded FeCO unit while in form II (1905cm^{-1}) the FeCO unit is tilted and H-bonded to Arg38 (*1-4, 84*). A review of the IR studies of HRPC-CO reveals a number of inconsistencies, with reports of time-independent, time-dependent and buffer-anion-dependent spectroscopic changes below pH 5. Most notable is the appearance under ill-defined conditions of a broad ν(CO) band at ~1970cm^{-1}.

With the goal of elucidating the low pH stability, and eventually the pH optima, of plant peroxidases, a *systematic* comparative study at pH 3.0 in phosphate, citrate and formate buffers was undertaken using HRPC purchased from two popular commercial suppliers. Time-dependent heme-pocket changes in HRPC-CO were followed using FTIR ν(CO) and Soret-CD spectra, and changes in ferric HRPC were probed by Soret absorption. Accompanying changes in secondary structure were monitored in the FTIR amide I' region (1600 - 1700cm^{-1}) at pD 3.0 and in the far-UV CD at pH 3.0, spectral regions that are highly sensitive to protein secondary structure (*64, 85, 86*). The spectroscopic measurements were repeated in the presence of 1mM Ca^{2+}, and the spectra obtained were both time-independent and buffer-anion-independent, indicating that

HRPC can exist in a stable conformation at pH 3.0. The results also allow identification of the spectral characteristics of acid-denatured HRPC [e.g., ν(CO) ~1970 cm^{-1}], and reveal that the literature discrepancies in the low-pH behavior of HRPC are due to buffer-anion-promoted leaching of the stabilizing Ca^{2+}. In the absence of added Ca^{2+}, the low-pH conformational stability of HRPC from the two suppliers varied significantly, which could be attributed to the differences in their carbohydrate content revealed by SDS-PAGE. A key inference from the present study is that the surface-shielding ability of critical glycans plays a major role in determining pH conformational stability, pK_as of catalytic residues, and hence pH optima of class II and III plant peroxidases.

2.3 Materials and Methods

2.3.1 Materials

Horseradish peroxidase isozyme C (HRPC) (EC 1.11.1.7) sample **A** was obtained from Boehringer Mannheim, now Roche Molecular Biochemicals (Grade I, salt-free, lyophilized, Ca^{2+}-bound, lot numbers 83696847-08 and 84955634-14) and sample **B** from Sigma (Type VI-A, essentially salt-free, lyophilized, Ca^{2+}-bound, lot numbers 62H95051 and 63H9516), and both samples were used without further purification. ABTS was purchased from Roche Molecular Biochemicals, CO gas (99.3%) from Prodair and 99.9% D_2O from Aldrich. All solutions were prepared using distilled water (specific resistance 18MΩ) from a Barnstead Nanopure system.

2.3.2 *Methods*

Solutions of 0.1-1.0mM ferric HRPC were prepared spectrophotometrically using a Hewlett-Packard 8431A diode array or a Beckman DU-630 spectrophotometer (ε_{403} = 102$cm^{-1}mM^{-1}$) (*82, 83*). The samples were dissolved in 100mM sodium phosphate (NaPi) buffer at pH 7.0 and 500mM NaPi, 100mM sodium citrate or 100mM sodium formate buffer at pH 3.0. All buffers contained 0.5M NaCl to maintain constant ionic strength. The pD values for buffers prepared in D_2O were calculated from pD = pH (measured) + 0.4 (*81*). The CO adducts were prepared by passing CO gas over 20μL of ferric HRPC in a sealed Eppendorf tube for ~2min, and a minimum amount of a saturated, degassed sodium dithionite in the appropriate buffer was added to reduce the ferric heme.

2.3.3 *Time-dependent FTIR spectra of HRPC and HRPC-CO at pH 3.0*

FTIR spectra were recorded on a Nicolet Magna 550 spectrometer equipped with a deuterated triglycerine sulfate (DTGS) detector and purged with dry air. A dismountable IR cell (Model 116) with 13 x 2mm CaF_2 windows and Teflon spacers were obtained from Wilmad. HRPC or HRPC-CO solutions (~10μL) were pipetted onto one window of the dismountable IR cell, which was rapidly reassembled. The UV-VIS absorbance of the HRPC-CO samples in the IR cell was measured at 422nm before and after the FTIR spectra were recorded to ensure complete formation of the CO adduct and that no oxidation occurred during IR data acquisition. The amide I' and ν(CO) FTIR spectra were recorded with a 50μm pathlength starting at 3, 23, 43, 63 and 123min after preparation. Each IR spectrum is an average of 256 scans recorded at a speed of 73scans/min and a resolution of $4cm^{-1}$. Spectral subtractions were carried out as

described previously (*87*). Amide I' resolution enhancement (Fourier self-deconvolution) was carried out with a bandwidth of $20cm^{-1}$ and a K factor of 2.0. The ν(CO) bands were plotted without any resolution enhancement.

2.3.4 Time-dependent CD spectra of HRPC and HRPC-CO at pH 3.0

CD spectra were recorded on a JASCO J-710 spectropolarimeter purged with N_2 at a flow rate of 5L/min. The dismountable IR cell also was used to record the CD spectra and the sample preparation method was the same as for the FTIR experiments. All CD spectra reported are the average of 5 scans at 0.2nm resolution, a bandwidth of 1.0nm and a scan speed of 100nm/min with a response time of 1.0s. Far-UV CD spectra were recorded in the FTIR cell with a 6μm spacer, while Soret-CD spectra were recorded with a 150μm spacer.

2.3.5 Time-dependent UV/VIS spectra of HRPC at pH 3.0

Samples (~2.0μM) were prepared in a 1.0cm pathlength quartz cuvette and spectra were immediately recorded on a Beckman DU-630 spectrophotometer at a scan speed of 600nm/min at 23°C.

2.3.6 Purity index, ABTS activity assay, SDS-PAGE and calcium analyses

The purity index or RZ value is expressed as a ratio of heme (403nm) to protein (275nm) absorbance (*20, 88*). The peroxidase assay mix contained 880μM (0.3 wt %) H_2O_2 and 91μM ABTS in 100mM NaPi (pH 5.0) at 23°C. Activities were calculated from the absorbance increase at 405nm following addition of ~ 200nM HRPC to the assay

mixture (*89*). For sample **A** the measured RZ and activity values were 3.27 and 1258 *vs* values of 3.37 and 1000 provided by the supplier. For sample **B** the corresponding values measured were 2.76 and 528 *vs* supplier values of 3.3 and 1100. The calcium content of the HRPC samples was measured using a Perkin-Elmer (Model 602) atomic absorption spectrophotometer. Lyophilized HRPC from the bottle was dissolved in water to a concentration of 5.0-8.0μM, and analyzed for Ca^{2+} in duplicate, following calibration of the spectrophotometer using a $CaCl_2$ standard. SDS-PAGE (12%) was performed as previously described (*90*).

2.4 Results

2.4.1 Time-dependent FTIR ν(CO) bands at pH 3.0 in phosphate buffer: Form III

At pH 7.0, both HRPC-CO samples exhibit essentially identical ν(CO) bands (Figure 2.1, inserts) to those reported previously. These bands have been assigned to tilted, H-bonded (form II, 1905cm^{-1}) and linear, non-H-bonded (form I, 1934cm^{-1}) conformers of the FeCO unit (*1-3*). Figure 2.1 also shows the ν(CO) spectra *vs* time of both HRPC-CO samples in phosphate buffer at pH 3.0. The HRPC-CO **A** spectra, which remain essentially unchanged between 3 and 123min. (Figure 2.1A), exhibit a strong form-I band at 1934cm^{-1} and a less intense form-II band at 1905cm^{-1}. The HRPC-CO **B** spectra (Figure 2.1B) are dramatically different from those obtained for HRPC-CO **A** at all times, and clearly undergo time-dependent changes. Sample **B** exhibits a major band at 1934cm^{-1} with a less intense band at 1969cm^{-1} within 3min. After 23min, the band at 1969cm^{-1} becomes dominant at the expense of the 1934cm^{-1} band, which possesses negligible intensity after 123min. The broad, blue-shifted 1969cm^{-1} band is assigned to a

third conformer of the FeCO unit (form III) that undergoes increased random polar interactions with time at acid pH. We conclude from the spectra in Figure 2.1 that HRPC-CO **B** undergoes heme-pocket unfolding over a 123min period at pH 3.0, while HRPC-CO **A** is more stable to local unfolding over the same time period.

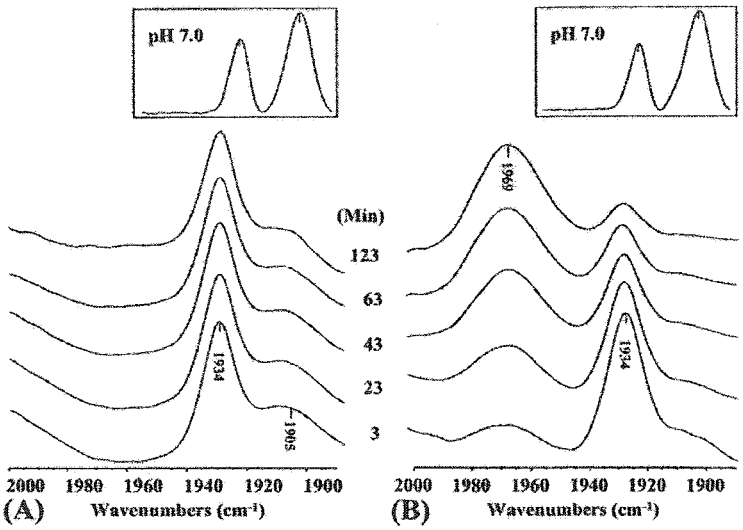

Figure 2.1. FTIR spectra of the ν(CO) region of 0.1–0.5mM HRPCO **A** and **B** at pH 3.0 in 500mM sodium phosphate buffer with 500mM NaCl *vs* time. Inserts show the ν(CO) spectra at pH 7.0. Each spectrum is the average of 256 scans recorded in 3.5min (73scans/min) and data acquisition was *started* at the times indicated on the spectra; 4cm^{-1} resolution; 50μm pathlength.

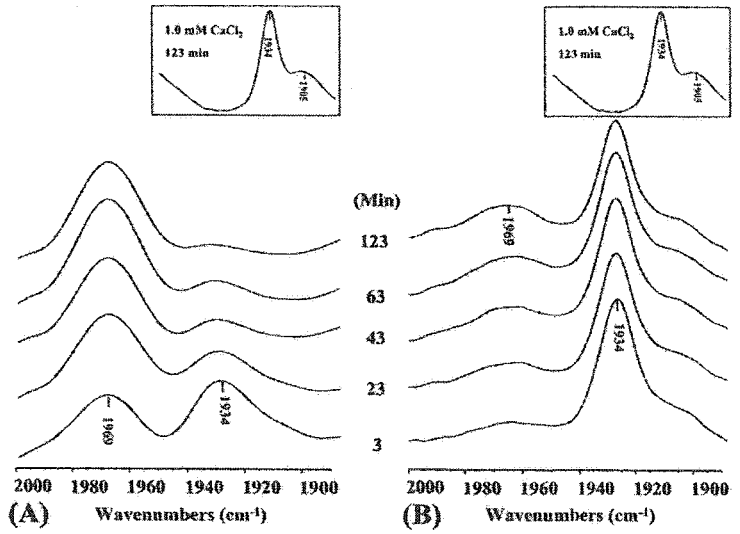

Figure 2.2. FTIR spectra of the ν(CO) region of 0.1 – 0.5mM HRPC-CO **B** at pH 3.0 in (A) 100mM sodium citrate and (**B**) 100mM sodium formate buffers with 50mM NaCl *vs* time. Inserts show the ν(CO) spectra at pH 3.0 in the same buffers with 1.0mM $CaCl_2$ after 123min. Experimental conditions are given in Figure 2.1.

2.4.2 Time-dependent FTIR ν(CO) bands at pH 3.0 in citrate and formate buffers

To compare the heme-pocket stability of the HRPC-CO samples at pH 3.0 in different buffers, the FTIR spectra were also recorded *vs* time in citrate and formate. Form I ($1934cm^{-1}$) of HRPC-CO **B** is rapidly converted to form-III ($1969cm^{-1}$) in citrate (Figure 2.2A) but not in formate (Figure 2.2B), while in phosphate (Figure 2.1B) the rate is intermediate. Clearly, the conformation changes induced in the heme environment of HRPC-CO **B** at acid pH exhibit a strong buffer-anion dependence. In contrast, no form-III band was observed in the HRPC-CO **A** spectra in citrate and formate (data not shown), consistent with the results observed in phosphate (Figure 2.1A).

2.4.3 Time-dependent HRPC-CO Soret-CD at pH 3.0 in phosphate buffer

Both HRPC-CO samples exhibit essentially identical positive and negative Soret-CD ellipticity peaks at pH 7.0 (Figure 2.3). When the pH is lowered to 3.0 in phosphate buffer, the HRPC-CO **A** bands lose elliptical intensity with time, but retain the same peak maximum (412nm) and minimum (427nm) as observed at pH 7.0 (Figure 2.3A). In sharp contrast, the HRPC-CO **B** spectra show a reversal in ellipticity within 3min, yielding essentially a mirror image of the pH 7.0 spectra (Figure 2.3B), following which the elliptical intensity decreases slightly with time. The Soret-CD results corroborate the FTIR ν(CO) data (Figure 2.1A) in revealing that HRPC-CO **A** and **B** undergo different conformational changes in the vicinity of the heme at low pH.

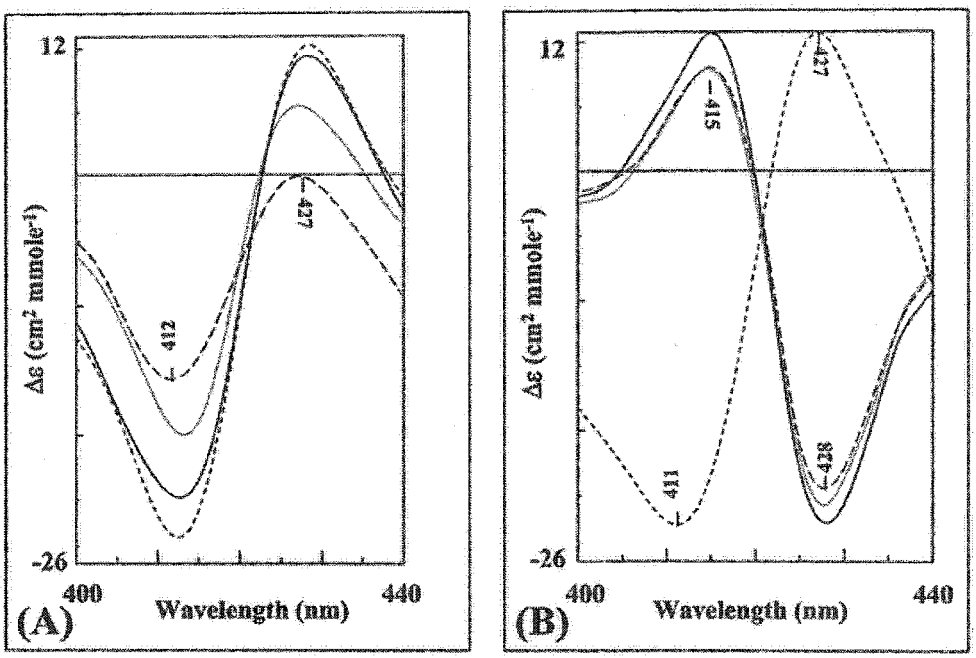

Figure 2.3. Soret-CD spectra of 1.0–2.0mM HRPC-CO A and B at pH 7.0 (---) and at pH 3.0 in 500mM sodium phosphate buffers with 500mM NaCl after (—) 3min, (···) 63min, (– – –) 123min. Spectra were recorded in the FTIR cell with a 150μm pathlength, and are the average of 5 scans at 0.2nm resolution, 1.0nm bandwidth, 100nm/min scan speed and 1s response time.

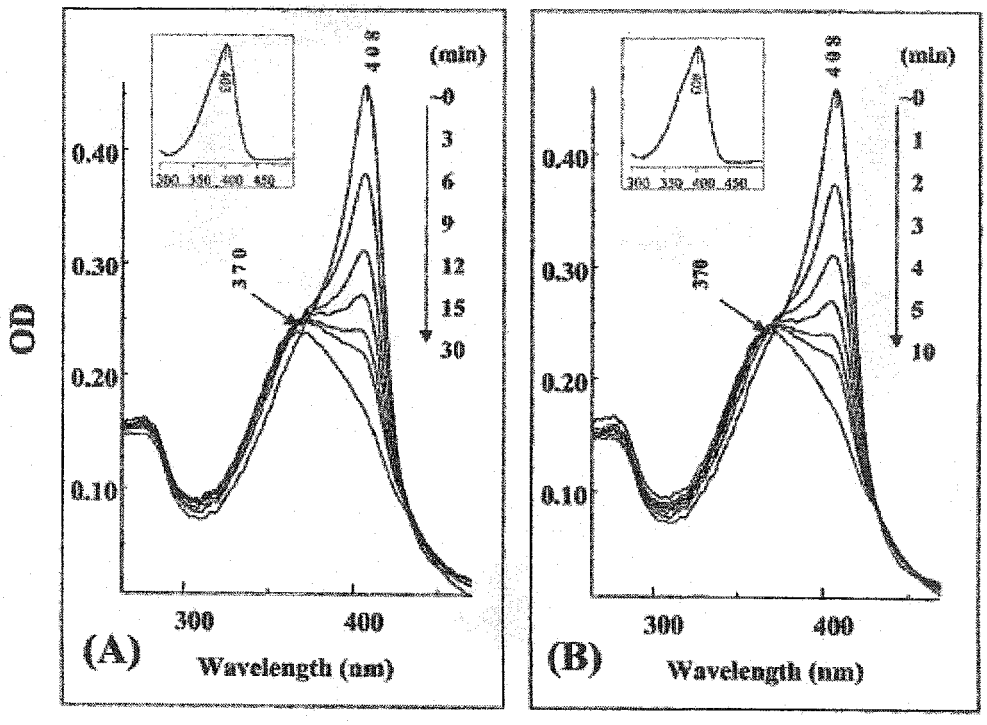

Figure 2.4. Soret absorption spectra of 2.0 – 4.0μM HRPC A and B at pH 3.0 in 500mM sodium phosphate buffer with 500mM NaCl *vs* time. Inserts show the Soret absorption spectra at pH 7.0. Spectra were recorded in a 1.0cm pathlength quartz cuvette at a scan speed of 600nm/min.

2.4.4 Time-dependent ferric HRPC UV/VIS spectra at pH 3.0

At neutral pH, the Soret spectra of both ferric HRPC samples are essentially identical with a peak maximum at 403nm (Figure 2.4, inserts). Immediately after preparation at low pH in phosphate buffer, the enzymes again exhibit similar spectra with a Soret maximum at 408nm, which loses intensity with time and gives rise to a broad band centered at 370nm characteristic of solvent-exposed heme (*91*). However, the different time-dependence of heme-exposure in the two samples is notable; HRPC **A** undergoes complete loss of the 408nm peak in 30min, while this loss is three times faster in HRPC **B**. When the pH is raised to 7.0 using NaOH, spectra identical to those seen when HRPC is first prepared at neutral pH are observed within mixing time (see insets of Figure 2.4), indicating that the conformational transitions are reversible for both ferric HRPC samples. Also, in agreement with the ν(CO) results, the 408nm band decayed ~2-fold slower in formate and ~1.5-fold faster in citrate (data not shown) compared to phosphate.

2.4.5 Time-dependent secondary-structure changes at pH 3.0 monitored by FTIR

HRPC is dominated by α-helices (*92*) which give rise to FTIR amide I' absorption between ~1640 and 1660cm^{-1}. The other structural elements present in HRPC and their characteristic amide I' frequencies include turns and loops (1671 - 1682cm^{-1}) and random coil (1630 – 1640cm^{-1}) (*93, 94*). Figure 2.5 shows the time-dependent deconvolved spectra of the amide I' region of the ferric HRPC samples in phosphate buffer. At pD 7.0, both samples possess very similar spectra, with α-helical peaks at 1658 and 1647cm^{-1}, which have been assigned to two types of α-helices (*1*) that differ slightly in H-bonding

and/or geometry (*95*). Upon lowering the pD to 3.0, both samples initially possess similar spectra, but while the HRPC **A** spectra remain relatively unchanged over 123min, those of HRPC **B** show significant changes. For example, the broadening of the amide I' envelope can be interpreted as an increase in unordered structure at the expense of α-helical content with time. Nonetheless, the presence of a peak at 1653cm^{-1} suggests that HRPC **B** still possesses some α-helical structure after 123min at pD 3.0. With time, both HRPC samples exhibit a band at 1622cm^{-1} that is characteristic of protein aggregation (*96, 97*). However, this band is much less intense in HRPC **A**, consistent with a higher degree of secondary structure in sample **A** compared to **B**. The curve-fitted FTIR spectra (Figure 2.7) clearly also revealed greater loss of helical character in HRPC **B**. CO binding resulted in little or no alteration in the amide I' absorption of HRPC at room temperature (Figure 2.7).

The spectra of HRPC **B** show obvious amide I' broadening immediately after preparation in citrate at pD 3.0 whereas this broadening is less evident in formate buffer. A well-defined aggregation band (1622cm^{-1}) also appears sooner in citrate (43min) and is more intense after 123min than the corresponding band in phosphate or formate buffers Figure 2.7). The HRPC **A** spectra are buffer-anion independent since the amide I' absorption in citrate and formate is the same as that in phosphate (Figure 2.5A). We conclude that HRPC **A** and **B** undergo different secondary structural changes at acid pH, regardless of the buffer anion present, but neither protein fully unfolds since the FTIR spectra indicate that residual secondary-structure elements are present after 123min.

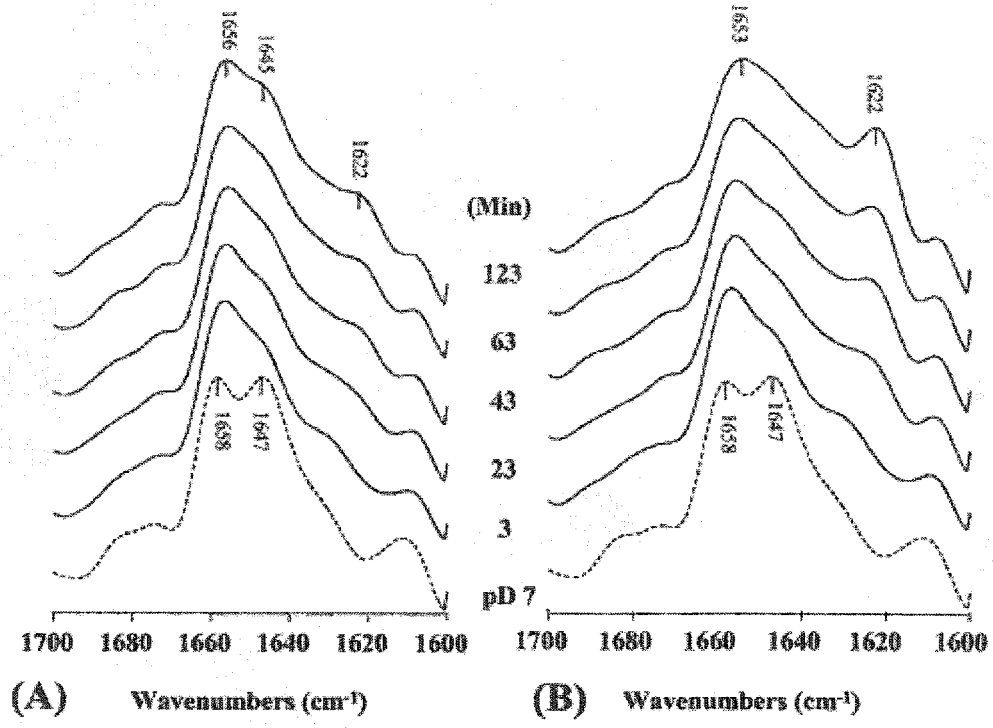

Figure 2.5. Deconvolved FTIR spectra of the amide I' region of 0.1–0.5mM HRPCO A and B at pD 7.0 (---) and at pD 3.0 in 500mM sodium phosphate buffers with 500mM NaCl *vs* time. Experimental conditions are given in Figure 2.1.

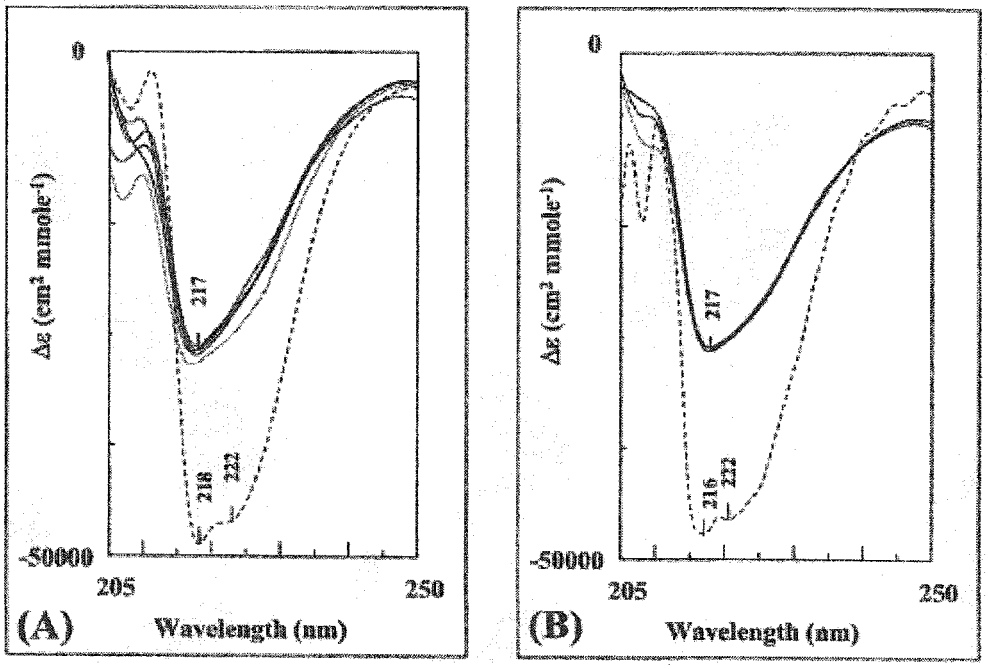

Figure 2.6. Far-UV CD spectra of 1.0–2.0mM HRPC A and B at pH 7.0 (---) and pH 3.0 in 500mM sodium phosphate buffers with 500mM NaCl after (···) 3min, (—) 23 to 123min. Spectra were recorded in the FTIR cell with a 6μm pathlength. Experimental conditions are given in Figure 2.3.

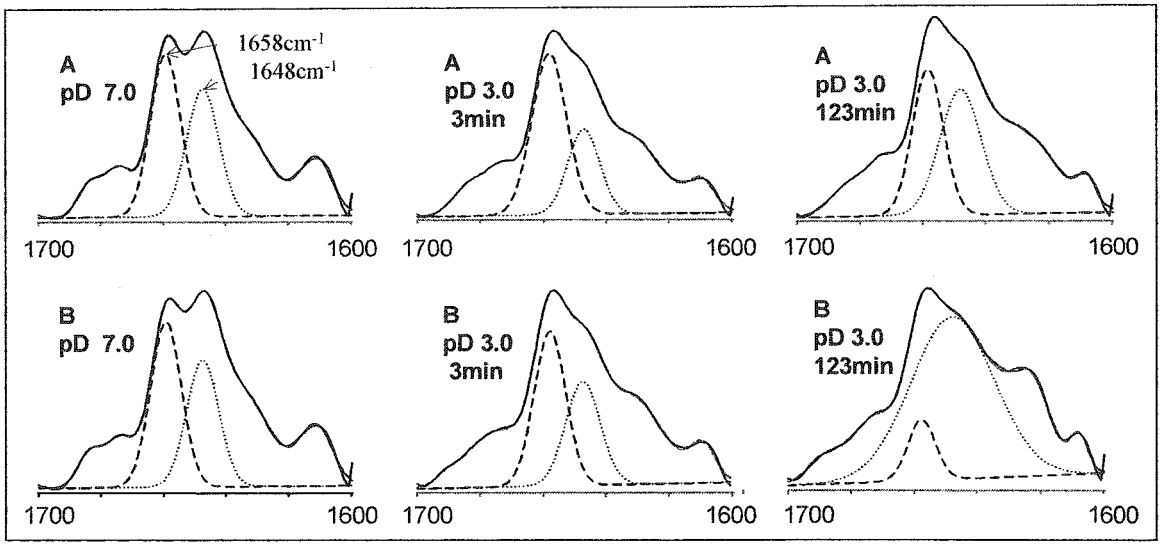

Figure 2.7. Curve-fitted deconvolved FTIR spectra of the amide I' region of 0.1–0.5mM HRPCO A and B at pD 7.0 and at pD 3.0 at 3 and 123min in 500mM sodium citrate buffer with 500mM NaCl *vs* time. The band at 1658cm^{-1} (---) is assigned to α-helical content, while the band at 1648cm^{-1} ( ) is assigned to unordered structure. Curve-fitting was performed as described by Dong *et al.* (*87*). Experimental conditions are given in Figure 2.1.

2.4.6 Time-dependent secondary-structure changes at pH 3.0 monitored by far-UV CD

The far-UV CD spectra of both ferric HRPC samples are similar at pH 7.0, with a negative peak at 222nm, characteristic of α-helical absorption, and a second peak at ~217nm (Figure 2.6). When the pH is lowered to 3.0, sample A undergoes ~40% loss of helical character as reflected in loss of the 222nm UV absorption (Figure 2.6A). Three minutes after preparation at pH 3.0, HRPC B shows ~45% loss of helical character and complete loss of the 222nm peak, with negligible additional spectral changes between 3 and 123min (Figure 2.6B). The far-UV CD results agree with the FTIR amide I' data in revealing that, while both proteins lose helical character within 3min after preparation at pH 3.0, HRPC A retains greater α-helical content over 123min. CO-binding resulted in no changes in the far-UV CD spectra at either pH 7.0 or 3.0 (data not shown).

2.4.7 *Effect of added $CaCl_2$ on HRPC spectra at pH 3.0*

HRPC binds two Ca^{2+} ions at distal and proximal sites (*98*). It is known that the Ca^{2+}-binding sites are selective for Ca^{2+} ions and Ca^{2+} is necessary for HRPC folding (*99, 100*). To determine whether the appearance of the form-III exposed-heme conformer in HRPC-CO **B** at low pH was due to loss of Ca^{2+}, the FTIR ν(CO) bands were examined in the presence of $CaCl_2$. The results reveal that excess Ca^{2+} completely inhibits the formation of the form-III band at 1969cm^{-1} since the HRPC-CO **B** spectra exhibit only form-I (1934cm^{-1}) and form-II (1905cm^{-1}) bands between 3 and 123min at pH 3.0 in formate, citrate (Figure 2.2, inserts) and phosphate (data not shown) buffers with 1mM Ca^{2+}. These results provide clear evidence that the acid-induced time-dependent conformation changes detected in the various buffers for HRPC-CO **B** are in fact due to Ca^{2+} leaching out of the protein. Presumably, protonation of Ca^{2+} ligands at low pH weakens the Ca^{2+}-binding affinity of HRPC (*100*), while the relative affinities of the buffer anions for Ca^{2+} account for the different rates of Ca^{2+} leaching. The Soret absorption of the ferric HRPC samples also was measured in 1mM $CaCl_2$ at pH 3.0 and negligible loss of 408nm intensity occurred over 30min (data not shown). These results underscore the stabilizing affects of Ca^{2+} which have been ignored in recent reports on the low-pH conformational stability of HRPC (*5, 6, 101*). It is also of note that both in the presence and absence of added Ca^{2+}, the Soret absorbance maximum returns to 403nm upon raising the pH to 7.0 within mixing time (Figure 2.6), indicating that acid-denaturation of ferric HRPC is reversible.

2.4.8 Calcium content of the HRPC samples

Although Ca^{2+}-leaching explains the buffer-anion-dependent rate of form III formation in HRPC-CO **B** (Figures 2.1A and 2.2), the question remains as to why HRPC-CO **A** does not lose Ca^{2+} under the same conditions (Figure 2.1A)? The Ca^{2+} content of both samples was analyzed by atomic absorption spectroscopy to determine if sample **A** contained excess Ca^{2+} that would inhibit acid denaturation. Samples **A** and **B** were found to possess Ca/heme molar ratios of 2.79 and 3.51, respectively, close to the expected ratio of 2.0 (*98*). Since sample **B** was found to possess the higher Ca^{2+}/heme ratio upon purchase, the heme-pocket stability of HRPC-CO **A** must be due to another factor.

2.4.9 Differences in HRPC Glycosylation

Glycans are likely involved in the proper folding, solubility, recognition, ligand binding and stability of proteins (*102*). HRPC has eight N-glycosylation sites, and possesses four different N-glycans (*103*), providing much scope for heterogeneous glycosylation. Figure 2.8 shows the 12% SDS-PAGE of HRPC **A** and **B** along with bovine serum albumin, a 66-kDa glycoprotein for comparison. Both HRPC **A** and **B** migrated less than expected for a 44-kDa glycoprotein compared to the glycosylated 45-kDa ovalbumin and the non-glycosylated 31-kDa carbonic anhydrase standards. HRPC **B** (lane 4) also migrated slightly further than HRPC **A** (lane 3) indicating that the former is of lower molecular weight than the latter. The band broadening seen in lanes 3 and 4 is characteristic of heterogeneous glycosylation, suggesting that this is one of the variables responsible for the differential stability of HRPC **A** and **B** at pH 3.0.

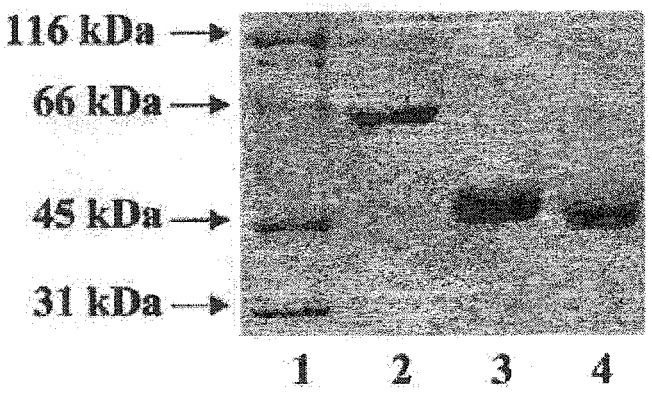

Figure 2.8. A 12% SDS-PAGE of molecular-weight standards (lane 1), bovine serum albumin (lane 2), HRPC **A** (lane 3) and HRPC **B** (lane 4).

2.5 Discussion

2.5.1 Time-Dependent Conformation Changes at pH 3.0

In the absence of added Ca^{2+}, HRPC-CO **B** undergoes dramatic time-dependent spectroscopic changes at low pH. Most notable are the growth of the broad ν(CO) band at 1969cm^{-1} (Figures 2.1B and 2.2) and the inversion of Soret CD absorption (Figure 2.3B). The 1969cm^{-1} band is assigned to a solvent-exposed FeCO unit (form III), where the CO ligand undergoes random interactions with the negative ends of the water dipoles which are reported to broaden and blue-shift the ν(CO) band (*104*). In support of this assignment, a similar ν(CO) band was reported for thermally-denatured HRPC-CO (1964cm^{-1}) (*1*), acid-denatured myoglobin-CO (1966cm^{-1}) (*105*) and base-denatured cytochrome P_{450}-CO (1966cm^{-1}) (*106*). A second marker of acid-denatured HRPC-CO is the reversal of the positive and negative CD bands as seen in Figure 2.3B for HRPC-CO **B**. Soret inversion also was reported by Smulevich *et al.* (*5*), who attributed it to a change in the relative orientation of the electric and magnetic dipole moments of the $\pi \rightarrow \pi^*$ heme transition (*107*). Thus, the conformation changes occurring on acid denaturation of HRPC-CO give rise to a solvent-exposed Fe-CO unit and alteration in the asymmetry of

the heme environment. HRPC-CO **A** exhibits neither of these markers of acid-denaturation (Figures 2.1A and 2.3A), but it does show a time-dependent decrease in the CD band intensity at pH 3.0, in agreement with the results of Coletta *et al.* (*108*).

Less dramatic differences are seen in the Soret absorption of the two ferric HRPC samples at pH 3.0 (Figure 2.4). In both cases the Soret broadens and blue-shifts over time to form a band with a maximum at 370nm which resembles that of solvent-exposed heme (*91*). Ferric HRPC **A**, however, it more resistant to acid denaturation than HRPC **B** since the Soret 408→370nm transition occurs three-fold more slowly (30 *vs* 10min) in the former. Smulevich *et al.* (*5*) reported slow formation (30min) of the 370nm peak in HRPC **B** at pH 3.1 but they also observed isosbestic points at 382 and 430nm, and concluded that HRPC forms a metastable species at low pH. Our spectra show no isosbestic points at these wavelengths indicating no direct interconversion of species. A comparison of the ferric HRPC and HRPC-CO data reveal that CO binding results in increased heme-pocket stability at pH 3.0. A time-dependent Soret shift (403→370nm) in formate is observed for the ferric samples (data not shown), whereas negligible changes are detected in the ν(CO) bands of both HRPC **A** or **B** under the same conditions (Figure 2.2B).

Based on the intensity of the far-UV CD band centered at 222nm, ferric HRPC **A** and **B** are assumed to lose ~40% and 45%, respectively, of their helical character after 3min at pH 3.0 in phosphate (Figure 2.6). The FTIR amide I' absorption also shows that ferric HRPC **B** undergoes greater loss of helical character compared to HRPC **A** (Figure 2.5). Interestingly, Smulevich *et al.* (*5*), reported only ~20% loss of CD-monitored α-

helical intensity in HRPC **B** following a 30min incubation at pH 3.1 in phosphate, which may be due to lot-to-lot variability in HRPC **B** (*vide infra*).

2.5.2 Conformational Stabilization of HRPC at pH 3.0 by Ca^{2+}

Feis *et al.* (*6*) were the first to report a buffer-anion-dependent rate of HRPC-CO form-III formation at low pH. In agreement with our results for HRPC-CO **B**, they found (using HRPC from a third commercial supplier) that form III appeared at a faster rate in citrate than in formate (*6*). We attribute this to buffer-anion-promoted leaching of the stabilizing proximal and/or distal Ca^{2+} from HRPC since the formation constant (K_f, Table 2.1) for calcium formate is $>10^3$-fold smaller than that of the citrate complex. Based on the relative K_f values alone, no form-I band was expected in phosphate but such is not the case (Figure 2.1B *vs* 2.2A), indicating that other factors, (*e.g.*, size and shape of the buffer anion) also may play a role. Nonetheless, consistent with our hypothesis, addition of 1mM Ca^{2+} resulted in time- and buffer-anion independent ν(CO) spectra at pH 3.0 with a dominant form-I band at 1934cm^{-1} in both HRPCO-CO samples (Figure 2.2, inserts). The Soret absorption at pH 3.0 of the Ca^{2+}-stabilized ferric HRPC samples is also time- and buffer-anion independent, and is the same as the sharp 408nm absorption at 0min shown in Figure 2.4. The dramatic effects of Ca^{2+} on the ν(CO) and heme spectra are consistent with NMR experiments which indicate that one of the Ca^{2+} ions is necessary for maintaining the integrity of the heme pocket (*109*). The Ca^{2+} ions are seven-coordinate with backbone carbonyl and side-chain carboxylate ligands. The distal Ca^{2+} is structurally coupled to the active site through Asp43, which provides two ligands to the ion, and is adjacent in sequence to the essential distal His42. Extremes of pH or

Ca^{2+}-depletion affect the position of His42 and the catalytic performance of the enzyme (*100, 101*) and, as shown here, the spectral properties of the heme. In contrast to the reported data, the conformationally stable low-pH forms of ferric HRPC and HRPCO are time and buffer-anion independent with a Soret maximum at 408nm, and a dominant ν(CO) band at 1934cm^{-1}.

Addition of Ca^{2+} following acid-denaturation of ferric HRPC or HRPC-CO at pH 3.0 results in formation of the stable low-pH conformations. Addition of NaOH to acid-denatured HRPC results in formation of the native forms at neutral pH within mixing time, revealing that acid-denaturation is reversible. This resembles the release and uptake of Ca^{2+} by calsequestrin in sarcoplasmic reticulum vesicles which are regulated by the luminal pH due to the protein's reduced affinity for Ca^{2+} at acid compared to neutral pH (*110*). Of even more direct relevance to the present study is the report that reversible alkaline inactivation of LIP involves the release of both the distal and proximal Ca^{2+} ions (*111*), and that Ca^{2+}-leaching was faster in borate than in Tris.

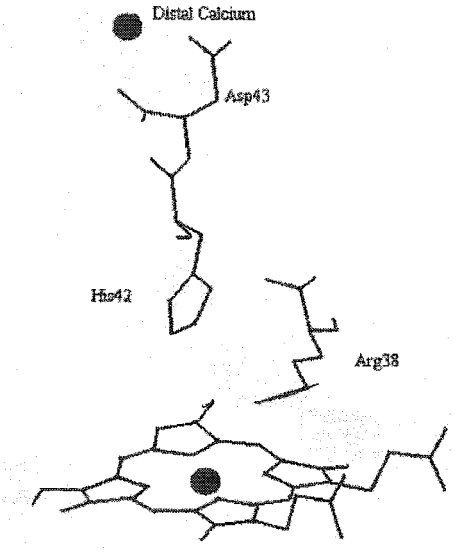

Figure 2.9. The heme, distal calcium ligand, and active-site residues in the crystal structure of HRPC (*31*). The δ-meso edge, facing the viewer, lies at the bottom of the substrate access channel that leads into the active site of heme peroxidases.

Table 2.1. Formation constants (K_f)[a] for calcium complexes of buffer anions

Calcium Complex	K_f	Ref.
$Ca_3(PO_4)_2$[b]	2.88 X 10^6	(*112*).
$Ca_3(C_6O_7H_5)_2$[c]	4.78 X 10^4	(*112*).
$Ca(HCO_2)_2$[d]	2.69 X 10^1	(*112*).
Ca_2(HRPC)	1.6X 10^4	(*97*).

[a]pH 7.0, 25°C, ionic strength (μ) ~ 0

[b]Calcium phosphate

[c]Calcium citrate

[d]Calcium formate

2.5.3 Role of Glycans

Since the commercial samples contained comparable amounts of Ca^{2+}, the greater low-pH stability of HRPC **A** relative to **B** must be due to another factor. The band broadening seen for the HRPC samples in Figure 2.8 is characteristic of heterogeneous glycosylation, which was observed at each of the N-linked sites of HRPC **B** using MALDI-ToF-MS (*113*). It has been pointed out (*114*) that the glycans of HRPC belong to the flexible protein-surface-shielding-type analyzed extensively in ribonuclease, where glycans reduce solvent access to the peptide backbone up to ~30Å from the glycosylation sites (*115-117*). Examination of the crystal structure of HRPC (*31*) reveals that of the eight N-glycosylation sites, glycans on Asn13, Asn57 and Asn158 are within shielding distance (30Å) of the distal Ca^{2+}, those on Asn13, Asn198 and Asn268 the proximal Ca^{2+}, and those on Asn57, Asn186 and Asn214 the heme pocket, providing many possible shielding scenarios.

The results reported here strongly support a proposal that variation in critical glycans is responsible for the dramatic differences in the low-pH conformational stability of HRPC from different suppliers. Supporting evidence for this hypothesis comes from the report of Feis *et al.* (*6*) that the form-III ν(CO) band appeared faster in non-glycosylated *r*HRPC-CO from *E. coli* than in glycosylated HRPC-CO. Also, the lot-to-lot variability in the low-pH stability of HRPC from the same supplier (*e.g.*, the reversal in Soret-CD ellipticity at pH 3 seen in Figure 2.3 and by Smulevich *et al.* (*5*) but not by Coletta *et al.* (*108*) for HRPC-CO **B**) can be attributed to differences in glycosylation since ESI-MS data revealed that two lots of HRPC **B** differed considerably in N-glycan composition (*113, 118*). Variation in glycosylation also could explain why the ν(CO) peak at 1965cm^{-1} reported for HRPC-CO **A** in formate buffer at pH 3.0 (*1*) was not seen under the same conditions in this study.

The glycosylation of recombinant glycoproteins is exquisitely sensitive to variations in growth conditions (*119*). Also, peroxidase isozymes that differ in carbohydrate content are correlated with specific developmental events (*120*). Thus, growing horseradish plants under different nutrient conditions or harvesting different tissue types at various stages of plant development could affect the carbohydrate content of their glycoproteins (*121*) and give rise to the heterogeneous glycosylation of HRPC seen here (Figure 2.8) and elsewhere (*113, 118*).

2.6 Conclusions

The variation in low-pH conformational stability of HRPC in the absence of added Ca^{2+} calls into question all previous work carried out at low pH on this protein. Of

particular interest is the pK_a of the distal His42 because of its critical role in acid-base catalysis. In the absence of added Ca^{2+}, a pK_a of ~4 represents the consensus value for ferric HRPC and values of 4.0 and 8.7 have been proposed for HRPC-CO from kinetic and ν(CO) titration measurements (*6*). Since decreasing the pH promotes loss of stabilizing Ca^{2+} in certain buffers, the pK_a values clearly need to be remeasured in non-chelating or Good's buffers (*122*) with the addition of supplementary Ca^{2+}. The spectral markers established here for the conformationally stable low-pH forms of HRPC should be used to insure that acid-denaturation in not taking place.

Class II peroxidases function at acid pH but possess essentially identical active sites and Ca^{2+} ligands as those that function at neutral pH. Apart from relatively weak sequence similarity, the other noticeable difference between class II and III peroxidases is in the attached glycans. For example, LIP, which is optimally active at pH 2-3 (*76, 77, 123*), possesses one N- and one O-linked glycan (*33*). Although both are within shielding range (~30Å) of the heme pocket and the proximal Ca^{2+}, glycosidase treatment revealed that only the O-linked glycan plays a role in stabilizing LIP at pH 7.9 (*124*). It is of interest to note that other class III plant peroxidases such as tobacco, soybean and barley peroxidase all possess conserved active sites, Ca^{2+} binding sites, disulfide bonds, similar glycosylation sites, and ~50% sequence similarity to HRPC (*125*). However, these three enzymes have been shown to retain significant catalytic activity at extremely low pH, unlike HRPC **B** (*126-128*). Presumably, the low pH stability of HRPC **A** is due to the nature of its glycans.

In summary, the results presented here lead us to hypothesize that the positioning of key glycans could determine the acid-base conformational stability, and hence activity,

of class II and III plant peroxidases by preventing Ca^{2+} leaching. Analysis of *r*HRPC and different glycosylation-site mutants from Sf9 (*9*) and yeast cells (*8*), which possess the machinery for protein glycosylation, would allow this novel hypothesis to be tested. Such studies are planned as well as investigation of pH-activity profiles of HRPC in the presence of various amounts of added Ca^{2+} in different buffer systems.

3.0 Scavenging with TEMPO$^{\bullet}$ to Identify Peptide- and Protein-based Radicals by Mass Spectrometry: Advantages of Spin Scavenging over Spin Trapping

3.1 Abstract

The detection and characterization of radicals in biomolecules is challenging due to their high reactivity and low concentration. MS provides a tool for the unambiguous identification of protein-based radicals by exploiting their reactivity with suitable reagents. To date, protein-radical detection by MS has been modeled after electron paramagnetic resonance experiments, in which diamagnetic spin traps, such as 3,5-dibromo-4-nitrosobenzenesulfonate (DBNBS), convert unstable radicals to more stable spin adducts. Since MS detects mass changes, and not unpaired spins, conversion of radicals to stable diamagnetic adducts is more desirable. The use of 2,2,6,6-tetramethylpiperidinyl-1-oxy (TEMPO$^{\bullet}$) in the MS identification of protein-based radicals was explored here to establish whether scavenging via radical combination would give rise to TEMPO-adducts that were stable to MS analysis. The horseradish peroxidase (HRPC)/H_2O_2 reaction was used to generate radicals in derivatives of tyrosine, tryptophan and phenylalanine as models of protein-based radicals. TEMPO$^{\bullet}$ was added as a radical scavenger and the products analyzed by ESI-MS. Dramatically higher mass-adduct yields were obtained using radical scavenging *vs* radical trapping, which greatly enhanced the sensitivity of radical detection. The efficiency of TEMPO$^{\bullet}$ in protein radical scavenging was examined in horse heart myoglobin (Mb) and cytochromes c peroxidase (CCP) from *Saccharomyces cerevisiae*. On H_2O_2 binding to their ferric hemes,

two oxidizing equivalents are transferred to the proteins as an Fe^{IV}=O species and a polypeptide-based radical. In addition, CCP has been shown to reduce up to 10 equivalents of H_2O_2 using endogenous donors, thereby generating as many as 20 radicals on its polypeptide. Following myoglobin and CCP incubation with a 10-fold molar excess of H_2O_2 and $TEMPO^{\bullet}$, MALDI-ToF analysis of the tryptic peptides derived from the proteins revealed 1 and 9 TEMPO-adducts of myoglobin and CCP, respectively. Given the high scavenging efficiency of $TEMPO^{\bullet}$ and the stability of TEMPO-labeled peptides in ESI and MALDI sources, scavenging by stable nitroxide radicals coupled with MS analysis should provide sensitive and powerful technology for the characterization of protein-based radicals.

3.2 Introduction

Protein radicals can lead to cross-linking, backbone cleavage, and formation of peroxy radicals and protein peroxides. In some cases, these radical reactions are physiologically relevant, but in many other cases, protein radicals promote pathological or toxicological processes. Despite their importance, the factors and mechanisms that control the formation, localization, delocalization, and propagation of protein radicals remain obscure. Their direct observation is often disadvantaged by their low concentration (10^{-7} M) and high rates of self-reaction (10^{7}-10^{9} $M^{-1}s^{-1}$) (*51*). Radical detection has been assisted by the use of diamagnetic ST containing a nitroso or nitrone function that is reactive with primary radicals to form more stable radical adducts (*53-55*). To date, electron paramagnetic resonance (EPR) spectroscopy has been the main tool used in protein-based radical detection (*52*). In an EPR spin-trapping experiment, the ST

is added to a radical-generating reaction, and detection of the spin adduct (R-ST$^{\bullet}$) is considered evidence that R$^{\bullet}$ is an intermediate in the reaction (*54*). However, this is not always the case. For instance, in an attempt to provide evidence for OH$^{\bullet}$ radical production in the Fenton reaction, Lai and Piette (*129*) assigned EPR signals to the MNP-OH$^{\bullet}$ spin adduct, but it was later shown that an identical spectrum was obtained by enzymatic or chemical reduction of the diamagnetic ST, 2-methyl-2-nitrosopropane (MNP) (*130*). "Inverted spin-trapping" represents another complication in the use of STs. Here, an enzyme or other component oxidizes the ST, which then reacts with an amino-acid residue, producing the same product as the direct reaction of the ST with a protein radical. It also has been shown that ene addition of DBNBS to peptides containing W gives rise to EPR signals upon oxidation of the resultant hydroxylamine (*131, 132*). Such processes obviously lead to incorrect assignments of R$^{\bullet}$ (*19*).

In addition to the chemical problems associated with spin trapping, difficulties in EPR spectral interpretation (*18, 52*) often prevent the unambiguous identification of radical sites in proteins. For instance, DeGray *et al.* (*56*) misassigned W14 and W7 as sites of radical formation in H_2O_2-oxidized Mb due to ambiguity in the EPR signals. Radicals in CCP also eluded identification, and it was only after considerable investigation that satisfactory simulations provided conclusive evidence that the unusual behavior of the W191 radical in CCP can be attributed to its coupling with the Fe^{IV} center (*27*).

To complement and overcome the limitations of EPR approaches for the analysis of protein-based radicals, spin trapping was combined in our laboratory with mass spectrometric detection of the labeled species. Specifically, spin trapping was coupled

with peptide mass mapping and sequencing using high-performance liquid chromatography (HPLC) and ESI-MS (ST/LC/MS) to localize the actual protein residues labeled by the ST (*18, 19*). ST/LC/MS has greatly increased the specificity and sensitivity of radical identification, and has been used by a number of groups to identify sites of protein-based radicals (*18, 19, 57, 58, 133*). For example, ST/LC/MS has been successful in unambiguously identifying the amino-acid radicals formed in H_2O_2-oxidized Mb, lactoperoxidase and CCP (*18, 50, 57, 133*). Nonetheless, the technology does suffer from the drawbacks of spin trapping mentioned above. Also, the relatively low reactivity of STs with proteins requires the use of 100- to 1000-fold excess ST, which complicates the MS analysis. A recent demonstration of this was the assignment of noncovalent mass adducts of cytochrome c and DBNBS to spin adducts (*19*).

Stable nitroxide radicals, such as TEMPO$^{\bullet}$ (Figure 3.1A), have been known for some time to scavenge carbon-centered radicals *in vivo* and *in vitro* (*134-139*). TEMPO$^{\bullet}$ and its derivatives also have been used extensively as scavengers to control polymerization or polymer degradation in living polymerization reactions (*60, 139-141*). Since a spin adduct is not required for MS detection, nitroxide radicals should be effective tools for the identification of peptide and protein-based radicals using MS. The reported rate constants for scavenging (k_S = $5\text{x}10^7$ – $2\text{x}10^9$ $M^{-1}s^{-1}$) (*51, 142*) or combination of a carbon-centered radical with TEMPO$^{\bullet}$ are faster than those for trapping ($k_T = 10^6 - 10^7$ $M^{-1}s^{-1}$) (*53-55*) or spin-adduct formation with a diamagnetic ST.

$$R^{\bullet} + \text{TEMPO}^{\bullet} \overset{k_S}{\rightleftharpoons} \text{R-TEMPO} \qquad (3.1)$$

$$R^{\bullet} + \text{ST} \overset{k_T}{\rightleftharpoons} \text{R-ST}^{\bullet} \qquad (3.2)$$

In this study, the use of TEMPO$^{\bullet}$ in scavenging peptide and protein-based radicals and characterization of the TEMPO adducts by MS were explored. Specifically, HRP was used to catalyze the one-electron oxidation by H_2O_2 of the aromatic amino acid derivatives, N-acetyl-*l*-tyrosinamide (NAYA) (Figure 3.1B), N-acetyl-*l*-tryptophanamide (NAWA) (Figure 3.1C), and N-acetyl-*l*-phenylalanine (NAF) (Figure 3.1D). These derivatives were selected as peptide models since Y and W are frequently oxidized amino-acids in biology whereas F is rarely oxidized (*16*). The adducts formed by spin-combination reactions (eqn 3.1) of the one-electron oxidized derivatives ($R^{\bullet}$) were analyzed by ESI-MS. For all three amino-acid derivatives, formation of a stable R-TEMPO adduct competed favorably with self-dimerization (R-R formation). Also, scavenging by nitroxide radicals provided a clear kinetic advantage over spin trapping, which greatly enhanced the sensitivity of MS detection of the mass adducts.

Horse heart Mb and yeast CCP were used as protein model systems. CCP efficiently catalyzes the oxidation of ferrocytochrome c by H_2O_2 in yeast mitochondria. In the absence of donor substrates, CCP reduces up to 10 molar equivalents of H_2O_2 using endogenous donors on its polypeptide, including Y and W residues, via a heme mediated process (eqns 3.3-5) (*17*). The first molecule of H_2O_2 reacts with ferric CCP (Fe^{III},P) to form compound I (Fe^{IV}=O,$P^{\bullet+}$, where the oxygen atom is assigned an oxidation number of –II). Intramolecular electron transfer to the Fe^{IV}=O heme leads to the formation of a new protein-based radical, $P_x^{\bullet+}$ (or $P_x^{\bullet} + H^+$) (*27*), and reaction of a second H_2O_2 molecule with the newly formed Fe^{III} regenerates Fe^{IV}=O and an additional protein radical $P_y^{\bullet+}$.

$$Fe^{III},P + H_2O_2 \rightleftharpoons Fe^{IV}{=}O,P^{\bullet+} + H_2O \qquad (3.3)$$

$$Fe^{IV}{=}O,P^{\bullet+} + 2H^+ \rightleftharpoons Fe^{III},P^{\bullet+}, P_x^{\bullet+} + H_2O \qquad (3.4)$$

$$Fe^{III},P^{\bullet+}, P_x^{\bullet+} + H_2O_2 \rightleftharpoons Fe^{IV}=O, P^{\bullet+}, P_x^{\bullet+},P_y^{\bullet+} + H_2O \qquad (3.5)$$

Up to 10 molar equivalents of H_2O_2 can be consumed in reactions 3-5 with no heme damage and no O_2 evolution, eliminating H_2O_2 disproportionation as a mechanism of H_2O_2 consumption (*50*). The protein-based radicals formed in CCP have received much attention since $P^{\bullet+}$ in eqn 3.3 represents a cation radical on W191, which was the first catalytically-active tryptophanyl radical identified in an enzyme (*27*).

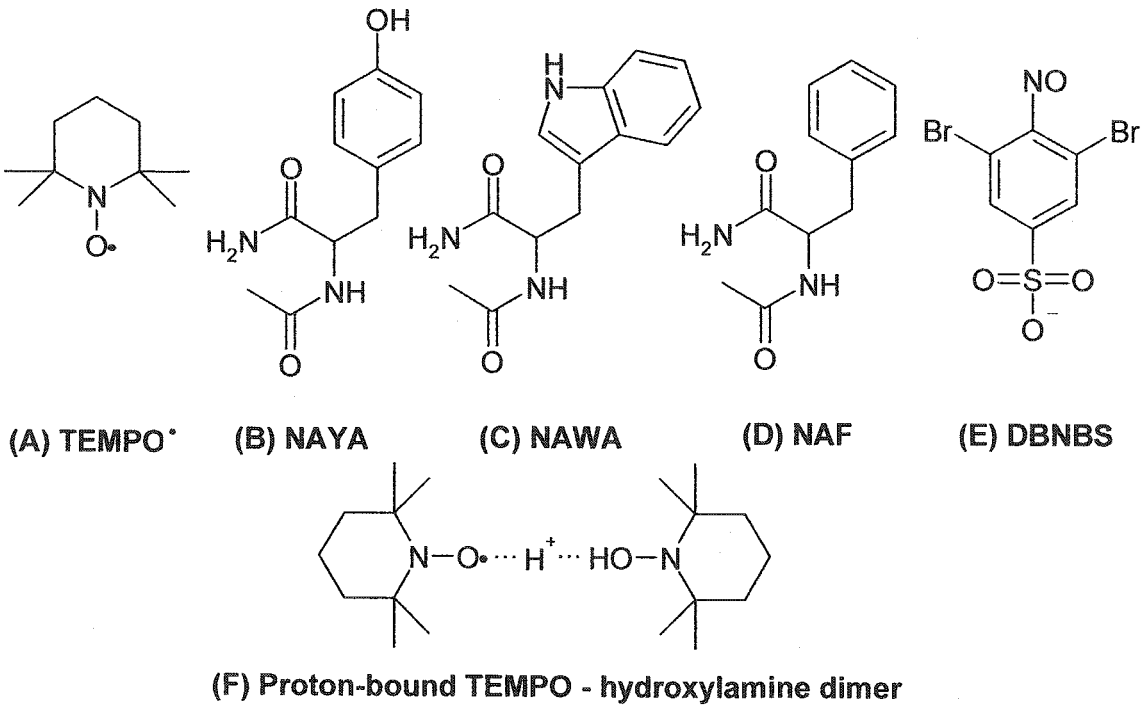

Figure 3.1. Structures of the reagents and the proton-bound TEMPO•-hydroxylamine dimer. TEMPO• (2,2,6,6-tetramethylpiperidinyl-1-oxy), NAYA (N-acetyl-*l*-tyrosinamide), NAWA (N-acetyl-*l*-tryptophanamide), NAF (N-acetyl-*l*-phenylalanine), DBNBS (3,5,-dibromo-4-nitrosobenzenesulfonate).

Like heme peroxidases, Mb reacts with H_2O_2 to form an oxyferryl (Fe^{IV}=O) heme and unstable protein radical species (*143*). It has been established by several groups using EPR, ST/LC/MS and site-directed mutagenesis that Y103, which is in van der Waals contact with the heme and solvent exposed, is the primary site of radical formation in horse heart Mb (*18, 19, 47, 143-145*). Thus, Mb is a well characterized model to use in the development of protein-based radical detection methods.

The low-molecular-weight R-TEMPO adducts examined here were stable to ESI-MS analysis. Furthermore, the TEMPO-labeled proteins were stable to tryptic digestion and peptide analysis by MALDI-ToF-MS. Thus, MS analysis of diamagnetic R-TEMPO adducts should provide an effective and sensitive method for the identification of radicals accessible to scavengers in biomolecules. Such capability should aid greatly in understanding the mechanisms of radical translocation, which in turn, will assist in comprehending the role of surface-exposed protein radicals in cellular redox signaling (*146*) and oxidative stress (*16*). The present results add to the extensive reports on biological applications of nitroxides in radical scavenging in the mitochondrial respiratory chain (*147*), in cytochromes P450 (*148*), and in preventing Haber-Weiss reactions (*149*). Scavenging by nitroxides also has been implicated in protecting against oxidative DNA scission in *Escherichia coli*, membrane damage, loss of contractility in beating cardiomyocytes, the deleterious effects of cardiac reperfusion after ischemia, and lipid peroxidation in hepatic microsomes (*134, 137, 138, 150, 151*).

3.3 Materials and Methods

3.3.1 Materials

Wild-type recombinant CCP was prepared as described previously (*28*). HRPC (Grade I) was purchased from Roche. Horse heart Mb, bovine catalase, N-acetyl-*l*-tyrosinamide, N-acetyl-*l*-tryptophanamide, N-acetyl-*l*-phenylalanine, 2,2,6,6-tetramethylpiperidinyl-1-oxy, sodium 3,5,-dibromo-4-nitrosobenzene and trifluoroacetic acid were from Sigma and used without further purification. HPLC grade acetonitrile was purchased from EM Industries, and H_2O_2 from Fisher. Sodium phosphate (ICN) buffers were prepared using distilled water (specific resistance 18MΩ) from a Millipore Simplicity 185 system. All buffers contained 100μM DTPA (Fisher) to prevent trace-metal redox chemistry.

3.3.2 Radical generation in the aromatic amino-acid derivatives

500μM NAYA, NAWA or NAF, 150μM H_2O_2, and 1 or 10 molar equivalents of TEMPO$^{\bullet}$ (500μM or 5mM) were added to 500μM NaPi buffer (pH 7.4) containing 100μM DTPA. The reaction was initiated by addition of HRP to a concentration of 36nM and let stand at room temperature for 5-10min, flash frozen and stored at –80°C for MS analysis. The samples were diluted 10-fold in 50% acetonitrile/0.05% TFA and directly infused using a syringe pump (Harvard Apparatus) into the ESI source of a ThermoFinnigan SSQ 7000 single quadrupole mass spectrometer at a flow rate of 3μL/min. Ultrapure N_2 (Praxair) was used as a nebulizing gas. Typical MS operating

conditions were: needle voltage, 4.0kV; spray current, 2.3mA; capillary temperature, 180°C; electron multiplier, 1200V. The mass range was scanned from 100-1000u at 3s/scan in positive-ion mode. Data analysis was performed using Xcalibur software (ThermoFinnigan).

3.3.3 Heme protein-based radical generation reactions

H_2O_2 (5mM) was added to a mixture of 500μM CCP (or Mb) and TEMPO$^{\bullet}$ (500μM or 5mM) and allowed to react for 10min at room temperature in 500μM NaPi buffer (pH 7.4) containing 100μM DTPA. Although the reduction of H_2O_2 by CCP should be completed in ~1min (*152*), 10nM catalase was added after 10min to ensure that all H_2O_2 was removed. The product mixture was directly infused into the ESI source of the mass spectrometer at a flow rate of 3μL/min or flash frozen and dried at 25°C in a Speed Vac (Savant) for 1h. For further ESI-MS analysis of the intact protein, the lyophilizate was diluted in 50% acetonitrile/0.05% TFA. The MS operating conditions were the same as those used for the amino-acid derivatives except the mass range was scanned from 500 to 2000amu.

Prior to tryptic digestion, heme-free CCP and Mb were formed by diluting the lyophilizate in 20μL 50% acetonitrile/0.05% TFA and removing the heme on a reversed-phase C18 4.6 x 250-mm HPLC column (Zorbax) with a 10-50% acetonitrile gradient in 0.05% TFA at 1mL/min over 20min. The HPLC purifications were performed using an Agilent HPLC (Model 1090) equipped with a control module, binary pump, manual

injector and diode-array UV-VIS detector. The heme-free proteins were lyophilized and resuspended in 100mM NaPi buffer (pH 7.4). Sequencing-grade trypsin (1μg/μL, Roche) was added at a sample to trypsin ratio of 10:1 (w/w) and digestion was carried out at 25°C overnight. Digestion was quenched by freezing in liquid N_2 and the recovered peptides were dried in the Speed Vac, resuspended in 10μL of 5% methanol (Fisher)/0.1% TFA, and desalted on C_{18} Zip Tips (Millipore). The desalted peptides were collected from the Zip Tips in 1.5μL of 60% acetonitrile/0.1% TFA and mixed with 1.5 μL of MALDI matrix solution prepared by combining 10 volumes of acetone saturated with α-cyano-4-hydroxycinnamic acid (Sigma), 1 volume of acetone with 20mg/mL nitrocellulose (Sigma), 4 volumes of acetone (Fisher), and 5 volumes of 2-propanol (Fisher). Samples (1.5-2.5μL) were spotted on the MALDI target plate (Applied Biosystems), and analyzed using a Voyager DE Linear MALDI-ToF mass spectrometer (Applied Biosystems) with a resolution of ~500. Mass spectra were acquired as the sum of the ion signals generated by irradiation of the target with 128 laser pulses, and subjected to two-point internal calibration using the trypsin autolysis peptides with M_r 804.9 and 2163.3. This resulted in a mass accuracy of ± 0.14% based on the masses obtained for the peptides derived from trypsin autodigestion and human keratin present in the samples as impurities. Average peptide masses were assigned and used in the database search. Peptides were selected in the mass range of 1000-4200Da.

3.4 Results

3.4.1 Products of free-radical generation in the aromatic amino-acid derivatives

Based on the oxidation of free Y by HRP/H_2O_2 (*153*), the expected radical combination reactions following HRP-catalyzed NAYA (Figure 3.1B) oxidation by H_2O_2 in the presence of TEMPO$^\bullet$ are:

$$NAYA^\bullet + NAYA^\bullet \rightleftharpoons \text{diNAYA} \quad (3.6)$$

$$NAYA^\bullet + TEMPO^\bullet \rightleftharpoons \text{NAYA-TEMPO} \quad (3.7)$$

The mass spectral analysis of the NAYA reaction mixture (36nM HRP, 150μM H_2O_2, 500μM NAYA, 500μM TEMPO$^\bullet$) revealed the presence of 2 product ions (Figure 3.3A). Peaks at m/z 378.1 and 443.3 are assigned to the MH^+ ions of the NAYA-TEMPO adduct (eqn 3.7) and diNAYA (eqn 3.6), respectively, while the peak at m/z 222.8 matches that predicted for MH^+ of unreacted NAYA. Peaks at m/z 156, 157, and 158 due to unreacted TEMPO$^\bullet$ (*68*), which undergoes unusual ion chemistry in the ESI source (see below), were observed with high relative abundance in all spectra recorded but are omitted for clarity. When 10-fold excess TEMPO$^\bullet$ over NAYA was added to the radical-generating reaction (36nM HRP, 150μM H_2O_2, 500μM NAYA, 5mM TEMPO$^\bullet$), the NAYA-TEMPO peak (m/z 378.1) is the most abundant product ion, while diNAYA (m/z 443.3) is undetectable, and the peak containing unreacted NAYA (m/z 222.8) is weak (Figure 3.3B). When the same experiments were performed using 1:2 and 1:5 NAYA/TEMPO ratios, no diNAYA formation was detected by MS in either case (data not shown). The peak at m/z 314.1 in Figure 3.3B is assigned to a noncovalent proton-linked TEMPO$^\bullet$–hydroxylamine dimer (Figure 3.1F) since nitroxides tend not to dimerize covalently (*53*). The intensity of the dimer peak, which was not seen at <1mM

TEMPO•, is dependent on concentration, and indirectly related to capillary temperature and spray voltage (Figure 3.2), consistent with noncovalent dimer formation.

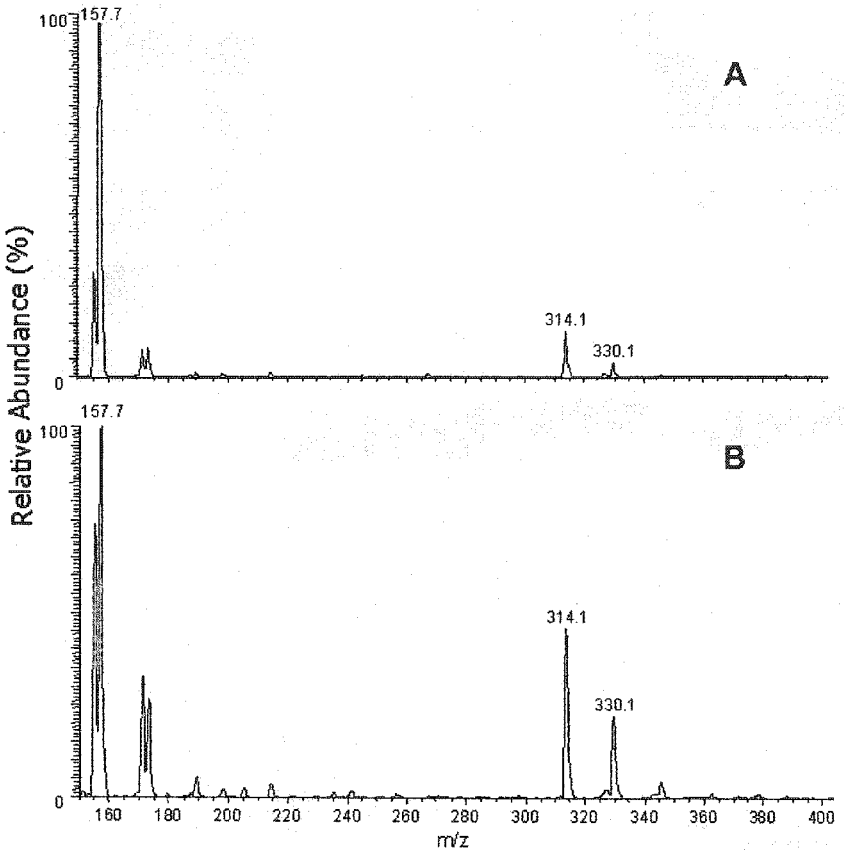

Figure 3.2. ESI mass spectrum of 500μM TEMPO• at a capillary temperature of (A) 235°C and (B) 180°C. TEMPO• was dissolved in 50% methanol/0.05% TFA, and directly infused at a rate of 3μL/min using a syringe pump into the ESI source of the mass spectrometer with a 4.0kV spray voltage. The peak at m/z 157.7 is assigned to $TEMPOH_2^+$ (see chapter 5), while the peak at m/z 314.1 is assigned to a TEMPO-$TEMPOH_2^+$ proton bound dimer.

To further characterize the efficacy of TEMPO• as a radical probe, oxidation of two other amino-acid derivatives, NAWA and NAF (Figure 3.1C and 3.1D), was examined. Free W and F also have been used as donor substrates for HRP/H_2O_2 but no reaction products were identified to date (*154*). Figure 3.4 shows the mass spectrum of the reaction products from the 1:1 NAF/TEMPO• reaction (36nM HRP, 150μM H_2O_2,

500μM NAF, 500μM TEMPO$^{\bullet}$). The low abundance of the MH^+ ions of NAF-TEMPO (m/z 363.0) and diNAF (m/z 413.0) *vs* that of unreacted NAF (m/z 207.7) clearly demonstrates that this amino-acid derivative is a poor donor substrate for HRP/H_2O_2. Nonetheless, the major product ion is NAF-TEMPO (Figure 3.4B), and this becomes the sole product detected by MS when NAF/TEMPO$^{\bullet}$ is $\leq 1:2$ (data not shown). These results mirror those found for NAYA, and reveal that scavenging of NAF$^{\bullet}$ by TEMPO$^{\bullet}$ is faster than NAF$^{\bullet}$ dimerization. Similar results were obtained in a series of NAWA experiments, and Figure 3.5 shows the mass spectra of the products from 1:1 (A) and 1:10 (B) NAWA/TEMPO$^{\bullet}$ reactions (36nM HRP, 150μM H_2O_2, 500μM NAWA, 500μM and 5mM TEMPO$^{\bullet}$).

The high efficiency of spin scavenging with TEMPO$^{\bullet}$ is recognized when adduct yields are compared to those obtained in spin-trapping experiments. For example, in a competition reaction for NAYA$^{\bullet}$ containing equimolar NAYA and TEMPO$^{\bullet}$ and 100-fold excess of the ST, DBNBS (Figure 3.1E), both NAYA-TEMPO (peak T, m/z 377.9) and NAYA-DBNBS (peak D, m/z 581.3) adducts are detected with similar intensities (Figure 3.6). $DBNBSNa^+$ and $DBNBSH^+$ ions are observed at m/z 365.9 and 343.9, respectively, as well as a number of unidentified peaks (marked with asterisks in Figure 3.6) that also are present in the ESI mass spectrum of DBNBS alone. These DBNBS-derived species cause ion suppression that significantly decreases the sensitivity of NAYA-adduct detection. A NAWA-DBNBS adduct, which may have been formed by ene addition of DBNBS to W (*131, 132*), was observed in radical-generating reactions containing 100-fold excess DBNBS (36nM HRP, 150μM H_2O_2, 500μM NAWA, 5mM

DBNBS), but no NAF-DBNBS adduct was detected in the corresponding NAF reaction (data not shown).

Since TEMPO$^{\bullet}$ catalyzes, via formation of TEMPO^{+}, oxidation of alcohols in the Anelli reaction (*155-157*), we investigated the possibility of "inverted spin scavenging". This would involve formation of the NAYA-TEMPO adduct from direct reaction between NAYA and TEMPO^{+}, generated by HRP/H_2O_2 oxidation of TEMPO$^{\bullet}$, rather than via spin scavenging. Specifically, 5mM TEMPO$^{\bullet}$ was oxidized by HOCl, and the preformed TEMPO^{+} incubated with 500μM NAYA for 10min. The ESI mass spectrum of the products revealed no NAYA-TEMPO adduct formation, indicating that inverted spin scavenging does not occur under the present experimental conditions (500μM NaPi, pH 7.4).

3.4.2 TEMPO$^{\bullet}$ adducts formed in H_2O_2-oxidized Mb

The reaction of Mb with H_2O_2 produces both an Fe^{IV}=O heme and a globin-centered radical (eqn 3.3) (*47*). The MALDI-ToF mass fingerprint of the tryptic digest of untreated Mb contained 14 peaks, 12 of which were identified as Mb peptides (including two isobaric peptides, Table 3.1) by searching the NCBI database (www.ncbi.nlm.nih.gov) using the Mascot search engine (Matrix Science) (*158*), and provided 97% sequence coverage. The presence of 5mM TEMPO$^{\bullet}$ during the 10min reaction of 500μM Mb and 5mM H_2O_2 at pH 5.0 or 7.4, followed by quenching with catalase, tryptic digestion and MALDI-ToF analysis of the digest, resulted in the identification of TEMPO-labeled tryptic peptide T_{16} which contains Y103 (Table 3.1).

No labeled peptides were observed when the Mb/H_2O_2/TEMPO$^{\bullet}$ reaction was repeated at pH 3.0 and 10.0 (data not shown).

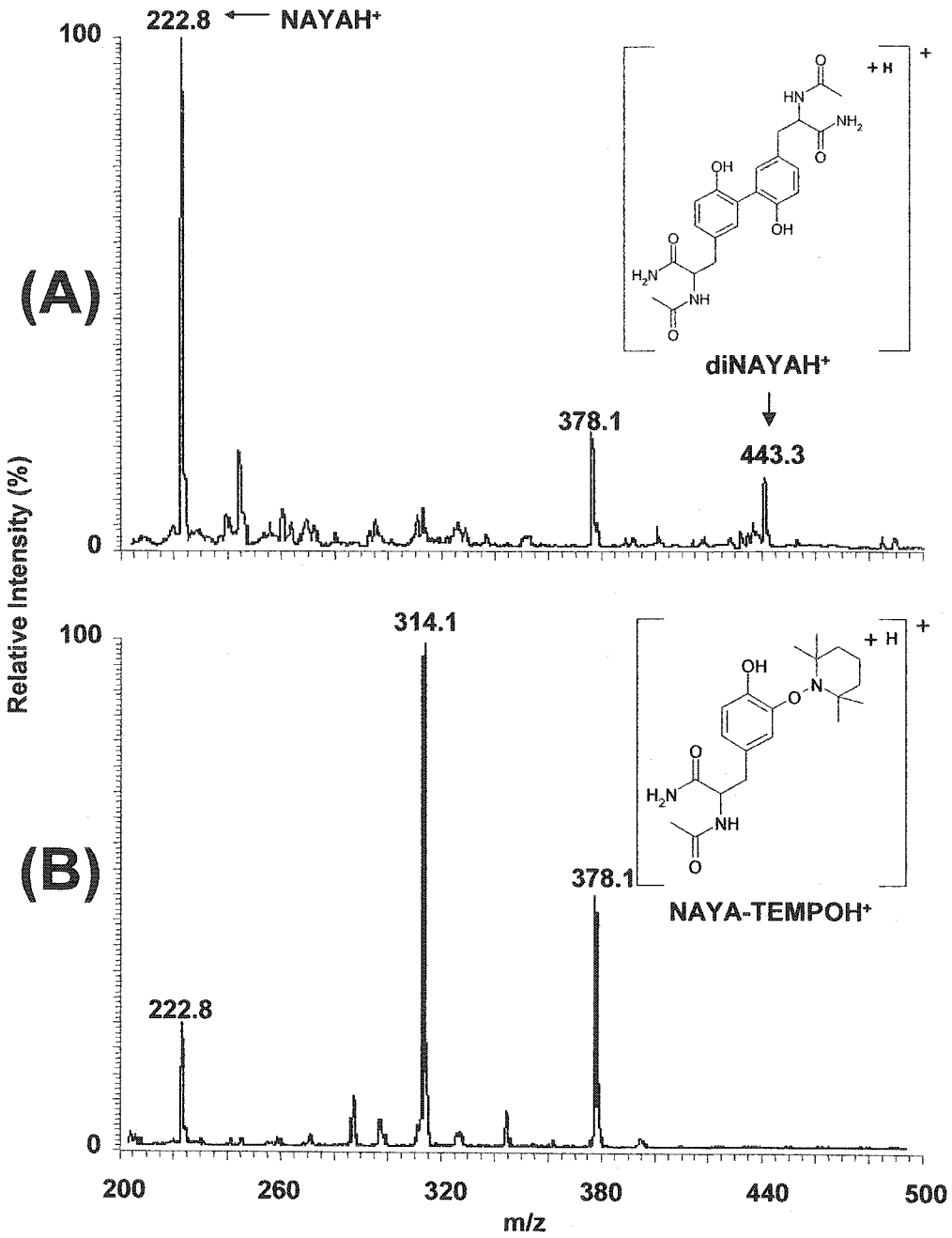

Figure 3.3. Product ESI mass spectrum of the reaction of 36nM HRP, 150μM H_2O_2, 500μM NAYA with (A) 500μM and (B) 5mM TEMPO$^{\bullet}$. The reaction was carried out for 5min in 500μM NaPi (pH 7.4) with 100μM DTPA, diluted 10-fold in 50% acetonitrile/0.05% TFA, and directly infused at a rate of 3μL/min using a syringe pump into the ESI source of the mass spectrometer. ESI conditions: 4.0kV spray voltage, 180°C capillary temperature. Insets show proposed structures of the radical combination products at m/z 443.3 and 378.1 (*58*).

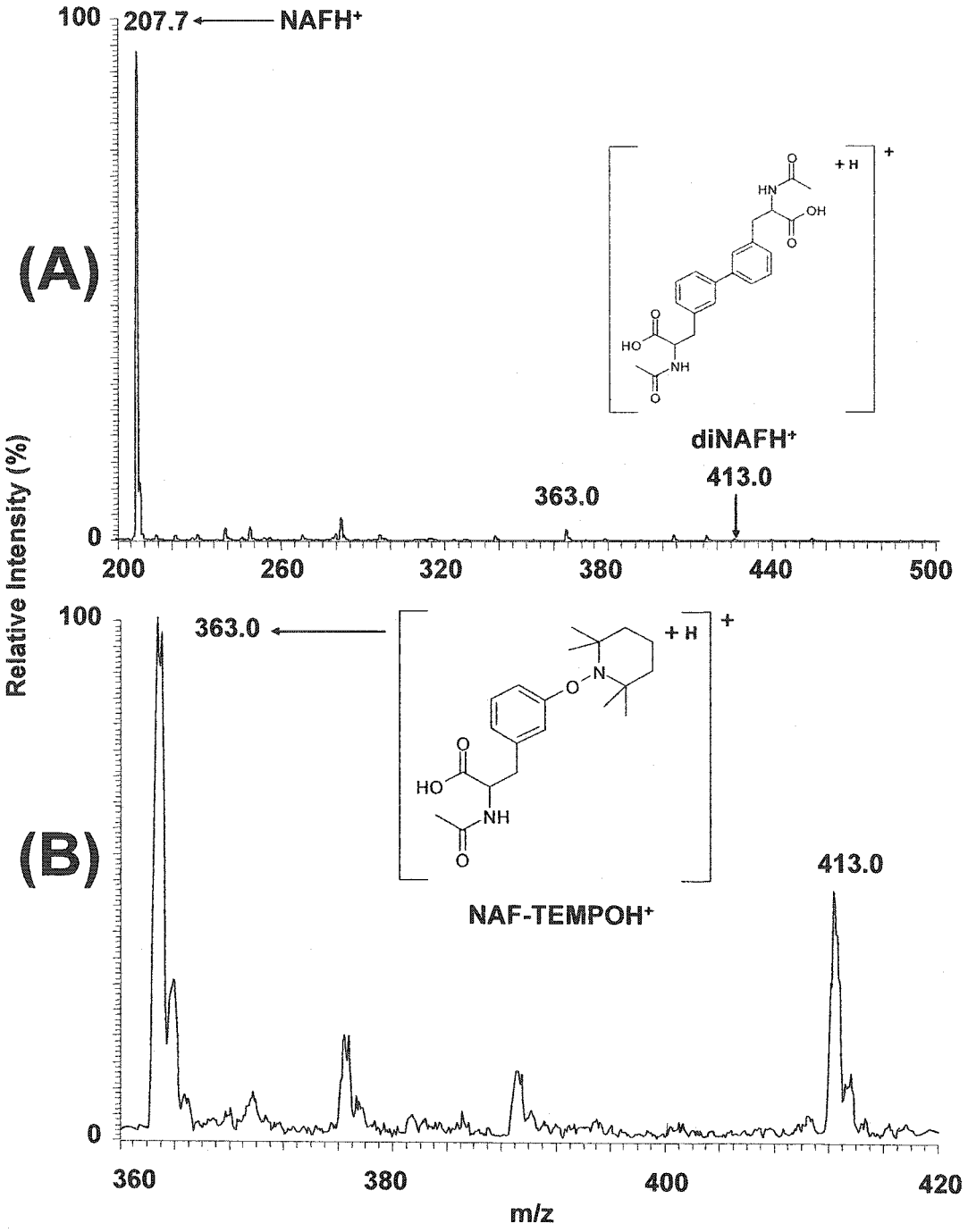

Figure 3.4. Product ESI mass spectrum of the reaction of 36nM HRP, 150μM H_2O_2, 500μM NAF with 500μM TEMPO• (A) between m/z 200 and 500 and (B) between m/z 360 and 420. The spectrum in B was expanded 50-fold. Insets show proposed structures of the radical-combination products at m/z 413.0 and 363.0 (*159*). The experimental conditions are given in the legend to Figure 3.3.

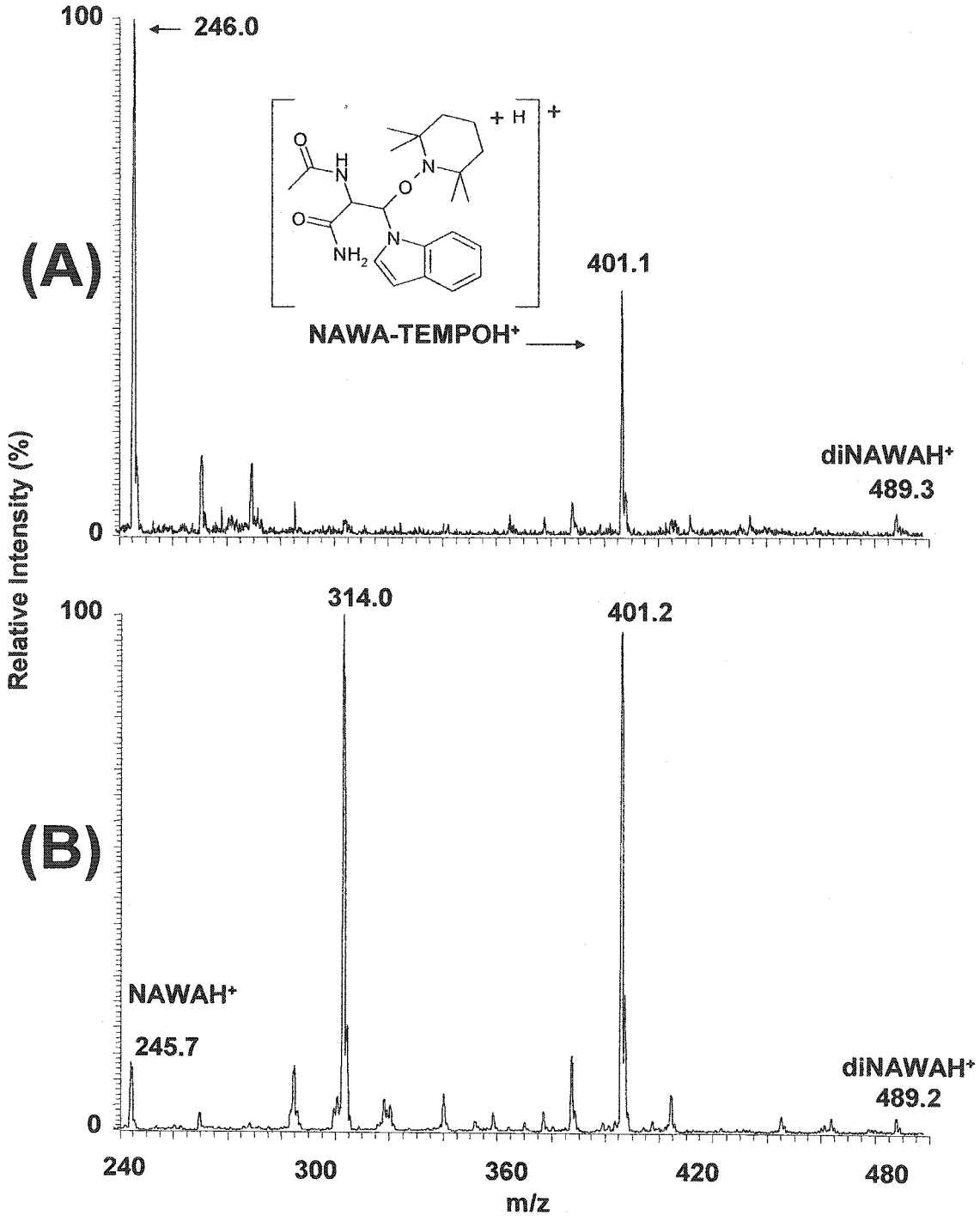

Figure 3.5. **Product ESI mass spectrum of the reaction of 36nM HRP, 150μM H_2O_2, 500μM NAWA with (A) 500μM TEMPO• and (B) 5mM TEMPO•.** The inset shows the proposed structure of the radical-combination product at m/z 401.1 (*159*). The experimental conditions are given in the legend to Figure 3.3.

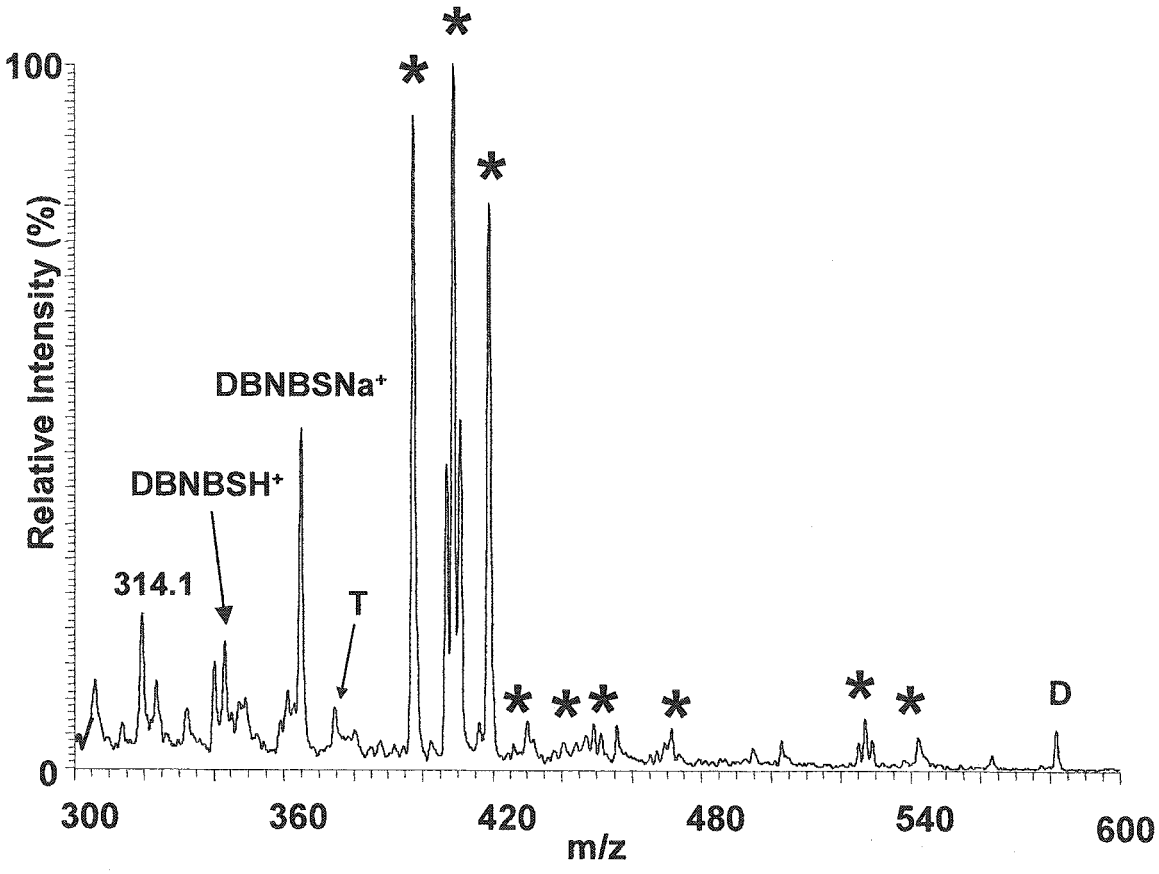

Figure 3.6. Product ESI mass spectrum of the reaction of 36nM HRP, 150μM H_2O_2, 500μM NAYA with 50mM DBNBS and 500μM TEMPO•. The NAYA-TEMPOH$^+$ (peak T, m/z 377.9) and NAYA-DBNBSH$^+$ (peak D, m/z 581.3) adducts are labeled, as are the DBNBSH$^+$ and DBNBSNa$^+$ ions at m/z 343.9 and 365.9, respectively. Unidentified peaks present in the spectrum of DBNBS only are labeled with asterisks (*). The experimental conditions are given in the legend to Figure 3.3.

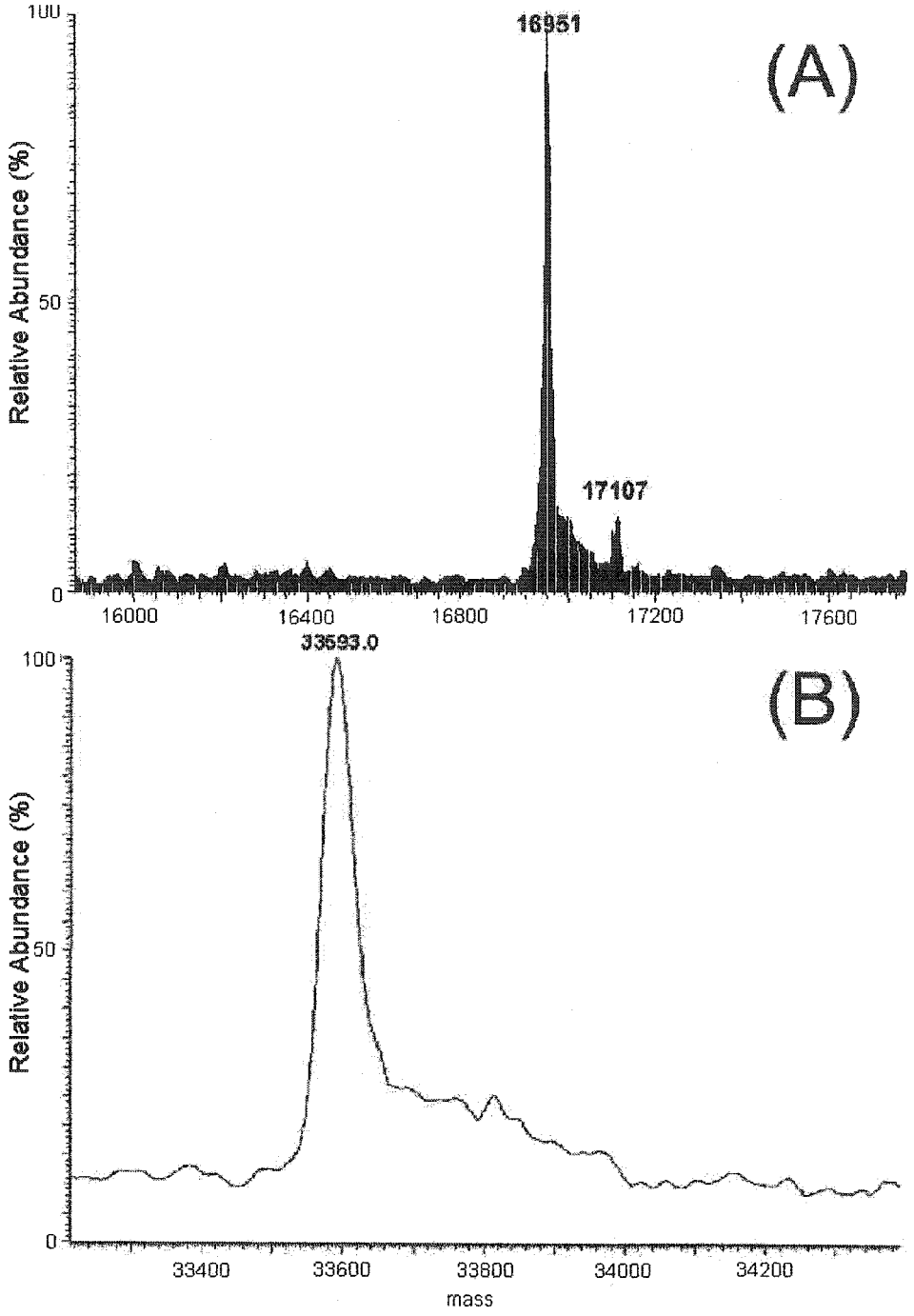

Figure 3.7. Deconvolved ESI mass spectra of the intact proteins from the 10min reactions of 500μM heme protein with 5mM H_2O_2 in the presence of 5mM TEMPO in 500μM NaPi containing 100μM DTPA. (A) Mb from a reaction carried out at pH 5.0; (B) CCP from a reaction carried out at pH 7.4. The HPLC-purified protein products were collected, lyophilized, resuspended in 50% acetonitrile/0.05% TFA to a concentration of ~1μg/mL, and directly infused at a rate of 3μL/min using a syringe pump into the ESI source of the mass spectrometer. The ESI conditions are given in the legend to Figure 3.3.

Table 3.1. Tryptic peptides from the MALDI-ToF mass fingerprints of myoglobin[a]

Peptide[b]	Residues[c]	M_r(obs)[d]	M_r(calc)[e]	Sequence[f,g]
T_{18}	134 – 139	748.2	747.9	ALELFR
T_{6+7}	48 – 56	1084.4	1086.3	HLKTEAEMK
T_{5+6+7}	46 – 56	1362.2	1361.6	FKHLKTEAEMK
T_{8+9}	63 – 77	1507.6	1506.8[h]	KHGTVVLTALGGILK
T_{9+10}	64 – 78	1507.6	1506.8[h]	HGTVVLTALGGILKK
T_2	17 – 31	1607.4	1606.8	VEADIAGHGQEVLIR
$T_{18+19+20}$	134 – 147	1649.6	1651.9	ALELFRNDIAAKYK
T_{16}	103 – 118	1885.9	1885.2	YLEFISDAIIHVLHSK
T_{16}+TEMPO		**2041.3**	**2040.4**	
T_{3+4+5}	32 – 47	1938.1	1937.2	LFTGHPETLEKFDKFK
$T_{12+13+14}$	79 – 98	2248.8	2247.5	KGHHEAELKPLAQSHATKHK
$T_{18+19+20+21}$	134 – 153	2283.6	2283.6	ALELFRNDIAAKYKELGFQG
T_{1+2}	1 – 31	3405.4	3404.8	GLSDGEWQQVLNVWGKVEADIAGHGQEVLIR
$T_{16+17+18}$	103 – 139	4100.3	4099.7	YLEFISDAIIHVLHSKHPGDFGADAQGAMTKALELFR

[a]Tryptic peptides were prepared and analyzed as described in the Experimental Section.

[b]Peptides are assigned T_x in order of the expected site of cleavage (C-terminal to K and R residues) and listed based on increasing mass. Peptides found to be TEMPO-labeled at pH 7.4 are presented in bold font and the mass of the labeled species are given in the T_{16} +TEMPO row.

[c]Position of peptide in the protein's amino-acid sequence

[d]Observed average mass (M_r) of the peptides in Da. The mass accuracy of the MALDI-ToF mass spectrometer is 0.14% using human keratin and trypsin autodigestion peaks as internal standards.

[e]Calculated average M_r based on peptide sequence, and a mass increase of 155.2 per TEMPO label.

[f]Amino-acid sequence presented in one-letter code; peptides were identified by searching the NCBI database (www.ncbi.nlm.nih.gov) using the Mascot search engine (*158*).

[g]Y and W residues, which are considered possible sites of TEMPO-labeling, are underlined.

[h]These peptides are isobaric given the mass accuracy of the instrument (0.14%).

Interestingly, no evidence for TEMPO-adducts of undigested, intact Mb was obtained by either MALDI-ToF or LC/ESI-MS analysis at pH 7.4, although a low-intensity TEMPO-adduct peak was observed at 17107 Da (10%) in the deconvolved ESI mass spectra of the protein from the pH 5.0 reaction (Figure 3.7A). In contrast, the Mb-DBNBS spin adduct (17293Da) was found (*19*) to dominate the ESI mass spectrum when DBNBS was added as a ST. The Mb-TEMPO adduct was observed only under very soft ionization conditions, and increasing the spray voltage and capillary temperature revealed that cleavage of the Mb-TEMPO bond was quite facile. However, differences in sample preparation such as lyophilization of the heme-free protein at 25°C *vs* direct infusion of the reaction mixture, or changing the amount of TFA added did not affect the relative intensity of the Mb-TEMPO adduct observed in the mass spectrum. These results suggest that the Mb-TEMPO bond is less stable than the T_{16}-TEMPO bond due to steric hindrance in the intact protein. The observation of an Mb-TEMPO adduct at pH 5.0 in the ESI mass spectrum (Figure 3.7A) is consistent with this hypothesis since opening of the heme pocket occurs in Mb at low pH (*18, 160*).

3.4.3 TEMPO• adducts formed in H_2O_2-oxidized CCP

The ability of CCP to turnover 20 equivalents of H_2O_2 using endogenous donors (*17*) makes it an ideal protein to use in studies of TEMPO-labeling of protein-based radicals. MALDI-ToF analysis of the tryptic digests of untreated CCP revealed 29 peaks, 21 of which were identified as CCP peptides (including three pairs of isobaric peptides, Table 3.2) by searching the NCBI database with Mascot (*158*), and provided 88% sequence coverage (Figure 3.8). The presence of 5mM TEMPO• during a 10min reaction

of 500μM CCP with 5mM H_2O_2 resulted in the detection by MALDI-ToF-MS of eight TEMPO-labeled tryptic peptides (including singly and doubly labeled $T_{27+28+29+30}$, Table 3.2), but no labeled peptides in the absence of H_2O_2. Figure 3.9 compares the MALDI-ToF mass spectra of tryptic peptides in the m/z range 2500-2900 from the control and H_2O_2 reactions. The mass increases of MH^+ ions of peptides $T_{27+28+29+30}$ (m/z 2585.8, Δm 151.8 Da) and T_{7+8} (m/z 2680.8, Δm 153.7 Da) reveals that these peptides are singly TEMPO-labeled since an increase of 155.2Da is expected per label. Peaks attributed to sodium adducts (+23Da), which are commonly observed in MALDI-ToF spectra (*161*), are denoted with an asterisk in Figure 3.9.

Three of the singly TEMPO-labeled peptides contain a sole W or Y residue (W126 in $T_{14+15+16}$, Y153 in T_{18+19}, and Y251 in $T_{28+29+30}$), which are the likely sites of radical scavenging. The other peptides contain multiple W or Y residues (Y36, Y39 and Y42 in T_6; Y244 and Y251 in $T_{27+28+29+30}$ and $T_{27+28+29+30+31}$; Y187, W191, Y203 and W211 in T_{23}). In doubly TEMPO-labeled $T_{27+28+29+30}$ both Y244 and Y251 are assumed to be labeled, as is Y251 in singly TEMPO-labeled $T_{28+29+30}$. The other doubly TEMPO-labeled peptide, T_{23}, contains W191, the site of radical formation in compound I (*27*), in addition to Y187, Y203 and W211. Sequencing of the labeled peptides is currently underway to unambiguously determine the oxidized residues. The errors in M_r(obs) for some of the TEMPO-labeled CCP peptides (Table 3.2) fall outside the range of mass accuracy (±0.14%) obtained using keratin and trypsin autodigestion peaks as internal standards (Figure 3.8).

Although extensive TEMPO-labeling of CCP peptides was detected by MALDI-ToF analysis, as with Mb, labeling of the undigested protein was not detected by MS. For

example, when 500μM CCP was reacted with 5mM H_2O_2/5mM TEMPO$^{\bullet}$ for 10min at pHs 3.0, 5.0, 7.4 or 10.0, and analyzed by LC/ESI-MS or MALDI-ToF-MS, only native protein peaks (M_r ~33593Da) but no CCP-(TEMPO)$_n$ peaks were observed in the mass spectra (Figure 3.7B).

3.5 Discussion

3.5.1 Scavenging of radicals generated in the aromatic amino-acid derivatives

TEMPO$^{\bullet}$ is a π-radical molecule where the unpaired electron occupies a π*-orbital between the oxygen and nitrogen atoms. The result of this electron delocalization is a relatively stable structure that provides a unique means by which to scavenge radicals. The effective N-O bond order is 1.5, since there are also filled σ- and π-bonding orbitals between these atoms (*53*).

The generation of dityrosine in proteins *in vivo* is a normal physiological process in specialized cells such as those involved in the biosynthesis of thyroxin and melanin (*162*). Dityrosine is also a marker for assessing oxidative damage or exposure of proteins to harmful environmental agents such as UV radiation (*163*) *in vitro* and *in vivo* (*153, 164, 165*). HRPC (Fe^{III},P) catalyzes the oxidation by H_2O_2 of free Y ($E^{o'}$ = 0.93V) (*166*) via the mechanism shown in eqns 3.3, 3.8 and 3.9 with k_I and k_{II} values of 5.0 x 10^4 and 1.1 x 10^3 $M^{-1}s^{-1}$, respectively (*167, 168*):

$$Fe^{III},P + H_2O_2 \rightleftharpoons Fe^{IV}{=}O,P^{\bullet+} + H_2O \qquad (3.3)$$

$$Fe^{IV}{=}O,P^{\bullet+} + RH \overset{k_I}{\rightleftharpoons} Fe^{IV}{=}O,P + R^{\bullet} + H^{+} \qquad (3.8)$$

$$Fe^{IV}{=}O,P + RH + H^{+} \overset{k_{II}}{\rightleftharpoons} Fe^{III},P + R^{\bullet} + H_2O \qquad (3.9)$$

Cytochrome c Peroxidase (CCP)

1 MKTLVHVASV EKGRSYEDFQ KVYNAIALKL REDDEYDNYI GYGPVLVRLA

51 WHISGTWDKH DNTGGSYGGT YRFKKEFNDP SNAGLQNGFK FLEPIHKEFP

101 WISSGDLFSL GGVTAVQEMQ GPKIPWRCGR VDTPEDTTPD NGRLPDMDKD

151 AGYVRTFFQR LNMNDREVVA LMGAHALGKT HLKNSGYEGP WGAANNVFTN

201 EFYLNLLNED WKLEKNDANN EQWDSKSGYM MLPTDYSLIQ DPKYLSIVKE

251 YANDQDKFFK DFSKAFEKLL ENGITFPKDA PSPFIFKTLE EQGL

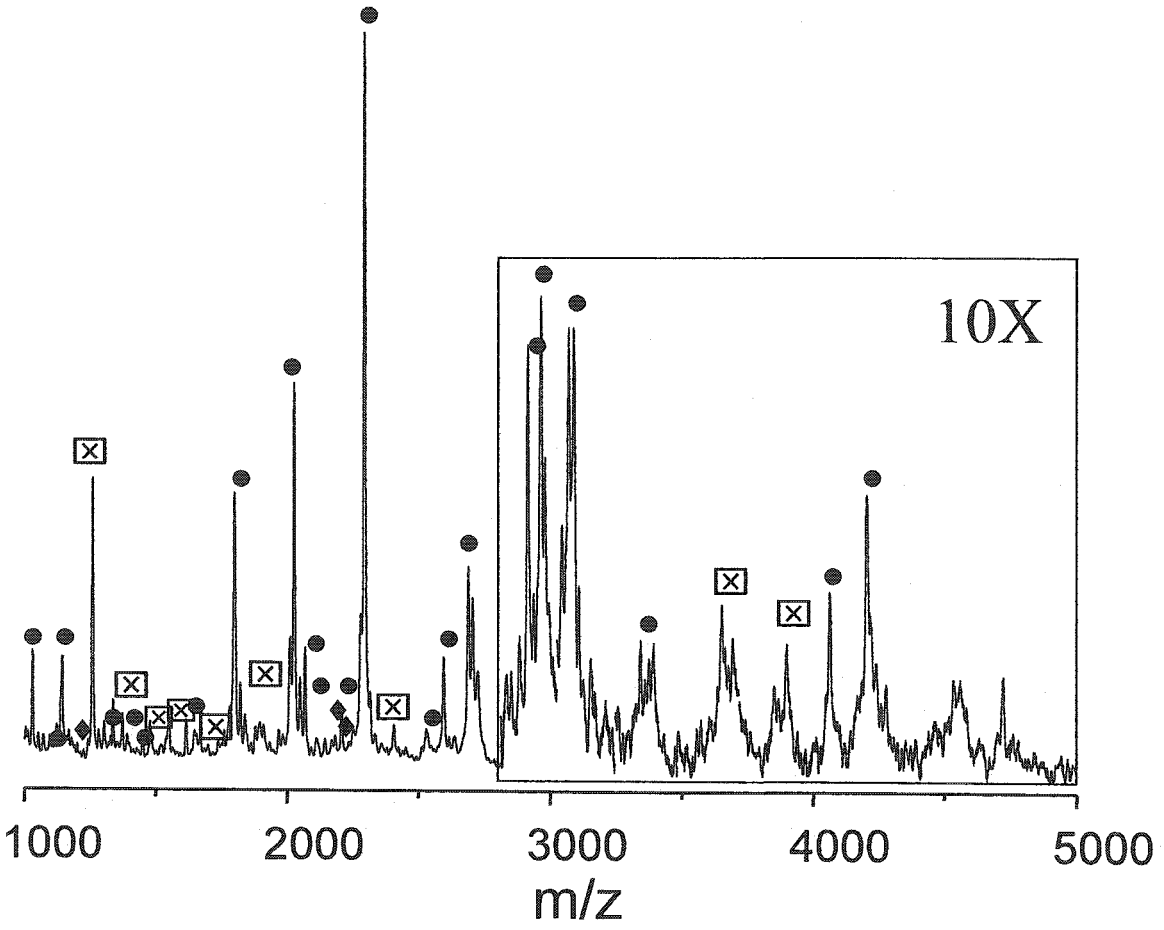

Figure 3.8. **MALDI-ToF mass fingerprint of the tryptic peptides of untreated CCP.** (●) Identified CCP tryptic peptides, which are listed in Table 3.2; (♦) trypsin autodigestion peptides, and (☒) human keratin peaks. The CCP sequence coverage was 88%, and the missing residues are underlined (insert). Tryptic peptides were prepared and analyzed as described in the Experimental Section. The MALDI-ToF mass spectrometer was operated in the linear, positive-ion, and delay modes with an accelerating voltage of +15 kV. Baseline correction and noise removal were performed using the default parameters (peak width 32, flexibility 0.5, degree 0.1, resolution, R ~500) of the Data Explorer software on the instrument.

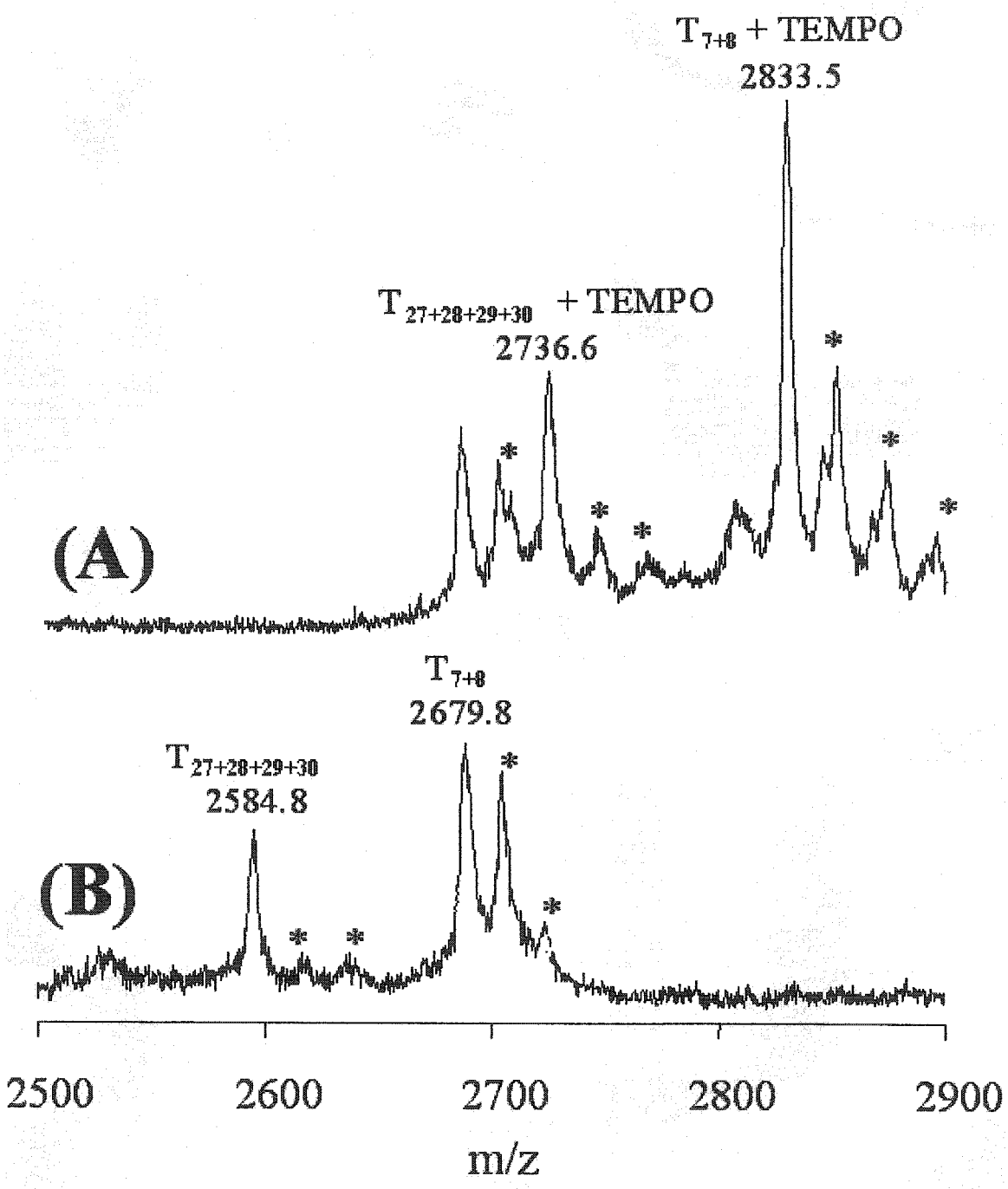

Figure 3.9. MALDI-ToF mass fingerprint in the region of tryptic peptides $T_{27+28+29+30}$ and T_{7+8} of (A) untreated CCP and (B) CCP oxidized by H_2O_2 in the presence of TEMPO$^{\bullet}$. Tryptic peptides were prepared and analyzed as described in the Experimental Section and MS conditions are given in the legend to Figure 3.8. Na^+ adducts (+23Da) are labeled with an asterisk (*). The doubly TEMPO-labeled MH^+ ion of $T_{27+28+29+30}$ is not observed in this particular spectrum.

Table 3.2. Tryptic peptides from the MALDI-ToF mass fingerprints of cytochrome c peroxidase[a]

Peptide[b]	Residues[c]	M_r(obs)[d]	M_r(calc)[e]	Sequence[g, h]
T_{33}	279 - 287	1022.4	1021.2	DAPSPFIFK
T_1	3 - 12	1083.5	1082.3	TLVHVASVEK
T_{32}	269 - 278	1132.3	1131.3	LLENGITFPK
T_{21}	167 - 179	1296.0	1295.6	EVVALMGAHALGK
T_{18+19}	150 - 160	1360.4	1359.5	DAGYVRTFFQR
T_{18+19}+TEMPO		**1519.2**	**1514.7**	
T_{31+32}	265 - 278	1607.3	1606.9	AFEKLLENGITFPK
T_{3+4}	15 - 29	1789.1	1789.0	SYEDFQKVYNAIALK
$T_{28+29+30}$	250 - 264	1880.1	1882.0	EYANDQDKFFKDFSK
$T_{28+29+30}$+TEMPO		**2037.2**	**2037.2**	
T_6	32 - 48	2015.9	2017.1	EDDEYDNYIGYGPVLVR
T_6+TEMPO		**2169.5**	**2172.3**	
T_{3+4+5}	15 - 31	2057.2	2058.4[h]	SYEDFQKVYNAIALKLR
T_{17+18}	131-149	2057.2	2056.1[h]	VDTPEDTTPDNGRLPDADK
T_{32+33}	269 - 287	2133.4	2134.5	LLENGITFPKDAPSPFIFK
T_{5+6}	30 - 48	2284.8	2286.5[h]	LREDDEYDNYIGYGPVLVR
$T_{14+15+16}$	124 - 143	2284.8	2285.5[h]	IPWRCGRVDTPEDTTPDNGR
$T_{14+15+16}$+TEMPO		**2440.7**	**2440.7**	
$T_{20+21+22}$	161 - 183	2518.3	2519.0	LNMNDREVVALMGAHALGKTHLK
$T_{27+28+29+30}$	244 - 264	2584.8	2585.9	YLSIVKEYANDQDKFFKDFSK
$T_{27+28+29+30}$+TEMPO		**2736.6**	**2741.1**	
$T_{27+28+29+30}$+2TEMPO		**2895.1**	**2896.3**	
T_{7+8}	49 - 72	2679.8	2679.9	LAWHISGTWDKHDNTGGSYGGTYR
T_{7+8}+TEMPO		**2833.5**	**2835.1**	
$T_{32+33+34}$	269 - 294	2907.2	2905.3[h]	LLENGITFPKDAPSPFIFKTLEEQGL-END
$T_{9+10+11+12}$	73 - 97	2907.2	2906.3[h]	FKKEFNDPSNAGLQNGFKFLEPIHK
T_{7+8+9}	49 - 74	2954.6	2955.2	LAWHISGTWDKHDNTGGSYGGTYRFK
$T_{27+28+29+30+31}$	244 - 268	3063.3	3061.4	YLSIVKEYANDQDKFFKDFSKAFEK
$T_{27+28+29+30+31}$+TEMPO		**3222.1**	**3216.6**	
T_{23}	184 - 212	3362.6	3363.6	NSGYEGPWGAANNVFTNEFYLNLLNEDWK
T_{23}+2TEMPO		**3674.7**	**3675.0**	
$T_{3+4+5+6}$	15 - 48	4053.3	4049.6	SYEDFQKVYNAIALKLREDDEYDNYIGYGPVLVR
$T_{12+13+14}$	91 - 127	4201.7	4198.9	FLEPIHKEFPWISSGDLFSLGGVTAVQEMQGPKIPWR

[a-h] See Footnotes to Table 3.1.

The resultant tyrosyl radical ($R^{\bullet}$) rapidly dimerizes to dityrosine (*163*), which provides a common method of dityrosine synthesis *in vitro* (*169*). Mass spectral analysis of the HRP/H_2O_2/NAYA(500μM)/TEMPO$^{\bullet}$(500μM) products revealed the presence of a NAYA-TEMPO peak and a less intense diNAYA peak (Figure 3.3A). These results were encouraging since they demonstrated that the NAYA-TEMPO adduct is stable under MS conditions, and that NAYA-TEMPO formation (eqn 3.7) competes with NAYA$^{\bullet}$ dimerization (eqn 3.6) in solutions containing equimolar NAYA and TEMPO$^{\bullet}$. Furthermore, the data in Figure 3.6 suggest that spin scavenging is much more efficient than spin trapping, and the large excess of ST required to trap the NAYA$^{\bullet}$ radical complicates the mass spectrum.

Dityrosine formation and the reaction of TEMPO$^{\bullet}$ with carbon-centered radicals both have rate constants in the range of 10^9 $M^{-1}s^{-1}$ (*51, 153, 170*). Thus, dimerization should not compete with scavenging by 10-fold excess TEMPO$^{\bullet}$ and no diNAYA peak was detected under such conditions (Figure 3.3B). Similar results were observed with NAWA ($E^{o'}$ ~1.1) and NAF ($E^{o'}$ ~1.4) (*16*) as substrates (Figures 3.3 and 3.4), demonstrating the ability of TEMPO$^{\bullet}$ to scavenge these less-easily-formed amino-acid radicals, and to compete with their dimerization. Interestingly, the homodimerization of both W and F has been shown to stabilize proteins against proteolytic cleavage *in vitro* (*171, 172*), and W dimers stabilize antiparallel β-structures in model peptides (*159*). A soluble fluorescent compound isolated from certain scorpions (*173*) was recently shown to be a ditryptophan derivative, revealing the biological relevance of W dimerization.

3.5.2 Protein-based radical scavenging

Much work has focused on the location of polypeptide-based radicals in H_2O_2-oxidized Mb (*18, 19, 47, 143-145*). TEMPO labeling of T_{16} was detected here by MALDI-ToF-MS (Table 3.1). This is attributed to scavenging of a radical localized on Y103 at pH 5.0 and 7.4 (Table 3.1), since we and several other groups have confirmed Y103-labeling by ST/LC/MS, site-directed mutagenesis and protein cross-linking experiments (*18, 19, 47, 143-145*).

With seven Ws and fourteen Ys, CCP contains an unusually high number of redox-active amino-acid residues for a 294-residue protein. These numbers are especially notable when compared with other peroxidases of similar size, such as HRP (one W and five Y) (*31*), ascorbate peroxidase (two W and seven Y) (*32*), lignin peroxidase (three W and no Y) (*33*) or manganese peroxidase (one W and no Y) (*34*). For many years, CCP was one of a few enzymes known to utilize a W (W191) radical during catalytic turnover (*27-30*). A function of CCP is believed to be the removal of H_2O_2 using electrons obtained (via ferrocytochrome c) from the electron-transport chain (*22, 23, 38, 174*). It was recently reported that CCP is also involved in conveying an oxidative-stress signal to the transcription factor, Pos9p (or Skn7p), in *Saccharomyces cerevisiae* (*42*). Since the W191F mutant, which has no ferrocytochrome c-oxidizing activity, also is able to activate Pos9p-dependent transcription (*42*), the signaling function of CCP is independent of electron-flux in the electron-transport chain. Therefore, identification of the sites of heme-mediated H_2O_2-induced radical formation in CCP (eqns 3.4 and 3.5) is of interest, since such radicals are likely involved in oxidative-stress signaling in yeast mitochondria (*42, 43*).

Previously we reported that the presence of the ST, MNP (11mM), during the reaction between 20μM CCP and 200μM H_2O_2 resulted in the detection by LC/ESI-MS of triply MNP-labeled CCP. Peptide mass mapping and sequencing by CID of the MNP-labeled peptides revealed the sites of adduct formation to be Y236, Y153, and peptide T_6 containing Y36, Y39 and Y42 (Figure 3.11) (*50*). Similar results were obtained by Zhang *et al.* (*133*) who found MNP adducts on Y39 and Y153. Although only a 10-fold molar excess of TEMPO$^{\bullet}$ over CCP was used here *vs* the 55- or 90-fold molar excess of MNP used in previous studies (*50, 133*), nine TEMPO-labeled peptides were found by MALDI-ToF-MS analysis of the CCP tryptic peptides (Table 3.2). These results highlight the much greater efficiency of spin scavenging compared to spin trapping as anticipated from the NAYA results (Figure 3.6).

Interestingly, Pfister *et al.* (*175*) found that sequentially mutating W191, W51, Y187, Y229, Y236, Y36, Y39 and Y42 to F residues resulted in higher stability of compound I, revealing the importance of these residues as endogenous donors. Such results reinforce the importance of the role played by Y and W residues in CCP compound I stability and possibly also in oxidative-stress signaling (*175*). With the exception of T_{26} (residues 227-243 including Y229 and Y236), which was not detected (Figure 3.8, inset), TEMPO-labeled peptides containing the residues altered were found here in the mass fingerprint (Table 3.2), as well as seven additional peptides with W or Y residues that were not changed by Pfister *et al.* (*175*) Intramolecular electron transfer to the CCP heme most likely involves radical hopping, forming transients until a radical is trapped in a relatively stable chemical environment or reaches the protein surface. Work

is underway in our lab to determine the sites of radical formation when CCP and several of its W and Y mutants are reacted with 1-10 molar equivalents of H_2O_2.

3.5.3 Radical scavenging vs electron donation by TEMPO•

In our previous ST/LC/MS studies on protein-based radicals, the STs used exhibited reduction potentials (E^o ~2 V) (*59*) more positive than those of the Fe^{IV}=O centers ($E^{o'}$ <1.2 V) (*18, 19, 57*) generated on reaction of heme proteins with H_2O_2 (eqn 3.3). In contrast, oxidation of TEMPO• to the nitrosium ion, $TEMPO^+$ (E^o ~ 0.64 V) (*156*), by HRP/H_2O_2 is thermodynamically favorable. To investigate if this occurs, the Soret band of 1μM HRP was monitored following addition of 1mM H_2O_2 with and without 2.5mM TEMPO•. H_2O_2 consumption in the absence of TEMPO• gave rise to a time-dependent Soret shift from 403 to 370nm, indicative of heme destruction and HRP inactivation (*11, 91, 176*), while in the presence of TEMPO•, the Soret band remained unaltered and all the H_2O_2 was consumed (Figure 3.10). The observation of a more abundant $TEMPO^+$ ion in the product mass spectrum of 36nM HRP, 150μM H_2O_2 and 500μM TEMPO• in the absence *vs* presence of NAYA confirms that TEMPO• acts as a donor substrate to HRP.

Heme destruction also was observed during 1μM HRP turnover in a solution of 1mM H_2O_2 and 2.5mM NAYA (data not shown). Although phenolic compounds are excellent donor substrates for HRP (*23*), studies have revealed that dityrosine is a competitive inhibitor of Y oxidation by HRP/H_2O_2 (*177*). Thus, diNAYA binding to the enzyme likely prevents access of NAYA to the HRP heme, which is then destroyed by reaction with excess H_2O_2. Heme destruction is eliminated when TEMPO• is present

because it acts as a NAYA$^{\bullet}$ scavenger, thereby preventing diNAYA product inhibition. Nonetheless, NAYA is the preferred substrate as evidenced by the large amount of NAYA-TEMPO detected in the mass spectra (Figures 3.2 and 3.4) presumably because HRP has a well-defined binding pocket for aromatic donors (*21*). Electron donation by TEMPO$^{\bullet}$ is not expected to be kinetically competitive with rapid radical scavenging since the buried hemes in peroxidases are reduced with rate constants of $< 10^7 M^{-1}s^{-1}$ (*178*).

In positive-ion mode, ESI sources typically produce protonated molecular ions (MH^+) (*179*). The ESI mass spectra of solutions containing only TEMPO$^{\bullet}$ exhibit peaks at m/z 156, 157 and 158 that are assigned to $TEMPO^+$, $TEMPOH^{\bullet+}$ and $TEMPOH_2^+$ ions, respectively. The relative abundance of the three species depends on the experimental conditions, and a systematic analysis of this unusual ion chemistry is discussed in Chapter 5 of this thesis.

3.5.4 Stability of the R-TEMPO bond

Evidence of TEMPO-labeling was observed at pH 5.0 (but not at pHs 3.0, 7.4 and 10.0) in the deconvolved ESI mass spectra of intact Mb (Figure 3.7A). The Mb-TEMPO adduct disappeared from the mass spectrum when the capillary temperature and spray voltage were increased. Similar results were obtained whether the Mb/H_2O_2/TEMPO$^{\bullet}$ reaction products were directly infused into the ESI source or HPLC-purified and lyophilized prior to infusion. No TEMPO-labeling of intact Mb was observed in the MALDI-ToF spectra. These results suggest that the T_{16}-TEMPO bond is weaker when the protein is in its folded conformation, and that the label is lost under the ionization conditions used to record the ESI and MALDI-ToF spectra.

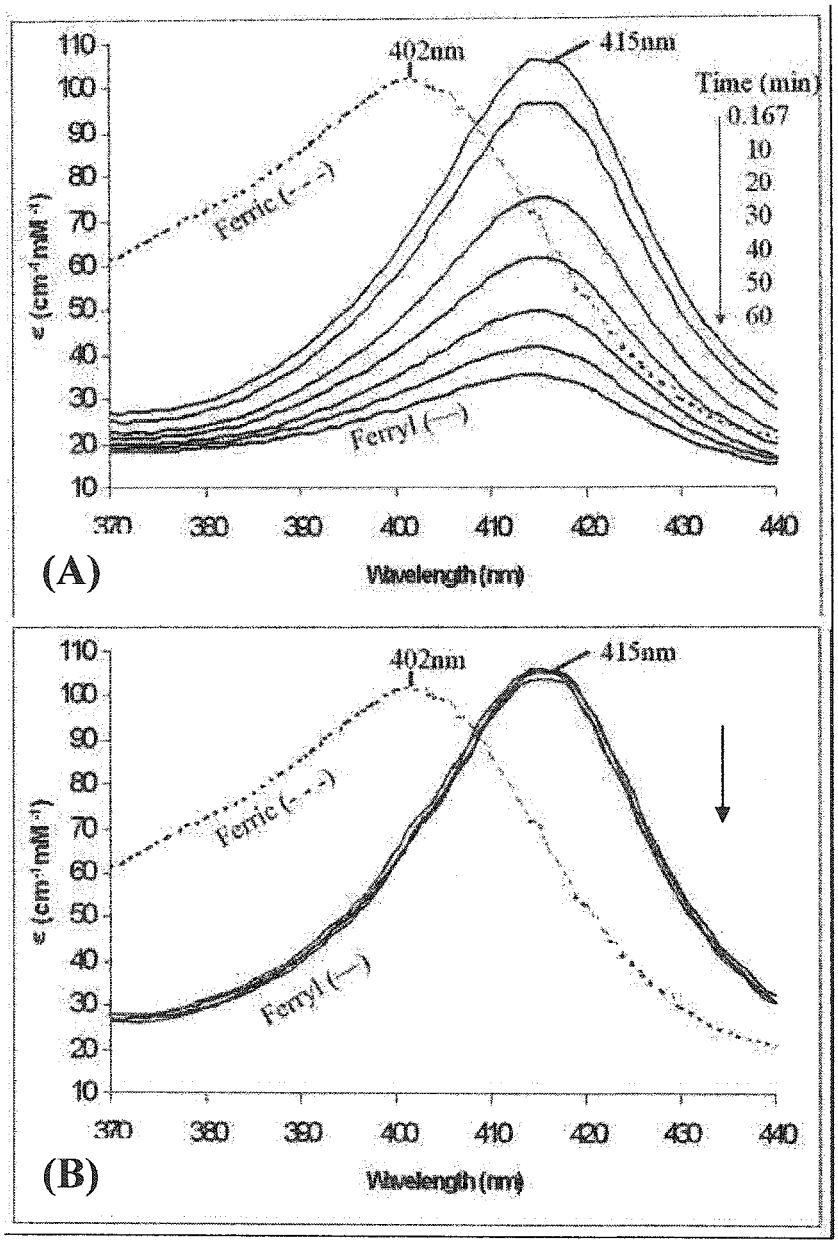

Figure 3.10.. The Soret-absorption spectra vs time of 1.8μM HRPC, 1mM H_2O_2, 2.5mM NAYA (A) in the presence of 2.5mM TEMPO$^{\bullet}$ and (B) without TEMPO$^{\bullet}$. The spectrophotometer was blanked with all reagents except HRPC. The cuvette pathlength was 1cm. Scans were taken every 10min at a scan rate of 600nm/min in 500μM NaPi buffer with 100μM EDTA at 25°C.

However, when Mb was subjected to tryptic digestion before MS analysis, TEMPO-labeled T_{16} was observed. Similar results were obtained for CCP, where no TEMPO-labeling of the intact protein was detected (Figure 3.7B), but nine labeled peptides were discovered when the enzyme was proteolytically cleaved prior to MS analysis (Table 3.2). Since the NAYA-, NAWA- and NAF-TEMPO adducts are stable in both the ESI and MALDI sources, steric constraints must destabilize the TEMPO label in a folded or partially folded protein. Given the low bond strength reported for similar carboxylamine (C-ON) bonds in alkoxyamine polymers (100-130kJ/mol) (*180, 181*), and the inherent instability of the C–ON bond to thermal homolysis (*180*), it is not surprising that TEMPO-labeled proteins are less stable to MS than their ST-labeled counterparts, which possess a stronger C-C bond (345kJ/mol) (*182*). Relief of steric overcrowding on protein digestion allows the C–ON bond to withstand the MS analysis, as seen clearly for the TEMPO-labeled aromatic amino-acid derivatives. In fact, it should be possible to exploit the thermal lability of the C–ON bond to confirm radical scavenging by establishing threshold temperatures for homolysis of peptide-TEMPO and protein-TEMPO adducts. Such investigations are discussed in Chapter 4, and the results demonstrate the intriguing possibility of generating polypeptide-based radicals reversibly as in nitroxide-mediated living polymerization (*60*). Radical capping may increase the stability of peroxidases, thereby expanding their utility in industrial applications, which currently include food production, fabric dying and paper-pulp manufacture (*7*).

3.6 Conclusions

The use of TEMPO$^{\bullet}$ as a reagent for the MS detection of biologically relevant carbon-centered free radicals has been shown to be highly effective in two very different radical-generating environments *in vitro*. In both the HRP-catalyzed peroxidation of aromatic amino-acid derivatives (NAYA, NAWA and NAF) and direct heme-mediated protein peroxidation, TEMPO$^{\bullet}$ significantly outperforms diamagnetic STs such as MNP and DBNBS in adduct yield. Also, the formation of a diamagnetic TEMPO-adduct rather than a spin-adduct greatly diminishes the probability of radical side reactions typically associated with STs. Spin scavenging also is expected to be more selective over spin trapping given the high reactivity of stable nitroxide radicals with carbon-centered radicals. Furthermore, the well-documented homolysis of the carboxylamine bond at elevated temperatures can be exploited to confirm spin scavenging. The technology described here should help elucidate mechanisms of translocation of protein radicals, and their roles in redox- and oxidative-stress-signaling pathways.

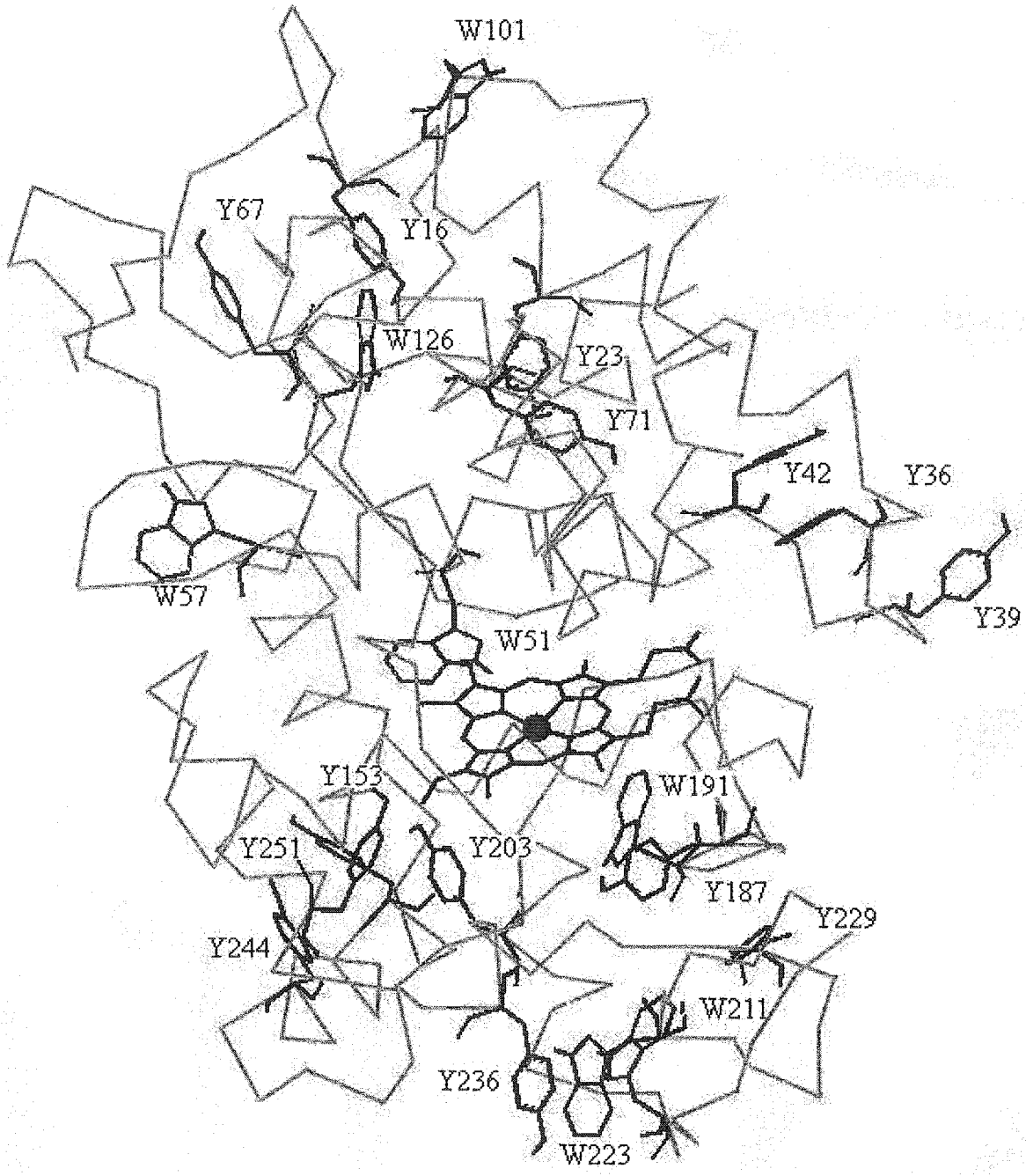

Figure 3.11. The C_α backbone of CCP showing the location of the 7 W and 14 Y residues relative to the heme (*183*).

4.0 Activation of TEMPO-Capped Protein-based Aromatic Radicals in Myoglobin and Cytochrome c Peroxidase at Low Temperatures

4.1 Abstract

The H_2O_2/TEMPO$^{\bullet}$ labeling reaction of horse heart myoglobin (2.5mM Mb, 10x H_2O_2, 4x TEMPO$^{\bullet}$) gives rise to protein that is singly TEMPO-labeled, most likely on Tyr103. Visible and EPR spectroscopy revealed the release of free 2,2,6,6-tetramethylpiperidinyl-1-oxy (TEMPO$^{\bullet}$) from the purified product (Mb_{TL}) of the labeling reaction on heating to 37°C. Release of TEMPO$^{\bullet}$ from trypsin-digested Mb_{TL} was observed at temperatures above 67°C. Incubation of 11mM of the spin trap 3,5-dibromo-4-nitrosobenzenesulfonate (DBNBS) with 500μM Mb_{TL} at 37°C allowed the exchange of the TEMPO label for a DBNBS label, which was detected by electrospray mass spectrometry. The steric hindrance experienced by the TEMPO label due to the interaction of its methyl groups with the aromatic side chain of Tyr103 and with the polypeptide, as well as increased solvation of the nitroxide radical in the aqueous solvent on binding to Mb weakens the carboxylamine bond such that thermolysis occurs at much lower temperatures in intact (37°C) and trypsin-digested Mb_{TL} (67°C) than in linear aliphatic polymers in organic solvents (120-130°C). Nine TEMPO-adducts were detected by mass spectrometry (*184*) in tryptic peptides of the digested product (CCP_{TL}) of the H_2O_2/TEMPO$^{\bullet}$ labeling reaction of yeast cytochrome c peroxidase (500μM CCP, 10x H_2O_2, 100x TEMPO$^{\bullet}$). Intact CCP_{TL} did not oxidize ferrocytochrome c [cytc(Fe^{II})] at 25°C, but 7.0 and 9.5 equivalents of cyt c(Fe^{II}) were oxidized per mole CCP_{TL} on

incubation for 10s at 37 and 47°C, respectively. Thus, oxidizing equivalents are stored and thermally activated in CCP_{TL}. Furthermore, since only 0.1 equivalents of the phenolic donor, 2,2'-azinobis(3-ethylbenzothiazoline-6-sulfonic acid (ABTS) was oxidized by CCP_{TL} at the elevated temperatures, activated CCP_{TL} behaves as a selective oxidant. Capping of protein-based radicals may contribute to peroxidase stability and lead to their cosmetic uses such as in hair dyes and environmental bleaching.

4.2 Introduction

Nitroxides have found widespread use in chemistry, such as the introduction of functionality and reducing properties (*185*) for synthetic purposes. They also can be used as protecting groups that can be photochemically cleaved (*186*). Recently, particular attention has been paid to their use in polymer chemistry (*60*). It has been known for some time that nitroxides can trap carbon-centered radicals (*139-141*), and they have been used as scavengers to inhibit polymerization or polymer degradation (*187*). Georges *et al.* (*61, 188*) found that stable nitroxide radicals can be used to control polydispersity during free radical polymerization, where lack of adequate molecular-weight control had been a major limitation. Incorporation of a nitroxide group renders the polymer "living," and the process is termed "living" free radical polymerization (LFRP) (*61*), since the thermally labile cap can be removed and polymerization resumed with the same or another monomer (*60*).

Nitroxides have also found many applications in biochemistry, including electron paramagnetic resonance (EPR) imaging (*189*) and spin labeling of biomolecules for further analysis by EPR spectroscopy (*53*). Work is underway to employ nitroxides for

pharmaceutical purposes by taking advantage of their antioxidant properties observed *in vivo* (*190*). Recently, we have exploited the ability of nitroxides to scavenge carbon-centered radicals to identify protein-based radicals (*37, 184*). Spin scavenging (SS) by the stable nitroxide, 2,2,6,6-tetramethylpiperidinyl-1-oxy (TEMPO$^{\bullet}$) of radicals generated in the aromatic amino-acid derivatives, N-acetyl-tyrosinamide (NAYA) and N-acetyl-tryptophanamide (NAWA), along with two heme proteins, myoglobin (Mb) and cytochrome c peroxidase (CCP), was combined with mass spectrometric detection of the labeled species. Identification of TEMPO-labeled sequences on the proteins involved tryptic digestion and peptide mass mapping by MALDI-ToF-MS (SS/MALDI) or HPLC and ESI-MS (SS/LC/MS) (*37, 184*).

Generation of protein radicals in Mb is thought to play a particularly important role in H_2O_2-mediated tissue damage through an intramolecular oxidation process that forms both an oxyferryl heme (Fe^{IV}=O) and unstable protein radicals ($P^{\bullet+}$) (*143, 160*):

$$Fe^{III},P + H_2O_2 \rightleftharpoons Fe^{IV}{=}O,P^{\bullet+} + H_2O \qquad (4.1)$$

Numerous EPR, MS, NMR and site-directed mutagenesis studies have attempted to characterize the radicals in Mb from horse heart (Figure 4.1A) (*18, 19, 47, 49, 56, 135, 143-145, 160, 191-193*). The consensus evidence is that the main site of radical stabilization in H_2O_2-oxidized Mb is the tyrosine (Y) residue, Y103 (*36*), which is consistent with our SS/MALDI results using TEMPO$^{\bullet}$ (*37, 184*).

The TEMPO$^{\bullet}$/H_2O_2 labeling procedure is presented schematically in Figure 4.2 for heme proteins. Curiously, TEMPO-labeled intact Mb was not observed in the deconvolved ESI

and MALDI-ToF mass spectra, with the exception of Mb from a labeling reaction carried out at pH 5 (*37, 184*). When Mb was subjected to tryptic digestion before MS analysis, TEMPO-labeled T_{16} (which contains Y103, the consensus site of radical formation (*36*)) was observed (*37, 184*). Similar results were obtained for CCP, which catalyzes the breakdown of up to 10 molar equivalents of H_2O_2 in the absence of substrate through intramolecular electron transfer to the Fe^{IV}=O heme. This could lead to the formation of up to 20 protein-based radicals, including Y and tryptophan (W) residues in a heme-mediated process (*22*). No TEMPO-labeling of intact CCP was detected, but nine TEMPO-labeled tryptic peptides, rich in Y and W residues, were detected when the enzyme was proteolytically cleaved prior to MS analysis (*37, 184*). Since TEMPO-labeled NAYA, NAWA and tryptic peptides were found to be stable in both ESI and MALDI-ToF sources (*37, 184*), we speculated that the carboxylamine (C-ON) bond formed between $TEMPO^{\bullet}$ and carbon-centered radicals, is weaker in proteins than in peptides so that the label is lost under the conditions used to record the ESI and MALDI-ToF mass spectra. Steric constraints between the polypeptide and the bound $TEMPO^{\bullet}$ likely destabilize the carboxylamine bond in a folded or partially folded protein, and relief of steric overcrowding on protein digestion allows the TEMPO-label to withstand the MS analysis.

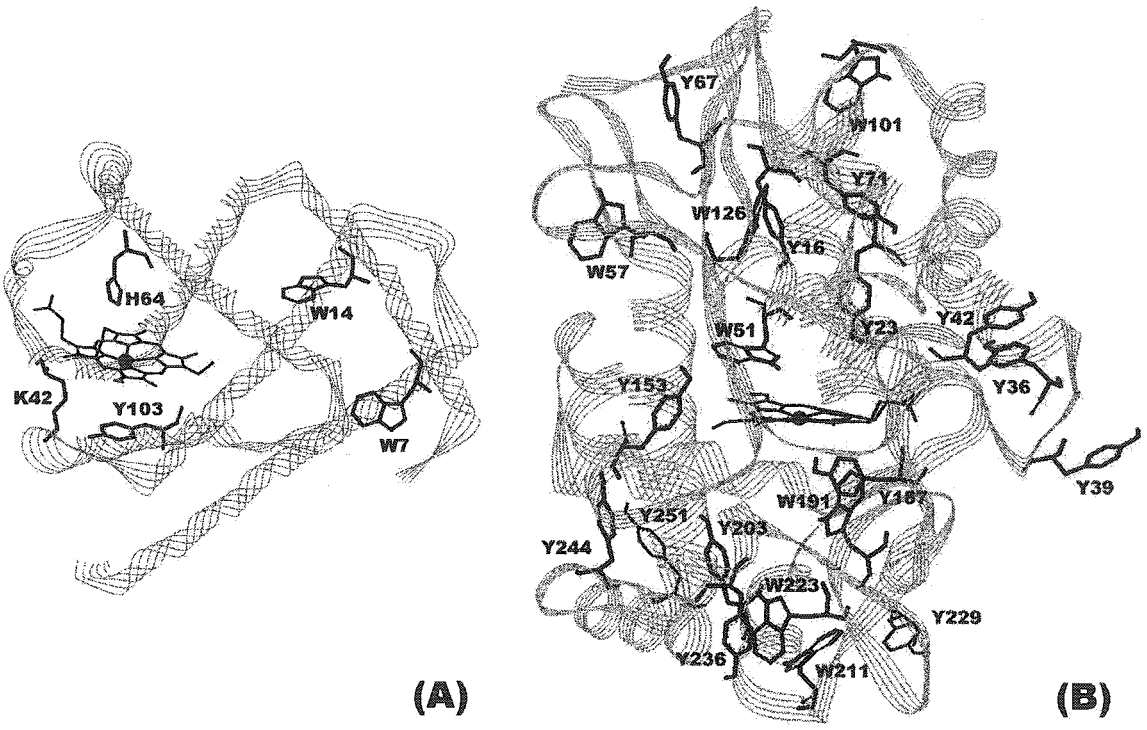

Figure 4.1 **Structures of (A) horse heart myoglobin (*194*), and (B) yeast cytochrome c peroxidase (*195*).** Tryptophan (W) and tyrosine (Y) residues are shown since these are possible sites of radical trapping or scavenging.

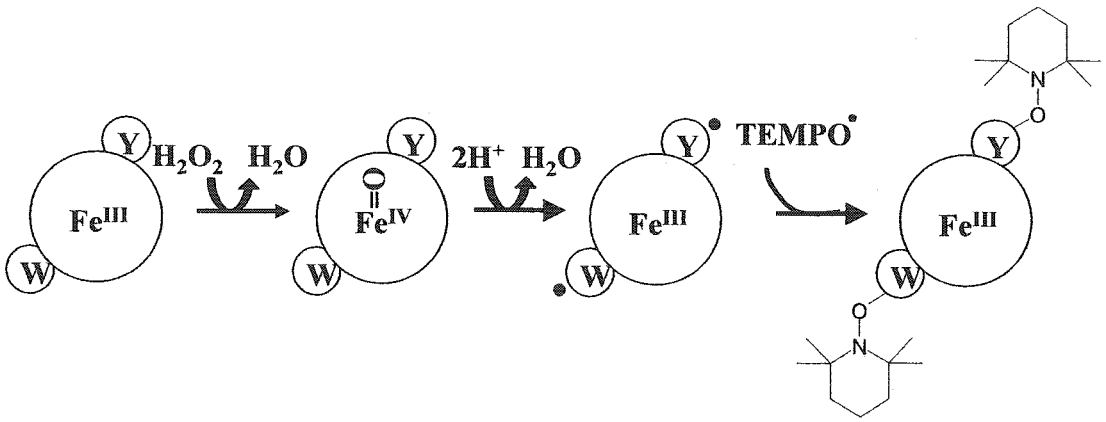

Figure 4.2. ***A schematic representation of the H_2O_2/TEMPO• labeling reaction in heme proteins.*** 500μM Mb or CCP was reacted with 5mM H_2O_2 in 100mM sodium phosphate buffer, pH 7.4, 25°C. The oxidizing equivalents of H_2O_2 are stored as an oxyferryl heme (Fe^{IV}=O) and polypeptide-based radicals (Y•, W•). The protein radicals are scavenged on formation of covalent carboxylamine bonds when TEMPO• is present. The excess TEMPO• is removed by gel filtration before analysis of the products.

To test this hypothesis, regeneration of TEMPO$^{\bullet}$ and protein-based radicals in the products from the TEMPO$^{\bullet}$/H_2O_2 labeling reactions of intact Mb (Mb_{TL}), CCP (CCP_{TL}) and in the Mb_{TL} tryptic peptides was investigated in the present study. Cleavage of the C-ON bond via thermolysis and the formation of TEMPO$^{\bullet}$ were directly probed by monitoring the characteristic nitroxide visible absorption at 445nm and EPR absorption with a g-factor of 2.055 upon heating Mb_{TL}. TEMPO$^{\bullet}$ formation in the tryptic digest of Mb_{TL} also was monitored by EPR. Regeneration of the Mb radical was probed by heating Mb_{TL} in the presence of a 100-fold excess of the spin traps, MNP and DBNBS, followed by ESI-MS analysis of the protein products. The number of oxidizing equivalents stored in CCP_{TL} and Mb_{TL} was examined at elevated temperatures using ABTS, and ferrocytochrome c [cytc(Fe^{II})]. Labeling of horseradish peroxidase isozyme c (HRPC), which reportedly does not form surface-exposed radicals on reaction with H_2O_2 (*20*), also was examined. The results presented here clearly indicate that the C-ON bond in proteins is less stable than that in peptides and free amino acids. This behavior offers an advantage in the characterization of protein products from spin scavenging reactions, since any peptide modification during the digestion process could be distinguished from labeling of the intact protein by heating the latter prior to digestion and MS analysis.

4.3 Materials and Methods

4.3.1 Materials

Wild-type recombinant cytochrome c peroxidase [CCP-MKT] was prepared as described previously (*195*). Horse heart myoglobin, bovine catalase, 2,2,6,6-

tetramethylpiperidinyl-1-oxy (TEMPO$^{\bullet}$), trifluoroacetic acid, and cytochrome c were from Sigma and used without further purification. Horseradish peroxidase isozyme C (Grade I) and 2,2'-azinobis(3-ethylbenzothiazoline-6-sulfonic acid) were purchased from Roche. HPLC-grade acetonitrile was purchased from EM Industries and H_2O_2 from Fisher. Sodium phosphate and ammonium acetate (ICN) buffers were prepared using distilled water (specific resistance 18MΩ) from a Millipore Simplicity 185 system. All buffers contained 100μM DTPA (Fisher) to prevent trace-metal-catalyzed redox processes.

4.3.2 TEMPO-labeling Reactions

Mb, CCP or HRPC (500 μM or 2.5mM) was added to 100x or 4x TEMPO$^{\bullet}$ and 10x H_2O_2 in 50mM ammonium acetate or 100mM sodium phosphate buffer (pH 7.4, NaPi) containing 100μM DTPA. Catalase (10nM) was added after 10min to remove any remaining H_2O_2, and excess TEMPO$^{\bullet}$ was separated from the proteins on an AmershamPharmacia HiTrap desalting G-25 size-exclusion column (1.0x2.5 cm). The concentrations of the protein products, Mb_{TL}, CCP_{TL}, and $HRPCC_{TL}$, from the TEMPO-labeling reactions were determined spectrophotometrically assuming ε_{409} = 171, (*191*) ε_{408} = 102 (*195*) and ε_{403} = 102 $cm^{-1}mM^{-1}$, (*82, 83*) respectively. Tryptic digestion was carried out as described previously, (*37, 184*) and covalent TEMPO-labeling was probed by ESI-MS or MALDI-ToF-MS (*37, 184*)

4.3.3 *Visible and EPR Spectroscopy*

The characteristic nitroxide band of free TEMPO$^{\bullet}$ at 445nm (ε_{445} = 11 $M^{-1}cm^{-1}$) (*196*) was monitored during the heating (37-67°C) in a 1cm thermostated cell of 2.5mM Mb_{TL} on an Agilent 8453 UV-visible diode-array spectrophotometer with ChemStation software. Formation of TEMPO$^{\bullet}$ also was monitored by EPR on a Bruker ESP-300 running on an OS/9 platform operating in the X-band with a modulation frequency of 100kHz. Mb_{TL} (2.5mM) or its tryptic digest (~500μM) was incubated at 37-87°C in a 0.3mm flat cell (Wilmad) for 10min before EPR analysis. The specific experimental parameters are given in Figure 4.3.

4.3.4 *Analysis of TEMPO/Spin Trap Exchange on Mb_{TL} by ESI-MS*

A spin trap, DBNBS or MNP (10mM), was added to Mb_{TL} (500μM), the sample heated to 37°C for 10min, diluted 10-fold with 50% acetonitrile/0.05% TFA and directly infused at a flow rate of 3μL/min into the ESI source of a ThermoFinnigan SSQ 7000 single quadrupole mass spectrometer using a syringe pump (Harvard Apparatus). The MS operating conditions were: needle voltage, 4.0kV; spray current, 2.3mA; capillary temperature, 200°C; electron multiplier, 1200V. Ultra pure N_2 (Praxair) was used as a nebulizing gas. The mass range was scanned from 500-2000u at 3s/scan in positive-ion mode. Data analysis was performed using Xcalibur software (ThermoFinnigan).

4.3.5 Donor Oxidation

The number of oxidizing equivalents stored in CCP_{TL}, $HRPC_{TL}$ and Mb_{TL} were determined by monitoring ABTS and cytc(Fe^{II}) oxidation spectrophotometrically on the diode-array spectrophotometer. Horse heart cytc(Fe^{III}) was reduced with dithionite, the low-molecular weight reagents were removed on a G25 size-exclusion column (AmershamPharmacia), and the cytc(Fe^{II}) concentration determined spectrophotometrically ($\varepsilon_{550} = 27.7 mM^{-1}cm^{-1}$) (*197*) CCP_{TL}, Mb_{TL} or $HRPC_{TL}$ (0.2nmol) was added to ~4μmol cytc(Fe^{II}) or ~9μmol ABTS in NaPi, the solutions were heated to 37-67°C, and cytc(Fe^{II}) or ABTS oxidation was monitored spectrophotometrically over 15s assuming $\Delta\varepsilon_{550} = 19.5$ (*198*) and $\Delta\varepsilon_{405} = 36.8 mM^{-1}cm^{-1}$ (*89*), respectively. The number of oxidizing equivalents stored in a protein from the H_2O_2/TEMPO$^{\bullet}$ labeling reaction is the number of donor equivalents oxidized by the treated proteins minus the number oxidized by the untreated protein (e.g., CCP_{TL} *vs* CCP).

4.4 Results

4.4.1 Direct Monitoring of Free TEMPO$^{\bullet}$ Formation in Intact Mb_{TL} and in its Tryptic Digest on Heating

The distinctive nitroxide band of TEMPO$^{\bullet}$ at 445nm was not observed in the spectrum of 2.5mM Mb_{TL} at 25°C. However, an increase in 445nm absorption in the difference spectra [37°C (or 47°C) spectrum minus 25°C spectrum] (data not shown) revealed that TEMPO$^{\bullet}$ was released on heating Mb_{TL} over 10min. Quantitation was not attempted due to the strong, temperature dependent, Soret absorption of Mb at 409nm (*191*). Consistent with the visible absorption results, Mb_{TL} was EPR silent at 25°C, but

heating to 37°C for 10min and subsequent EPR analysis revealed the presence of the characteristic three-line spectrum of the TEMPO$^{\bullet}$ radical (Figure 4.3C). The g-factor of 2.055 and hyperfine coupling constant (A_N) of 1.83mT are identical to those observed for free TEMPO$^{\bullet}$ (Figure 4.3A). The line broadening in Figure 4.3C is attributed to increased solution viscosity and possible nonspecific association of the released TEMPO$^{\bullet}$ with Mb_{TL}, since the incubation of 2mM TEMPO$^{\bullet}$ with 2.5mM native Mb yielded a similar EPR spectra (Figure 4.3B). Cooling of Mb_{TL} back to 25°C resulted in a loss of EPR signal (Figure 4.3D) suggesting some recombination of the TEMPO$^{\bullet}$ radical with the Mb-based radical. Tryptic digestion of Mb_{TL} followed by EPR analysis of the digest between 25 and 67°C yielded only EPR-silent species. However, when the digest was heated above 67°C for 10min, a three-line spectrum with a g-factor and an A_N identical to those observed for free TEMPO$^{\bullet}$ (Figure 4.3A) were observed (data not shown).

4.4.2 Probing Formation of Protein-based Radicals in Mb_{TL} on Heating

Figure 4.4A shows the deconvolved mass spectrum of Mb_{TL} formed in the H_2O_2/TEMPO$^{\bullet}$ labeling reaction at pH 5.0. The presence of a peak at 17107Da corresponds to Mb with a single TEMPO-label, while the dominant peak at 16951Da is due to the heme-free form of the unlabeled protein (*199*). When 500μM Mb_{TL} was heated to 37°C in the presence of 10mM DBNBS for 10min, a peak corresponding to singly DBNBS-labeled Mb was observed at 17312Da in the deconvolved mass spectrum (Figure 4.4B). Similar results were obtained when MNP was added as a spin trap (data not shown). Thus, heating Mb_{TL}, which is TEMPO-labeled (*37, 184*), to 37°C homolytically

cleaves the C-ON bond, and the newly formed Mb-based radical is trapped when a large excess of spin trap is present in solution.

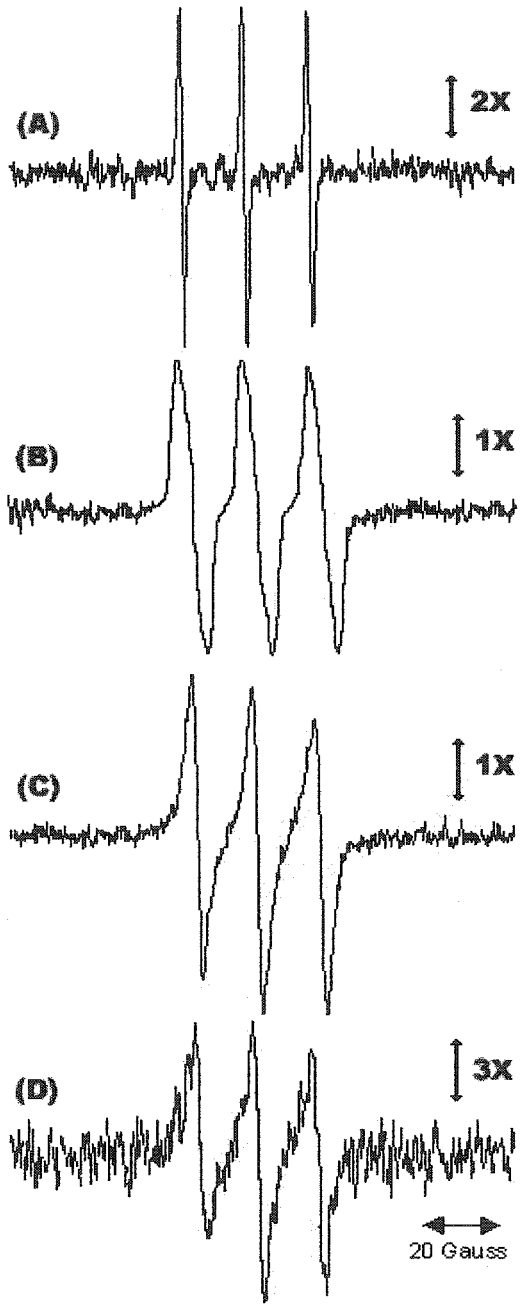

Figure 4.3. ***EPR spectra obtained following heating and cooling of Mb_{TL}.*** (A) 2mM TEMPO$^{\bullet}$ at 25°C. (B) 2mM TEMPO$^{\bullet}$ in the presence of 2.5mM Mb at 25°C. (C) 2.5mM Mb_{TL} after standing at 37°C for 10min. (D) Sample in C following cooling to 25°C. The samples were in 100mM sodium phosphate buffer, pH 7.4 in a 0.3mm flat cell. The instrumental parameters were: modulation amplitude, 1Guass; time constant, 20.48s; receiver gain, 100; microwave power, 20.11mW.

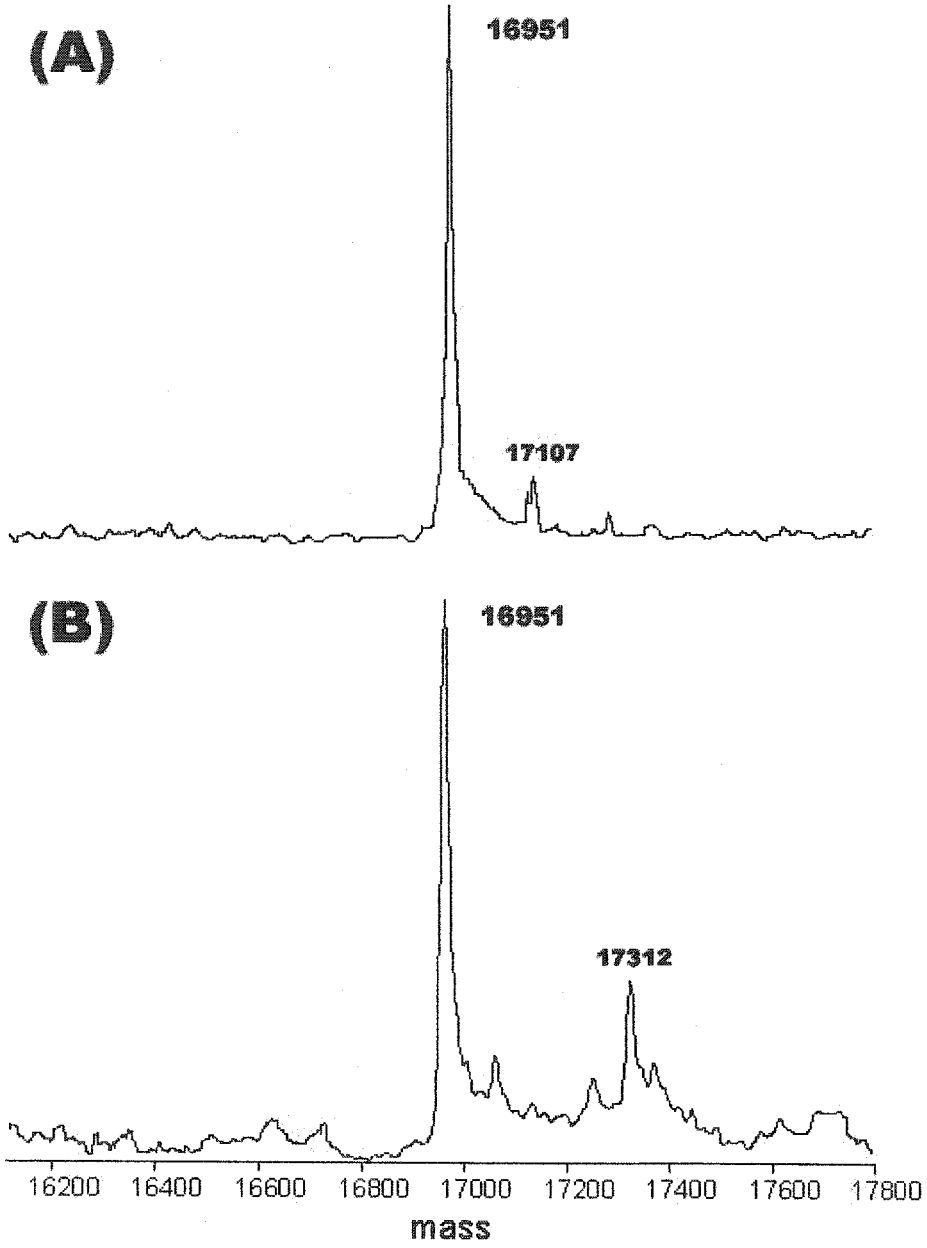

Figure 4.4. ***Deconvolved ESI mass spectra of (A) 500μM Mb_{TL} and (B) 500μM Mb_{TL} following heating to 37°C in the presence of 10mM DBNBS.*** The samples were diluted in 50% acetonitrile/0.05% TFA, and directly infused using a syringe pump at 3μL/min into the ESI source of the mass spectrometer. The MS operating conditions were: needle voltage, 4.0kV; spray current, 2.3mA; capillary temperature, 200°C; electron multiplier, 1200V.

4.4.3 Oxidizing Equivalents Stored in CCP_{TL}, Mb_{TL} and $HRPC_{TL}$ Based on Donor Oxidation

CCP_{TL} was heated to 37 and 47°C and donor oxidation was monitored spectrophotometrically. The absorption increase due to donor oxidation plateaued after 10s (Figure 4.5), and Table 4.1 lists the equivalents of donor oxidized per mole CCP_{TL} at different temperatures. When CCP_{TL} was added to either ABTS or cytc(Fe^{II}) at 25°C, the extent of donor oxidation was the same as in the untreated CCP control. However, upon heating to 37 and 47°C, 7.0±0.5and 9.5±1 equivalents respectively, of cytc(Fe^{II}) were oxidized per mole CCP_{TL}, while 0.10±0.5 equivalents of ABTS was oxidized at both temperatures. When CCP_{TL} was heated to 55°C, donor oxidation was only 10% that observed at 47°C, and no oxidation was observed above 55°C, most likely due to protein denaturation (*1*). Since donor oxidation by native CCP in the presence or absence of TEMPO$^{\bullet}$ (Figure 4.5) at the various temperatures is negligible, homolysis of the C-ON bond in CCP_{TL} is required to release oxidizing equivalents stored in the polypeptide.

Interestingly, CCP_{TL} exhibited lower peroxidase activity than untreated CCP. In an assay solution containing 0.2nmol peroxidase, 4μequiv H_2O_2 and 4μequiv cyt c(Fe^{II}), 802 *vs* 613nequiv cyt c(Fe^{II}) were oxidized in 10s when native CCP *vs* CCP_{TL} was present as a catalyst. Thus, the cytc(Fe^{II})-oxidizing activity of CCP_{TL} is ~76% that of native CCP. The ABTS-oxidizing activity of CCP_{TL} was only ~68% that of the native peroxidase (40nequiv ABTS/10s) under the same conditions. These results indicate that the TEMPO$^{\bullet}$ groups bound to CCP_{TL} likely impede electron transfer from the donor during catalytic donor turnover.

Negligible oxidizing equivalents were stored in Mb_{TL} (data not shown). This is presumably due to its low peroxidase activity (*200*) and the short lifetime of the Y103 radical (50-280ms) (*144, 201*) following cleavage of the carboxylamine bond. In the absence of donor substrates (*20*). HRPC turns over H_2O_2 mainly through catalatic activity ($2H_2O_2 \rightleftharpoons O_2 + 2H_2O$). Consistent with catalatic turnover, no TEMPO-labeling of $HRPC_{TL}$ tryptic peptides was detected by ESI-MS or MALDI-ToF-MS (data not shown), and $HRPC_{TL}$ possessed the same peroxidase activity as native HRPC using ABTS and cytc(Fe^{II}) as substrates. $HRPC_{TL}$ exhibited negligible cytc(Fe^{II}) oxidizing ability up to 47°C (Table 1). However, close to 10 equivalents of ABTS are oxidized per mole $HRPC_{TL}$ or native HRPC in 10s. This is close to 100-fold the ABTS-oxidizing power seen in CCP_{TL} at elevated temperatures, and is assigned to weak oxygenase activity in the plant peroxidase. The presence of a donor-binding site close to the heme of HRPC (*31*) likely promotes reduction of the ferric heme and O_2 binding. Further reduction of the oxyheme center leads to formation of HRPC(Fe^{V}=O) and donor oxidation (*202, 203*):

$$HRPC(Fe^{III}) + ABTS \rightleftharpoons HRPC(Fe^{II}) + ABTS^{\bullet+} \quad (4.2)$$

$$HRPC(Fe^{II}) + O_2 \rightleftharpoons HRPC(Fe^{II}\text{-}O_2) \quad (4.3)$$

$$2H^+ + ABTS + HRPC(Fe^{II}\text{-}O_2) \rightleftharpoons HRPC(Fe^{V}{=}O) + ABTS^{\bullet+} + H_2O \quad (4.4)$$

$$2H^+ + 2ABTS + HRPC(Fe^{V}{=}O) \rightleftharpoons 2ABTS^{\bullet+} + HRPC(Fe^{III}) \quad (4.5)$$

$$2ABTS^{\bullet+} \rightleftharpoons ABTS_{ox} \quad (4.6)$$

4.5 Discussion

The field of LFRP mediated by stable nitroxide free radicals, such as TEMPO•, has seen explosive growth in recent years (*60*). Materials with low polydispersity can be

readily prepared by heating the neat monomer with a nitroxide-based initiator at 120-130°C under an inert atmosphere. This process proceeds by the reversible termination of the growing polymeric radical by the stable nitroxide, producing an inactive species, in which the nitroxide is covalently bound to the polymer chain end. The carbon-oxygen bond is unstable to homolysis at high temperatures (120-130°C) and cleaves to give the nitroxide and polymeric radicals. The latter undergoes chain extension with the monomer to yield a similar polymeric radical in which the degree of polymerization has increased. Recombination with the nitroxide gives a new dormant species, which has the same structure as the original polymer with a one-monomer addition (*60, 61, 204*). The present results reveal that, analogous to LFRP, nitroxide-capped protein-based radicals are activated above room temperature.

4.5.1 Reformation of TEMPO•

EPR spectroscopy is a sensitive probe of paramagnetic species (*55*), and was used here to monitor the formation of free TEMPO• in Mb_{TL} solutions. At 25°C, Mb_{TL} is EPR silent because TEMPO• is covalently bound to a globin-based radical [R•, eqn 5.7] (*37, 184*). Upon heating Mb_{TL} to 37°C, a triplet with the same g-factor and A_N as native TEMPO• is observed (Figure 4.3C), which signals homolysis of the carboxylamine bond (eqn 5.8).

$$R^{\bullet} + TEMPO^{\bullet} \rightleftharpoons R\text{-}TEMPO \qquad (5.7)$$

$$R\text{-}TEMPO \overset{\Delta}{\rightleftharpoons} R^{\bullet} + TEMPO^{\bullet} \qquad (5.8)$$

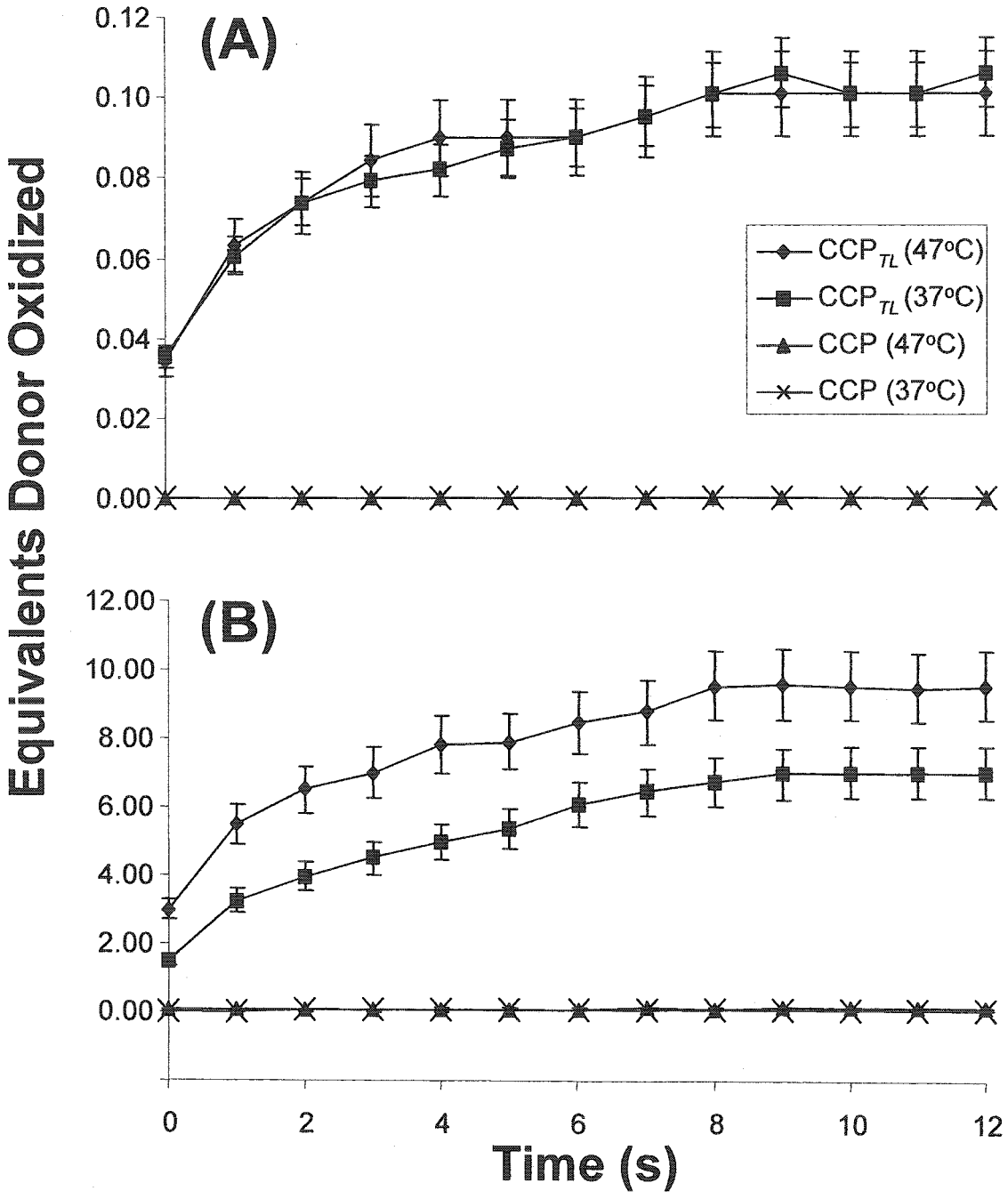

Figure 4.5. ***Oxidizing equivalents stored in CCP$_{TL}$ based on donor oxidation.*** Oxidation of (A) ABTS and (B) cytc(Fe^{II}) by 0.2nmol CCP$_{TL}$ or CCP in 100mM sodium phosphate buffer (pH 7.4) following heating to 37 and 47°C. Oxidation of cyt c(Fe^{II}) (4μequiv) and ABTS (9μequiv) was monitored in a 1cm cuvette at 550nm and 405nm, respectively. Each data point is the average of three trials. Where error bars are not visible, they are contained within the symbols.

Table 4.1. Equivalents of donor oxidized in 10s per mole of heme protein[a]

Protein[b]	Donor[c]	25°C	37°C	47°C
CCP	Cytc(Fe^{II})	0.14±0.1	0.15±0.1	0.09±0.1
	ABTS	$1.9x10^{-4}$±$1.0x10^{-4}$	$1.7x10^{-4}$±$1.0x10^{-4}$	$2.0x10^{-4}$±$1.0x10^{-4}$
CCP_{TL}	Cytc(Fe^{II})	0.14±0.1	7.0±0.5	9.5±1.0
	ABTS	$1.9x10^{-4}$±$1.0x10^{-4}$	0.10±0.05	0.10±0.05
HRPC	Cytc(Fe^{II})	$3.5x10^{-3}$±$2.0x10^{-3}$	$2.5x10^{-3}$±$1.5x10^{-3}$	$2.5x10^{-3}$±$1.0x10^{-3}$
	ABTS	10.0±1.0	5.5±1.5	12.5±1.0
$HRPC_{TL}$	Cytc(Fe^{II})	$3.1x10^{-3}$±$1.5x10^{-3}$	$2.5x10^{-3}$±$1.1x10^{-3}$	$3.0x10^{-3}$±$2.0x10^{-3}$
	ABTS	10.5±1.0	7.0±1.5	12.0±1.5

[a]Heme protein (0.2nmol) was incubated in 100mM sodium phosphate buffer (pH 7.4) at the temperatures indicated, and the equivalents of donor oxidized were measured spectrophotometrically (see Figure 4.5).

[b]CCP and HRPC, untreated ferric heme proteins; CCP_{TL} and $HRPC_{TL}$ proteins from the H_2O_2/TEMPO$^{\bullet}$ labeling reactions described in the caption to Figure 4.2.

[c]Incubations contained ~4μequiv cytc(Fe^{II}) or ~9μequiv ABTS.

In contrast, the alkoxyamine derivatives resulting from TEMPO$^{\bullet}$ scavenging of carbon-centered free radicals in vinyl polymers (*205*) are stable at temperatures close to 120°C. TEMPO$^{\bullet}$ release from trypsin-digested Mb_{TL}, where the C-ON bond should be less sterically hindered than in intact Mb, was observed around 67°C. Thus, the TEMPO-phenolic ring (in this case Y103 on T_{16} in Mb_{TL}) (*36*) bond in the aqueous buffer is less stable than the TEMPO-polyvinyl polymer bond in organic solvents (*139*). It is not surprising that a "capped" aromatic radical would experience increased steric interference

by the TEMPO$^{\bullet}$ methyl groups compared to a vinyl radical (*140*). Furthermore, the steric effects of the folded globin compound the destabilizing effects (*37, 184*). Hence, the C-ON bond is weakest in the intact protein, but weaker in the tryptic peptides as compared to those found in typical LFRP reactions (*60*).

Since the EPR signal observed on heating Mb_{TL} has similar intensity to that of 2mM TEMPO$^{\bullet}$ (Figure 4.3C *vs* 4.3B), nearly 2mM TEMPO$^{\bullet}$ must be regenerated on heating 2.5mM Mb_{TL}. This is consistent with the observation of a single site (Y103) of TEMPO-labeling by SS/MALDI (*37, 184*). However, additional, TEMPO-labeled peptides may have escaped detection by SS/MALDI, and radical stabilization at several sites in Mb has been reported (*18, 19, 47, 143-145*). Compared to Figure 4.3A, the spectra in Figure 4.3B and 4.3C exhibit line broadening. Since the spectra in both Figure 4.3A and 4.3C were measured at 25°C, the line broadening may be due to the increased solution viscosity in the presence of 2mM Mb or to interaction between free TEMPO$^{\bullet}$ and the protein, which would decrease the spin-lattice relaxation time thus influencing the extent of line broadening (*55*). Cooling did not regenerate an EPR-silent sample presumably because the short lifetime of the Mb radicals ($t_{1/2}$ ~ 50-280ms) (*144, 201*) competes with reformation of the carboxylamine bond at 25°C (*18, 57*). Monitoring the nitroxide band at 445nm by visible spectroscopy yielded similar results. At 37°C, nitroxide absorption at 445nm was detectable in the spectrum of gel-purified Mb_{TL} (or CCP_{TL}) but not at 25°C (data not shown).

4.5.2 *Regeneration of Protein-based Radicals*

MNP and DBNBS successfully have been used to trap protein-based radicals on both Mb (*18, 19*) and CCP (*50, 133*). Also, unlike the TEMPO-adducts, the spin adducts of the intact proteins are stable under ESI-MS conditions (*18, 50, 55, 133*). When excess spin trap was incubated with Mb_{TL} at 37°C for 10min, Figure 4.4B reveals that exchange of TEMPO$^{\bullet}$ for DBNBS occurred following homolysis of the carboxylamine bond. Thus, 10mM DBNBS (Figure 4.4B) or MNP (data not shown) can compete with regenerated TEMPO$^{\bullet}$ for the Mb-based radicals confirming that homolysis of the TEMPO-Mb bond activates the Mb-based radical(s).

4.5.3 *Stored Oxidizing Equivalents*

Activation of protein-based radicals at elevated temperature should "unleash" the oxidizing power of H_2O_2 stored in the TEMPO-labeled proteins. The results presented in Table 4.1 indicate that one mole of CCP_{TL} can oxidize 7 equivalents of cytc(Fe^{II}) on homolysis of the carboxylamine bond at 37°C. Since nine sites of TEMPO-labeling were detected by MALDI-MS in CCP_{TL} (*37, 184*), a maximum of nine oxidizing equivalents were expected to be stored in its polypeptide. When the temperature was raised to 47°C (Table 4.1), 9.5 equivalents of cyt c(Fe^{II}) were oxidized per mole CCP_{TL}, close to the maximum expected. The high reactivity of the stored oxidizing equivalents with cytc(Fe^{II}) raises the question as to how the cytochrome is oxidized by CCP_{TL}. Is this a heme-mediated process or are electrons donated directly to the protein radicals? At temperatures above 55°C, the oxidation of cytc(Fe^{II}) diminished to ~10% of that observed at 47°C, suggesting that the structural integrity of the protein is necessary for efficient

transfer of the oxidizing equivalents since CCP has been shown to denature above 55°C (*1*). Further studies are clearly required to elucidate the mechanism(s) of electron transfer between cytc(Fe^{II}) and activated CCP_{TL}. The oxidation of ABTS by CCP_{TL} also increased at high temperature but only 0.1 equiv was consumed. The low reactivity of ABTS with the CCP-based radicals may be due to the fact that CCP_{TL} may retain the donor specificity of the native enzyme. Thus CCP_{TL} and other heme enzymes may serve as thermally-activatable oxidants with some donor specificity.

Using cytc(Fe^{II}) as a donor, CCP_{TL} exhibited ~76% of the activity of native CCP. Pfister *et al.* (*175*) found that the sequential mutagenesis of two W and six Y residues in CCP resulted in an increase in compound I stability, and a decrease in cyt c(Fe^{II})-oxidizing ability, providing evidence that several aromatic residues in the CCP polypeptide are redox-active during normal catalytic turnover. Since CCP_{TL} presumably has 9 TEMPO-labeled Y and W residues, the labels may interfere both chemically and sterically with donor oxidation. TEMPO-capping of W191, for example, should greatly diminish the cytc(Fe^{II})-oxidizing capability of CCP since electron transfer between the hemes occurs via W191. The W181F mutant of CCP exhibits negligible cytc(Fe^{II})-oxidizing activity although it reacts rapidly with H_2O_2 (*16, 152, 175*).

Additional donor oxidation was not detected upon heating $HRPC_{TL}$ (Table 4.1). This is not surprising since HRPC (5Y, 1W) does not possess a large number of oxidizable aromatic residues like CCP (14Y, 7W), and it turns over H_2O_2 by a catalatic mechanism ($2H_2O_2 \rightleftharpoons O_2 + 2H_2O$) in the absence of other donors (*20*). The increased ABTS oxidation observed for HRPC and $HRPC_{TL}$ compared to CCP_{TL} is attributed to the presence of an aromatic substrate binding pocket near the distal heme in HRPC that is not

present in CCP (*20*). HRPC can therefore oxidize ABTS by its inherent oxygenase activity since aromatics are able access the distal heme cavity [eqns 4.2-4.5] (*20*). Heating $HRPC_{TL}$ did not generate any donor-accessible oxidizing equivalents since, as can be seen from Table 4.1, there is no difference in the number of ABTS equivalents oxidized by HRPC and $HRPC_{TL}$.

4.6 Conclusions

The use of the stable nitroxide, $TEMPO^{\bullet}$, to reversibly cap protein-based radicals has been confirmed. Steric hindrance experienced by the methyl groups of $TEMPO^{\bullet}$ on scavenging aromatic radicals (*140*), unfavorable TEMPO-polypeptide interactions (*37, 184*) and solvation (*139*) in aqueous buffers weakens the carboxylamine bond. Thus, TEMPO-capped aromatic radicals in Mb_{TL} (37°C) and in Mb_{TL} peptides (67°C) are activated at much lower temperatures than those reported for alkyl radicals in linear polymers (120°C). The intact TEMPO-labeled proteins are less stable to MS than their DBNBS spin adducts, which possess a carbon-carbon bond. However, the thermal lability of the carboxylamine bond can be exploited to confirm radical scavenging by measuring the threshold temperatures for free $TEMPO^{\bullet}$ appearance. Additionally, TEMPO-capped phenols could provide an alternative oxidant to H_2O_2 for cosmetic use such as in hair dyes, and TEMPO-capping may stabilize CCP in the presence of the high H_2O_2 concentrations desired in industrial applications.

5.0 Oxidation and Reduction of 2,2,6,6-tetramethylpiperidinyl-1-oxy (TEMPO$^{\bullet}$) in the Electrospray Ion Source

5.1 Abstract

Positive-ion ESI mass spectra of TEMPO$^{\bullet}$ revealed three peaks that were assigned to (pseudo)molecular ions with relative abundances sensitive to solvent, and to a lesser extent spray voltage and the presence of TFA. MS/MS analysis of each ion gave different fragment spectra confirming that the three peaks arise from ions formed in the ESI source by different mechanisms. Since the ions are observed at m/z 156 (TEMPO^{+}), 157 (TEMPOH$^{\bullet}$) and 158 (TEMPOH$_2^{+}$), TEMPO$^{\bullet}$ must be converted to TEMPO^{+} and TEMPOH in the ESI source. Electrolysis of TEMPO$^{\bullet}$ to TEMPO^{+} likely occurs at the metal electrospray capillary to maintain charge balance in the charged droplets by counterbalancing the buildup of negative charge created by the high positive potential applied to the capillary. The formation of TEMPO^{+} promotes subsequent solvent oxidation that generates TEMPOH through an Anelli-like reaction. Since the electrochemical reduction of TEMPO^{+} to TEMPOH is irreversible, TEMPOH, which is detected as TEMPOH$_2^{+}$, acts as an electron sink in the ESI source. The results presented here suggest the suitability of TEMPO$^{\bullet}$ as a probe of electrochemistry occurring in a particular ESI source.

5.2 Introduction

Stable nitroxides such as TEMPO$^{\bullet}$ are π-radical molecules where the unpaired electron occupies a π^* orbital between the oxygen and nitrogen atoms. Since there is also an N-O σ-bond and two electrons fill a π-bonding orbital between these atoms, the effective N-O bond order is 1.5 resulting in a stable structure (*53*). The existence of an unpaired electron confers unique chemical and magnetic properties to many nitroxide reactions. For instance, nitroxides have been shown to possess antioxidant activity *in vivo* and protect against a range of agents that impose oxidative stress, including superoxide, hydrogen peroxide, and ionizing radiation (*137, 150, 151, 206, 207*). Recent research has shown that TEMPO$^{\bullet}$ administered to mice prevented them from becoming obese and decreased incidences of age-related spontaneous tumor formation (*190*). Nitroxides in biological systems have been shown to be reduced by several enzymes and ascorbic acid to their corresponding hydroxylamines (*208*). The reduction of TEMPO$^{\bullet}$ with ascorbate readily proceeds to completion with the consumption of two moles of nitroxide per mole of ascorbate, and TEMPOH and dehydroascorbic acid are the products (Scheme 5.1) (*209*). TEMPO$^{\bullet}$ can be oxidized to the nitrosium ion, TEMPO^{+}, by strong oxidants such as HOCl (*155, 156*). In the nitroxyl radical-catalyzed oxidation of alcohols by the Anelli reaction (Scheme 5.2) (*155, 156, 185*), which plays an increasingly important role in organic synthesis (*185*), TEMPO$^{\bullet}$ is redox cycled between TEMPO^{+} and TEMPOH.

With its low molecular weight (M_r 156.23) and water solubility, along with its ability to undergo reversible redox chemistry, TEMPO$^{\bullet}$ has applications in many areas of chemistry and biochemistry such as "living" free-radical polymerizations (*60*), EPR imaging (*189*), and spin labeling of biomolecules for further analysis by EPR (*53, 210*).

In our lab, spin scavenging by TEMPO$^{\bullet}$ has been developed into a sensitive method of protein-based radical detection by MS (*37, 184*). It also has been shown that covalently linked nitroxide-fluorophore adducts can be employed as sensitive optical sensors of radical/redox reactions (*186, 211-213*).

Although TEMPO$^{\bullet}$ is widely used, its ESI mass spectra have not been well characterized. Previously, a peak at m/z 156 due to $TEMPO^{+}$ was shown to dominate the ESI mass spectrum recorded in positive-ion mode. This differs from the usual detection of MH^{+} ions (*179*). Weak peaks at m/z 157 and 158 were assigned to the odd-electron ion, $TEMPOH^{\bullet+}$, and the protonated hydroxylamine, $TEMPOH_2^{+}$, respectively (*68*). However, when we recorded the ESI mass spectra of TEMPO$^{\bullet}$ under the same conditions (100μg/mL TEMPO$^{\bullet}$ in acetonitrile, 5μL/min flow rate, 65°C source temperature, 40V cone voltage, 4.0kV spray voltage), dominant peaks were present at m/z 157 and 158, in addition to a weaker $TEMPO^{+}$ peak at m/z 156. Furthermore, the relative intensities depended on the solvent, pH and instrumental parameters, and the extent of in-source fragmentation (ISF), most noticeable being the loss of $^{\bullet}CH_3$ from $TEMPOH^{\bullet+}$ ($TEMPOH^{+}$-$^{\bullet}CH_3$; m/z 142).

TEMPO$^{\bullet}$ appears to be both oxidized and reduced in the ESI source under positive-ion conditions. Van Berkel and co-workers (*214-216*) have shown that metallocenes, metalloporphyrins and polycyclic aromatic hydrocarbons are oxidized during positive-mode ESI. The basis for this phenomenon is that the ESI source behaves as a two-electrode controlled current electrochemical (CCE) flow cell (Figure 1.4) (*217*). The metal capillary from which the ES droplet plume is generated (emitter) acts as the working electrode, while the counter electrode is the atmospheric sampling aperture plate

or inlet capillary of the MS (see Figure 1.4). In order to maintain continuous production of charged droplets and gas-phase ions, oxidation occurs where the emitter electrode contacts the solution and reduction dominates at the counter electrode. Thus, the electrospray current (i_{ES}) that is generated is maintained by solvent and solute electrolysis, and is dependent on the magnitude of the ESI voltage, the solvent, the solution flow rate, and the reduction potentials and concentrations of the solute (*69*).

Although protonated molecular ions are traditionally seen by ESI in positive-ion mode (*179, 218*) analyte oxidation is not uncommon (*69, 217*). The detection of reduced species is rare and was first reported for the reduction of N-phenyl-1,4-phenylenediamine using a copper capillary emitter as an electrochemical buffer (*219*). Recently, a reduced heme group (Fe^{II}) in cytochrome c was detected by Fourier transform ion cyclotron resonance (FTICR) MS (*220*). However, both of these examples involved the chemical reduction of the analyte prior to injection into the ESI-MS.

Here, we report on the oxidation and reduction of $TEMPO^{\bullet}$ by means of an electrochemical/chemical (EC) process occurring in the ESI source. The electrochemical production of $TEMPO^{+}$ from $TEMPO^{\bullet}$ catalyzes Anelli-like oxidation of the solvent, generating TEMPOH, which is detected as $TEMPOH_2^{+}$. $TEMPO^{\bullet}$ provides the first reported case of oxidation and reduction occurring simultaneously in the ESI source without prior chemical reduction. The effects of experimental parameters on the ratio of oxidized to reduced ion abundances are of interest. Hence, the mass spectra of $TEMPO^{\bullet}$ in acetonitrile, methanol and water in the presence and absence of 0.01% TFA at needle voltages of 3, 4 and 5kV were recorded to determine the effects of these variables on $TEMPO^{\bullet}$ ionization in the ESI source.

Based on the results presented here, the redox chemistry of TEMPO$^{\bullet}$ could be used as a sensitive probe of the factors that control the magnitude of i_{ES} in a particular ESI source. This information would be useful when electrochemical reactions are of concern, such as in the analysis of compounds with low oxidation potentials (E < 1.0V) (*69, 70*), and in studying the mechanisms of biological redox systems (*221*) or those pertinent to electrochemical organic syntheses (*214*).

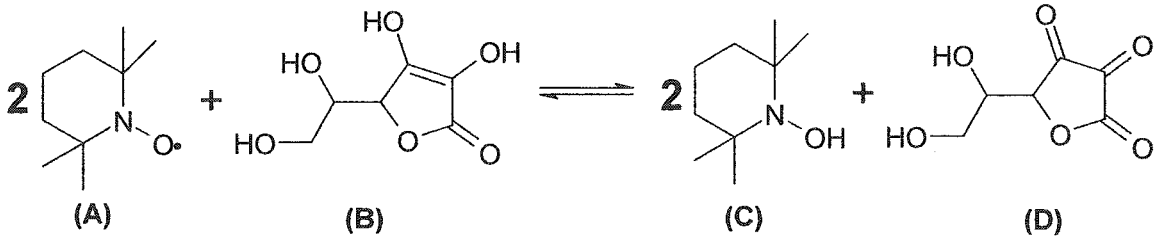

Scheme 5.1. Reduction of TEMPO$^{\bullet}$ (A) with ascorbate (B) proceeds to completion with the consumption of two moles of nitroxide per mole of ascorbate. 2,2,6,6-tetramethylhydroxylamine (TEMPOH) (C) and dehydroascorbic acid (D) are the products.

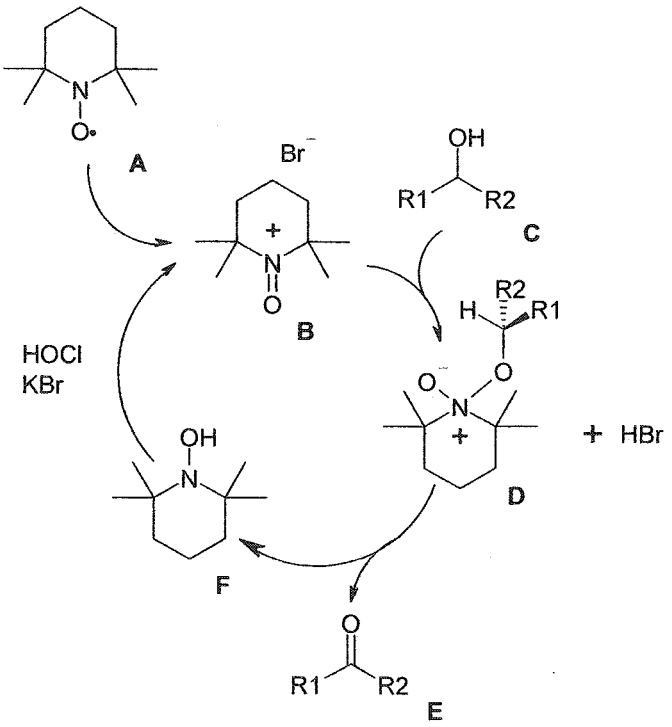

Scheme 5.2. Catalytic cycle in the Anelli reaction in solution. TEMPO$^{\bullet}$ catalyzes the oxidation by HOCl of the alcohol R_1R_2CHOH to the corresponding ketone $R_1R_2C{=}O$.

5.2 Material and Methods

5.2.1 Materials

2,2,6,6-tetramethylpiperidinyl-1-oxy ($TEMPO^{\bullet}$) and trifluoroacetic acid (TFA) were from Sigma and used without further purification. HPLC grade acetonitrile and methanol were purchased from EM Industries, while HPLC-grade water was from Fisher.

5.2.2 $TEMPO^{+}$ and TEMPOH formation

Stock solutions of $TEMPO^{\bullet}$ were prepared in acetonitrile, methanol or water and quantitated spectrophotometrically (ε_{445} = 11 $M^{-1}cm^{-1}$) (*196*). Two molar equivalents of ascorbate or HOCl were added to ensure complete conversion of $TEMPO^{\bullet}$ to TEMPOH or $TEMPO^{+}$, respectively. The loss of the $TEMPO^{\bullet}$ band at 445nm was monitored on an Agilent 8453 UV-visible diode-array spectrophotometer with ChemStation Software.

5.2.3 ESI-MS

Samples (100μg/ml) were dissolved in acetonitrile, methanol or water, with and without 0.01% TFA (~pH 2). All MS and MS/MS spectra were obtained using a Micromass Quattro II triple quadrupole (Waters). The sample solutions were infused continuously at a flow-rate of 5μl/min into the ESI source operating at atmospheric pressure and a temperature of 200°C. Nitrogen was used as both nebulizing and drying gas. Cone voltages and gas-flow rates were optimized to ensure minimal fragmentation and to produce maximal molecular-ion intensity in positive-ion mode. Mass spectra were collected at needle voltages of 3.0, 4.0 and 5.0 kV at a scan rate of 200 amu/s from m/z 50 to 600. MS/MS was carried out by selecting the parent ion in the first quadrupole and

passing the selected ion through a collision cell pressurized with argon and operating in the *rf*-only mode. Collision energies between 10 and 40eV were used. Fragmentation patterns were generated with the aid of Mass Frontiers 3.0 from HighChem Ltd.

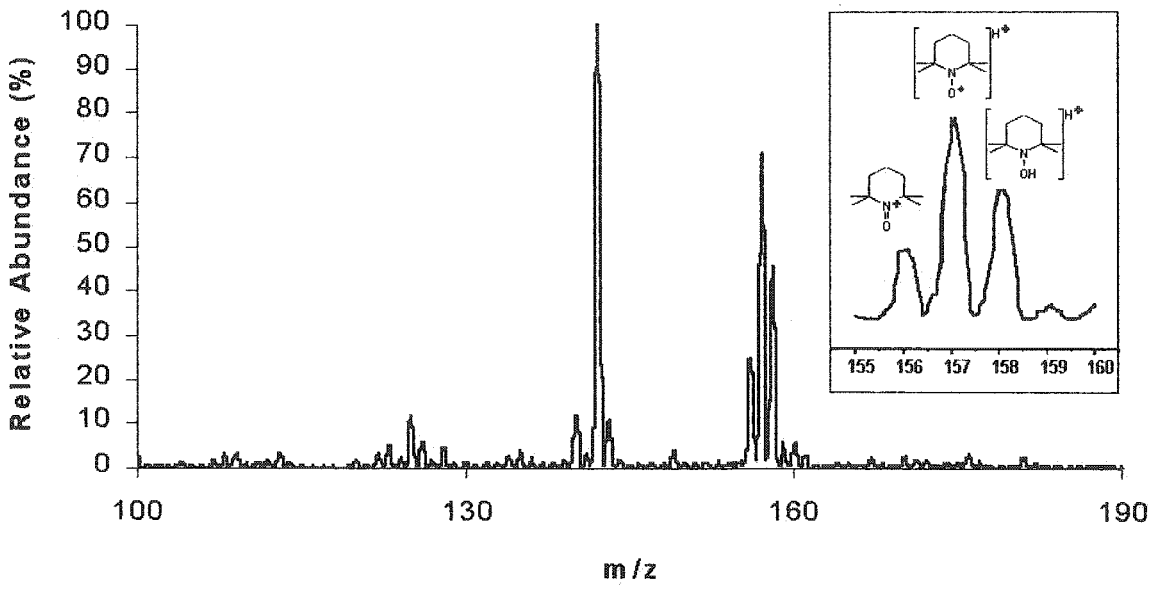

Figure 5.1. Q1MS spectra of 100μg/mL TEMPO$^{\bullet}$ in acetonitrile. Inset shows the expanded region between m/z 155 and 160, and the structures of the (pseudo)molecular ions. Experimental condition: 5μL/min flow rate, 65°C source temperature, 40V cone voltage, 4.0kV spray voltage. The spectra are an accumulation of 30 scans between m/z 50 and 200 recorded at a rate of 100amu/z.

5.4 Results

5.4.1 ESI-MS of TEMPO$^{\bullet}$

Smith *et al.* (*68*) were the first to provide a detailed interpretation of the ESI mass spectra of stable nitroxide free radicals in acetonitrile. Following the direct infusion of TEMPO$^{\bullet}$ in acetonitrile into the ESI source of a Quattro II triple-quadrupole mass spectrometer, the dominant molecular ion was at m/z 156 (100%) corresponding to $TEMPO^{+}$, and smaller peaks at m/z 157 (15%), 158 (8%) and 123 (7%) corresponding to $TEMPO^{+\bullet}$, $TEMPOH_2^{+}$ and $TEMPO^{+}$- NH_2OH, respectively. However, using the same

commercial instrument under the same conditions as those of Smith *et al.*, the mass spectrum we obtained for $TEMPO^{\bullet}$ (Figure 5.1) is very different from the reported spectrum (*68*). The base peak is at m/z 142 (100%) and corresponds to $TEMPOH^{+}$-$^{\bullet}CH_3$. Loss of the $CH_3^{\bullet}$ gives rise to the more stable even-electron species ($C_8H_{14}NOH$). The dominant (pseudo)molecular ion was $TEMPOH^{+\bullet}$ at m/z 157 (70%), and the relative abundances of $TEMPO^{+}$ (25%) and $TEMPOH_2^{+}$ (45%) are much greater than reported previously, while that of $TEMPO^{+}$-NH_2OH (10%) was similar. To probe further the reasons for the differences in the current (Figure 5.1) and reported results (*68*), the effects of spray voltage on the ESI behavior of $TEMPO^{\bullet}$ in different solvents were investigated.

5.4.2 MS/MS Analysis of TEMPO, $TEMPOH^{+\bullet}$, and $TEMPOH_2^{+}$ (Pseudo)Molecular Ions

The presence of $TEMPO^{+}$, $TEMPOH^{\bullet}$ and $TEMPOH_2^{+}$ ions in the positive-ion ESI mass spectrum of $TEMPO^{\bullet}$ has been reported previously, but only $TEMPO^{+}$ fragmentation was described (*68*). To confirm that the ions observed at m/z 156 and 157 were not fragments of the ion at m/z 158, MS/MS analysis was performed on each by selecting the desired mass in Q1 and analyzing the fragmentation patterns in Q3. The MS/MS spectra clearly reveal that the species at 156, 157 and 158 arise from distinct ions since their fragmentation patterns are noticeably different (Figure 5.2). The arrows in Figure 5.2 connect the precursor and fragment ions based on the fragmentation mechanisms given in Schemes 5.3-5.5. The even-electron ions, $TEMPOH_2^{+}$ and $TEMPO^{+}$, lose hydroxylamine (NH_2OH, -33Da), a common neutral fragment. The loss of

the $CH_3^{\bullet}$ (-15Da) from $TEMPOH^{\bullet+}$ is quite facile (Figure 5.1), forming the base peak at m/z 142, which then loses hydroxylamine to form the species at m/z 109.

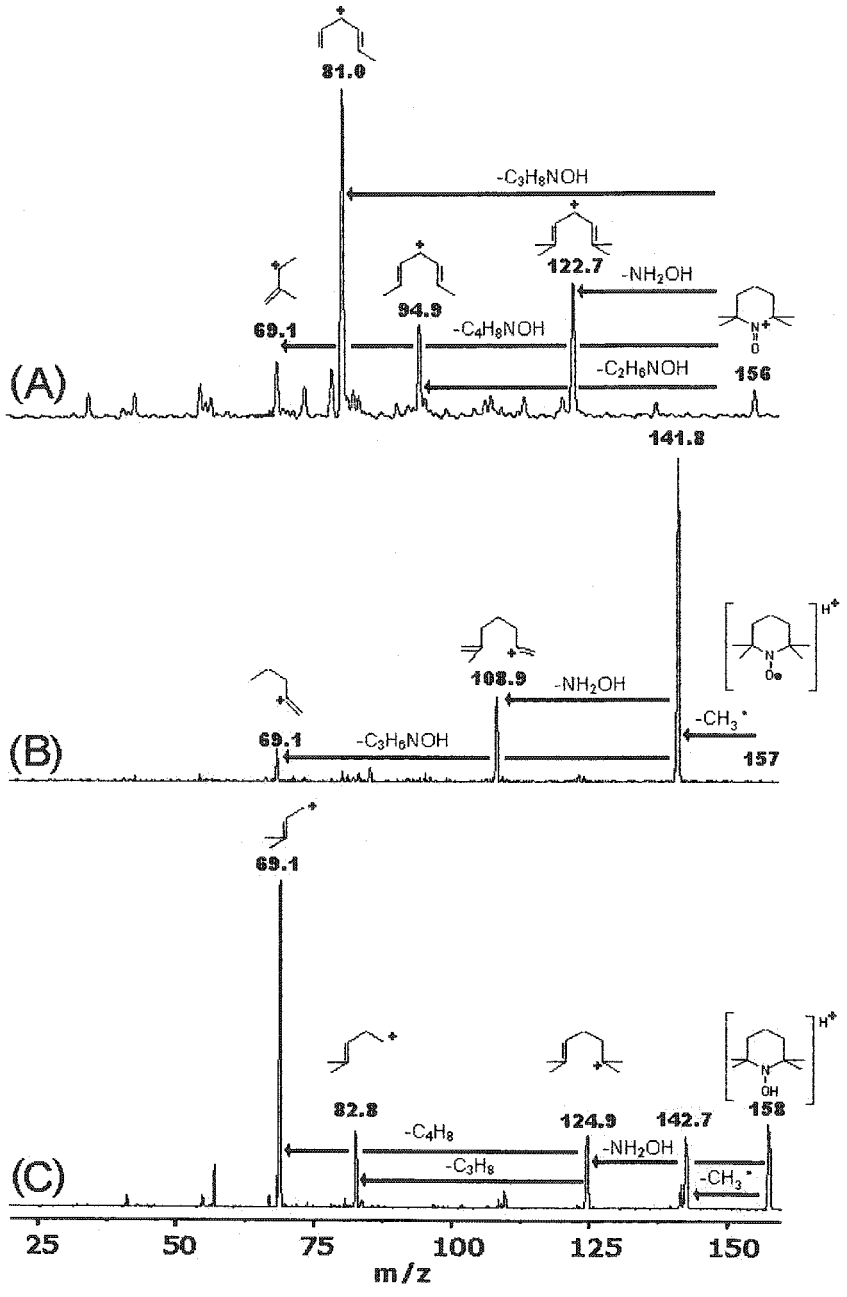

Figure 5.2. Q2MS product ion spectra of TEMPOH (A), TEMPO$^{\bullet}$ (B) and TEMPO^{+} (C). Arrows originate from the parent ion to the observed fragment ions. Experiments were carried out by selecting the parent ion in the first quadrupole and passing the selected ion through a collision cell operating in the *rf*-only mode and pressurized with argon using a Quattro II triplequadrupole (Micromass) mass spectrometer equipped with an ESI source. In a typical experiment, collision energies between 10 and 40eV were used. The analyte was prepared in water and infused at a flow rate of 5μL/min.

The loss of ethyl-methyl-hydroxylamine (C_3H_8NOH, -75Da) gives rise to the base peak m/z 81 for $TEMPO^+$. The loss of $CH_3^\bullet$ from $TEMPOH_2^+$ to give a radical fragment ion at m/z 142.7 is interesting because even-electron ions fragment mainly by loss of non-radical neutrals. Although peaks with m/z 69 are present in all three fragmentation patterns, they most likely arise from different species as indicated in Schemes 5.3-5.5.

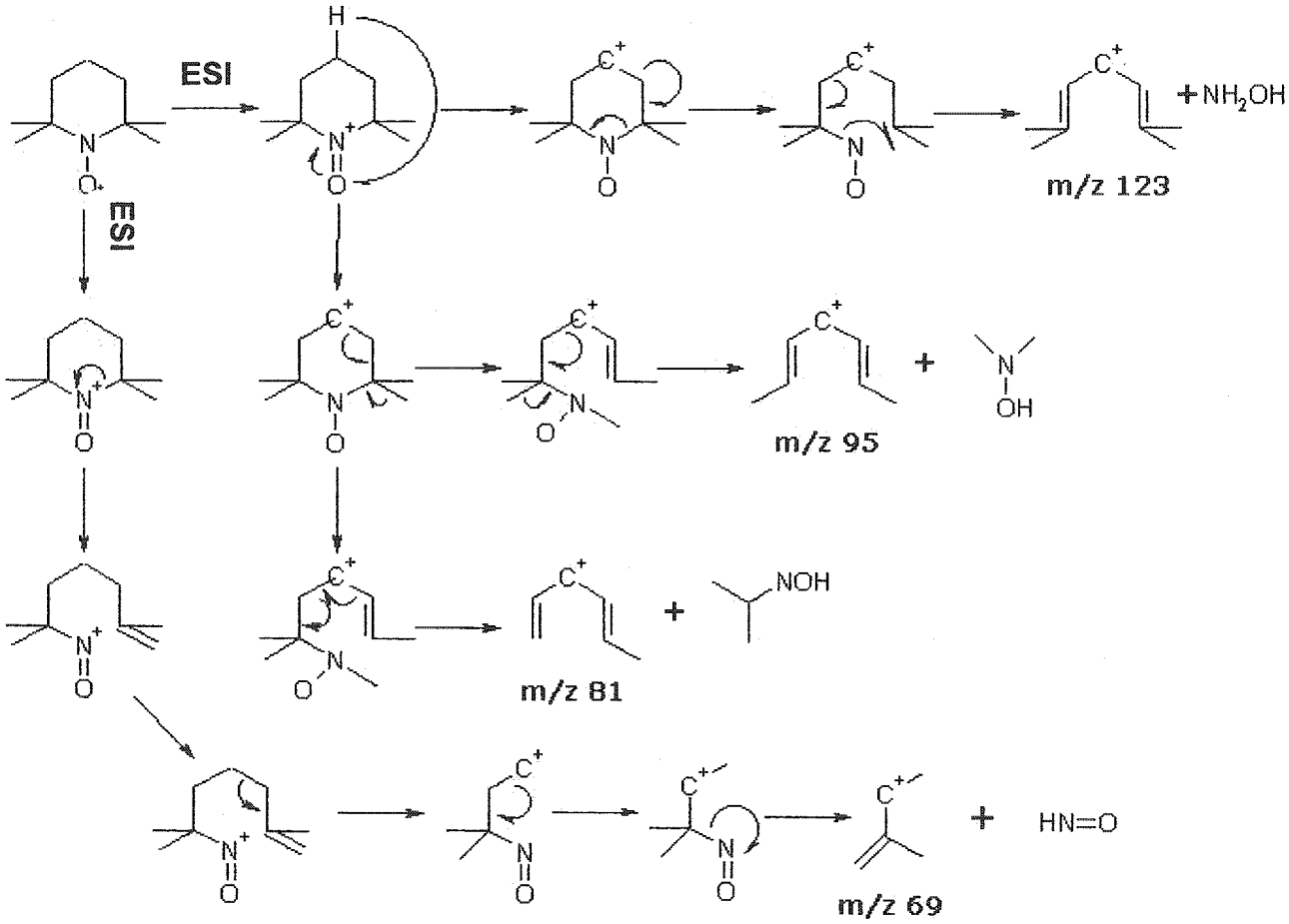

Scheme 5.3. Proposed fragmentation of $TEMPO^+$ ion (m/z 156) (*68*).

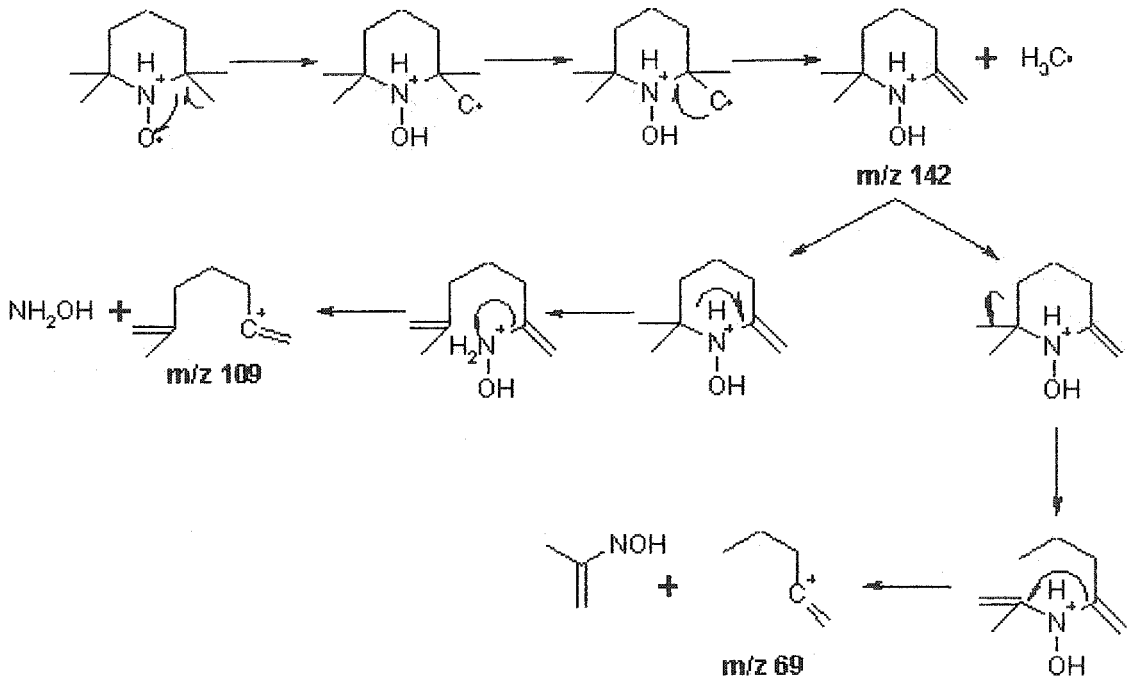

Scheme 5.4. Proposed fragmentation of $TEMPOH^{+\bullet}$ (m/z 157) (*68*).

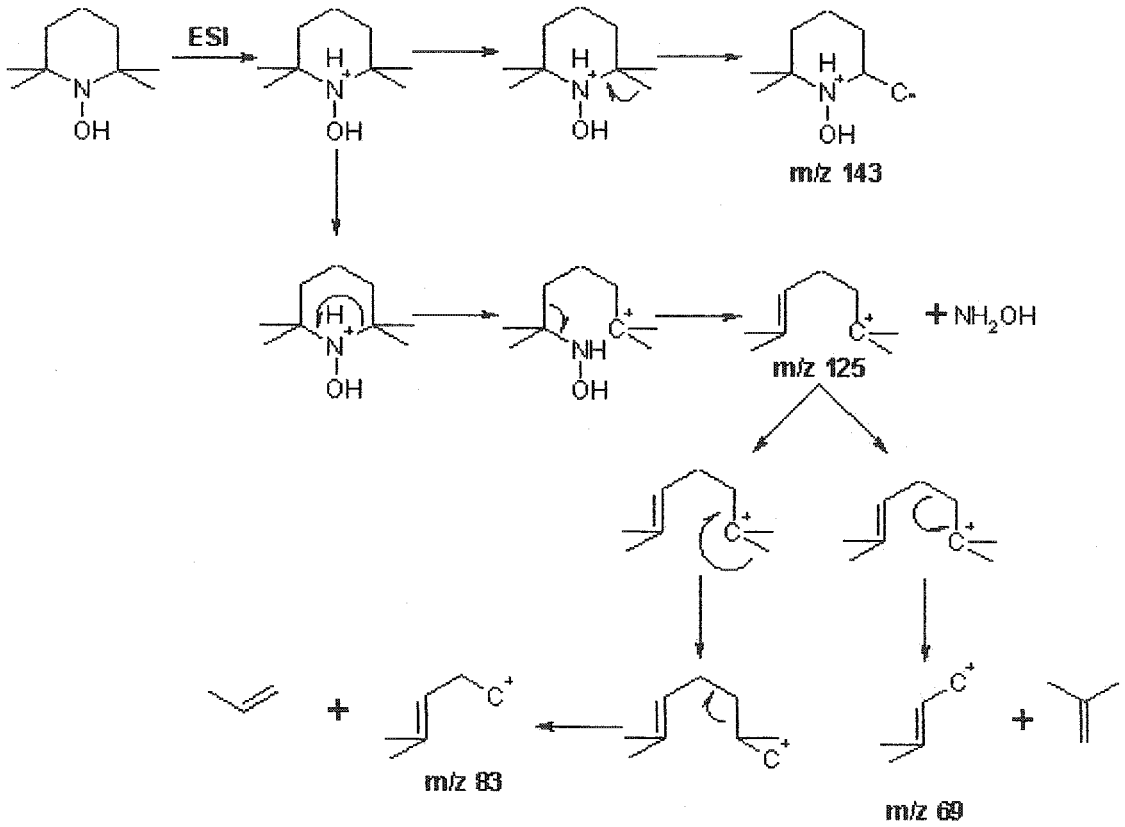

Scheme 5.5. Proposed fragmentation of $TEMPOH_2^+$ (m/z 158) (*222*).

5.4.3 *ESI-MS of Preformed $TEMPO^+$ and TEMPOH*

$TEMPO^{\bullet}$ was oxidized with HOCl in methanol to generate $TEMPO^+$ (*155-157*). Optical analysis of the resulting mixture revealed loss of the characteristic nitroxide band at 445nm (*196*), and ESI-MS in methanol confirmed the presence of $TEMPO^+$ as the major product (100%), with a low abundant $TEMPOH_2^+$ peak (5%, data not shown). The relative abundance of the $TEMPOH_2^+$ peak was dependent on the time spent in the ESI source. For instance, direct infusion of preformed $TEMPO^+$ into the ESI source for 1min followed by analysis for 5min increased the relative abundance of $TEMPOH_2^+$ to 10%. Reduction of $TEMPO^+$ in the electrospray source suggests that an Anelli-like reaction takes place, where the preformed $TEMPO^+$ catalyzes the oxidation of methanol to produce TEMPOH (Scheme 5.2), which is observed as $TEMPOH_2^+$ in the mass spectrum. Similar results were observed with water as solvent, but negligible (<1%) $TEMPOH_2^+$ was detected in acetonitrile.

When $TEMPO^{\bullet}$ was incubated with ascorbate in methanol, the 445nm absorption disappeared, and the sole molecular-ion peak in the ESI mass spectrum was at m/z 158, indicative of the $TEMPOH_2^+$ ion (data not shown). When TEMPOH in acetonitrile was infused into the ESI source at a spray voltage of 3.0kV, a white salt precipitated at the ESI needle. The inability to generate ions at low spray voltages is due to the absence of electrolysis required to maintain i_{ES}. Electrochemical charge balancing can involve electrolysis of the emitter (*71*), solvent, additives and contaminants (*217, 223*), and the analyte (*219*). However, heterogeneous oxidation of TEMPOH does not occur (*221*), so electrolysis of TEMPOH will not take place in the ESI source. Thus, oxidation of the solvent or some other species is necessary to counterbalance the buildup of negative

charge at the ESI needle. A needle voltage above 3.0kV must be required for acetonitrile oxidation since no i_{ES} is observed at 3.0kV. These studies on preformed $TEMPO^+$ and TEMPOH confirm that the former can catalyze solvent oxidation in the ESI source and that the latter is not oxidized electrochemically.

5.4.4 Effect of Solvent, Electrolyte and Spray Voltage

Figure 5.3 summarizes the fractional abundances of $TEMPOH^{+}$-$^{\bullet}CH_3$ (m/z 142), $TEMPO^+$ (m/z 156), $TEMPOH^{+\bullet}$ (m/z 157) and $TEMPOH_2^+$ (m/z 158) observed in the ESI mass spectra following the direct infusion $TEMPO^{\bullet}$ in acetonitrile, H_2O or methanol into the ESI source at various spray voltages in the presence or absence of 0.01% TFA. The fractional abundance of each species is given as a percentage of the total ion intensity detected under each set of conditions investigated. Other ISF fragment ions were observed in addition to that at m/z 142 (Figure 5.1) but these had <10% fractional abundance. The number above each set of columns is the sum of the fractional abundances of the $TEMPO^+$ plus $TEMPOH_2^+$ ions.

No ion current was detected at 3.0kV in acetonitrile (Figure 5.3A&B). However, when the spray voltage was increased to 4.0 or 5.0kV, TEMPOH-$^{\bullet}CH_3$ (m/z 142) has the highest fractional abundance in the presence or absence of TFA. This indicates that the major molecular ion formed in the ESI source in acetonitrile is $TEMPOH^{+\bullet}$ since the peak at m/z 142 arises from fragmentation of $TEMPOH^{+\bullet}$ only (Scheme 5.4, Figure 5.2). When the spray voltage is increased from 4.0 to 5.0kV in acetonitrile (Figure 5.3A), the fractional abundance of $TEMPOH_2^+$ increases from 19 to 33% at the expense of $TEMPOH^{+\bullet}$, which decreases from 29 to 13%. The abundance of $TEMPO^+$ also increased

slightly, suggesting that increased spray voltage promotes both oxidation and reduction of $TEMPO^{\bullet}$ in the ESI source. In fact, the percentage of species produced via EC increases from 29 to 46%. In the presence of TFA, $TEMPOH^{+}$ - $^{\bullet}CH_3$ is again the dominant species, but the sum of $TEMPO^{+}$ and $TEMPOH_2^{+}$ increases at the expense of $TEMPOH^{+\bullet}$ (29 *vs* 15%) at 4.0kV, whereas $TEMPOH_2^{+}$ increases to 35% at the expense of $TEMPO^{+}$ (5%) at 5.0kV (Figure 5.3B). The results at 5.0kV suggest that $TEMPOH_2^{+}$ is formed in an Anelli-type process at higher spray voltages. The addition of TFA increases the percentage of EC produced species since the addition of electrolyte increases i_{ES} (*69, 70*).

Since water likely acts as a better nucleophile than acetonitrile in Anelli-type reactions, the reduction of $TEMPO^{+}$ to TEMPOH is promoted (*185*) at all applied voltages in water. Nonetheless, combining the fractional abundances at m/z 142 and 157 reveals that $TEMPOH^{+\bullet}$ is also the major molecular ion formed in water. Fractional abundance shows little dependence on spray voltage or TFA addition (Figure 5.3C, D). In contrast, dramatic changes in fractional abundance with spray voltage are observed in methanol (Figure 5.3E&F). At 3.0kV, in the absence of TFA (Figure 5.3E), $TEMPO^{+}$ is the dominant ion (40%), but its intensity drops dramatically at 4.0 and 5.0kV when $TEMPOH_2^{+}$ (62%) becomes dominant. This reveals that extensive $TEMPO^{\bullet}$ and methanol oxidation occurs in the ESI source at the higher voltages to maintain i_{ES} (*69, 70*). In the presence of TFA, $TEMPOH^{+\bullet}$ is the dominant ion at 3.0kV, but at higher spray voltages, $TEMPOH_2^{+}$ becomes more dominant.

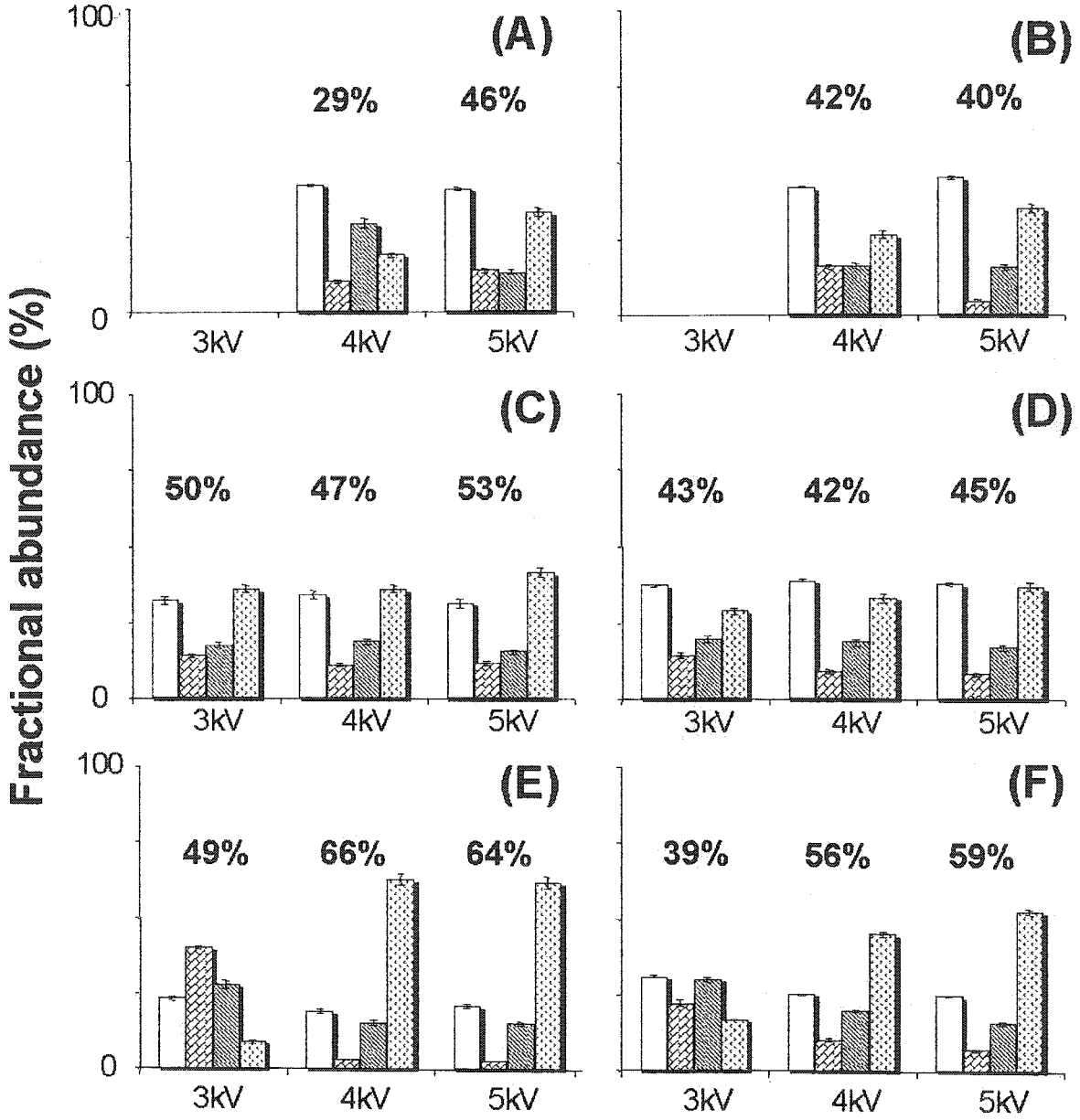

Figure 5.3 Fractional abundances of the $TEMPOH^+$-$^{\bullet}CH_3$ ion at m/z 142 (white), $TEMPO^+$ ion at m/z 156 (brick), $TEMPOH^{+\bullet}$ at m/z 157 (dashed) and $TEMPOH_2^+$ at m/z 158 (divots) *vs* spray voltage in presence (B,D,F) or absence of TFA (A,C,E) in (A,B) acetonitrile, (C,D) water and (E,F) methanol. The number above each set of columns is the sum of the fractional abundances of the $TEMPO^+$ plus $TEMPOH_2^+$ ions. Fractional abundances are given as a percentage of the sum of the total ion count of all four ions observed over an accumulation of 30 scans at a scan rate of 200amu/s from m/z 50 to 600. The ions were analyzed in Q1, following direct infusion at a rate of 5μL/min into the ESI source of a Quattro II triple quadrupole mass spectrometer.

5.5 Discussion

5.5.1 $TEMPO^+$, $TEMPOH^{+\bullet}$, $TEMPOH_2^+$ (Pseudo)Molecular Ions and Their MS/MS Analysis.

The oxidation of $TEMPO^\bullet$ to $TEMPO^+$ in the ESI source is not surprising since this process has been shown to be electrochemically facile (0.63eV) (*221*). Therefore, the positive potential at the emitter can easily oxidize $TEMPO^\bullet$ to $TEMPO^+$. This positive charge must be electrochemically counterbalanced in order for the spray droplets to reach the detector (*179*). The charge-balancing reactions that occur in the ESI source, and the extent to which these reactions take place, are a function of the relative concentrations and reduction potentials of the various species in the solution, the availability of electroactive species for reaction at the metal/solution interface (which is related to capillary dimensions, solution flow rate, and solute concentration), and the magnitude of i_{ES} (which is related to the nature of the solvent, solution conductivity, and the magnitude of the applied electric field at the capillary tip) (*69, 71*). The metal capillary also may contribute to electrochemical charge balancing since Blades *et al.* (*71*) observed gas-phase Zn^{2+} and Fe^{2+} ions using ESI capillary tips made of zinc metal ($Zn_{(s)} \rightarrow Zn_{(aq)}^{2+} + 2e^-$) and stainless-steel ($Fe_{(s)} \rightarrow Fe_{(aq)}^{2+} + 2e^-$), respectively. Although stainless steel capillary tips were used here, Fe^{2+} ions were not detected presumably due to the ease of $TEMPO^\bullet$ oxidation.

The system is further complicated by the fact that $TEMPO^+$ can catalyze solvent oxidation. Anelli and coworkers used bleach (HOCl) as a bulk oxidant (*155-157*) in the catalytic cycle involving TEMPO-mediated alcohol (R_1R_2CHOH) oxidation shown in Scheme 5.2 (*185*). $TEMPO^\bullet$ is oxidized to the $TEMPO^+$ ion **B** by the action of HOCl and

KBr. Addition of the alcohol to **B**, followed by an oxa-Cope fragmentation produces the ketone R_1R_2CO and TEMPOH **F**. Reoxidation of TEMPOH to **B** completes the catalytic cycle. In the ESI source, $TEMPO^+$ formed at the emitter can oxidize the solvent (depending on its nucleophilicity) in an Anelli-like reaction to generate TEMPOH, which will be detected as $TEMPOH_2^+$. It has been shown that the electrochemical reduction of $TEMPO^\bullet$ to TEMPOH is an irreversible process (-0.8eV) (*221*). Thus, TEMPOH acts as an irreversible electron sink in the ESI source, which would explain the high abundance of $TEMPOH_2^+$ detected under conditions that favor solvent oxidation. Smith *et al.* (*222*) recently published an ESI-MS analysis of iminyl nitroxide radicals and revealed that these free radical species produce a high abundance of the MH_2^+ ions in their mass spectra. They described the formation of the latter ions as the formal attachment of $H^\bullet$ and H^+ to the nitroxide radical due to the redox chemistry taking place at the ESI needle but did not elaborate on the mechanism (*222*).

5.5.2 Effect of Solvent on TEMPO$^\bullet$ Electrochemistry in the ESI Source.

The choice of solvent affects the $TEMPO^\bullet$-derived ions observed in the mass spectrum (Figure 5.3). Acetonitrile, methanol and water are frequently used solvents for organic electrochemistry (*224*) because of their high dielectric constants (37.5, 32.63 and 80.10) (*225*), wide accessible potential ranges (-3.5 to +2.4, -2.2 to +1.5 and –2.7 to +1.5 V *vs* SCE), and range of temperatures over which they remain liquid (-45 to +81.6, -98 to 64.7 and 0 to 100°C) (*225*). Although the electrochemical oxidation of $TEMPO^\bullet$ to $TEMPO^+$ is not likely affected by any of the solvents used, the extent of $TEMPO^+$-catalyzed solvent oxidation through the Anelli-type reaction, as reflected in the

$TEMPOH_2^+$ fractional abundance, varies considerably (Figure 5.3). $TEMPOH^{+\bullet}$ together with its fragment ion, $TEMPO^+$-$^\bullet CH_3$, constitute 71% of the fractional abundance observed in acetonitrile at a spray voltage of 4.0kV, whereas in methanol, under the same ESI conditions, the electrochemically produced $TEMPOH_2^+$ ion is dominant. In water, the fractional abundances of $TEMPOH^+$-$^\bullet CH_3$ and $TEMPOH_2^+$ fall between their values in acetonitrile and methanol (Figure 5.2). Hence, less $TEMPO^\bullet$ oxidation occurs in the ESI source in acetonitrile, and more $TEMPOH^{+\bullet}$ and its fragment ion are detected by the mass analyzer than when methanol and water are used as solvents. The dominance of $TEMPOH_2^+$ in methanol at 4.0 and 5.0kV is attributed to the relative ease of oxidation in methanol via an Anelli-like reaction (Scheme 5.2).

5.5.3 Effect of Spray Voltage on TEMPO$^\bullet$ Electrochemistry in the ESI Source.

The spray voltage affects the electrochemistry in the ESI source (*72*). An example is the absence of ions when $TEMPO^\bullet$ in acetonitrile is infused into the ESI source at a spray voltage of 3.0kV (Figures 5.3A&B). A white precipitate accumulated at the end of the spray needle since the oxidation potential of acetonitrile is too high for solvent oxidation to counterbalance the charge at the metal/solution interface (*73*). Ions are observed at spray voltages of 4.0 and 5.0kV but $TEMPOH^+$-$^\bullet CH_3$ and its parent $TEMPOH^{+\bullet}$ exhibit the highest fractional abundances as discussed in Section 5.5.2. Switching the solvent to water promotes electrochemical oxidation of $TEMPO^\bullet$ to $TEMPO^+$ at all spray voltages, which is then reduced to TEMPOH by an Anelli-like reaction (Figure 5.3A). TEMPOH cannot be electrochemically reduced (*221*) and no

suitable chemical oxidant is present in the ESI source, therefore the formation of TEMPOH is proportional to i_{ES}.

Interestingly, $TEMPO^+$ is the major species in methanol at a spray voltage of 3.0kV (Figure 5.3E). This is due to the ability of methanol to contribute to charge balancing because of its low potential limits. Increasing i_{ES} by increasing the spray voltage from 3.0 to 4.0kV dramatically increases the fractional abundance of the $TEMPOH_2^+$ ion (Figure 5.3E). Methanol is easily oxidized by $TEMPO^+$, which is formed at the capillary needle, and TEMPOH is produced in the Anelli reaction (Scheme 5.2).

The fractional abundances of the ions are relatively insensitive to the spray voltage when H_2O is used as the solvent, the $TEMPOH_2^+$ ion is more abundant at 3.0kV since H_2O has a lower oxidation potential than methanol (*225*). However, H_2O_2 or O_2 formed on water oxidation likely reoxidize the TEMPOH produced and prevent $TEMPOH_2^+$ from reaching the high fractional abundances seen in methanol.

5.5.4 Effect of TFA on TEMPO• Electrochemistry in the ESI Source.

In electrochemical experiments, high concentrations of supporting electrolyte are typically added to the solution to obtain sufficient conductivity and to maintain electroneutrality (*224*). High concentrations of electrolytes also are known to decrease the sensitivity of ESI-MS detection of analytes formed via proton attachment or proton removal (*226*). If the electrolyte has a high surface activity, like TFA, analyte suppression is further intensified due to increased competition for charge sites on the droplet surface (*227*). Therefore, the addition of 0.01% TFA to the TEMPO• solutions could alter the fractional abundances of the ions via two phenomena: (1 by competing for charge sites on

the droplet surface (*227*), and (2 by increasing i_{ES}, thus favoring $TEMPO^+$ production in solution (*69, 70, 72, 73*). No significant differences are observed in H_2O when 0.01% TFA is added, but in methanol the ratio of the $TEMPOH_2^+/TEMPO^+$ fractional abundances increases at 3.0kV but decreases at 4.0 and 5.0kV on addition of TFA (Figure 5.3E *vs* F). It has been known for some time that the Anelli reaction increases at low pH (*185*). Therefore, the reduction of $TEMPO^\bullet$ to TEMPOH should proceed more efficiently in the presence of TFA and more $TEMPOH_2^+$ should be detected. Since this is not the case, TFA may cause suppression of the $TEMPOH_2^+$ ion in methanol.

An examination of Figure 5.3 shows that the $TEMPO^+$ ion (m/z 156) is dominant only in methanol at a spray voltage of 3.0kV. Smith *et al.* (*68*) reported that $TEMPO^+$ was the dominant ion in acetonitrile at a spray voltage of 4.0kV, but clearly the ions derived from unoxidized $TEMPO^\bullet$ ($TEMPOH^{+\bullet}$ and $TEMPOH^+$-$^\bullet CH_3$) are found to be dominant here (Figure 5.3A). The reasons for the discrepancy between our results and those of Smith *et al.* are not apparent at present.

5.6 Conclusions

The molecular ions present in the ESI mass spectrum of the stable nitroxide radical $TEMPO^\bullet$ are strongly dependent on the solvent. The electrochemistry at the metal/solution interface is influenced by an Anelli-like reaction (*155-157*) that produces TEMPOH in the ESI source. Since the reduction of $TEMPO^\bullet$ to TEMPOH is electrochemically irreversible, the abundance of the $TEMPOH_2^+$ ion reflects the extent of solvent oxidation in the ESI source. With the dramatic increase in use of stable nitroxides such as $TEMPO^\bullet$ in many areas of chemistry and biochemistry care must be taken in

interpreting the ESI mass spectra of products from reactions involving TEMPO$^{\bullet}$. Furthermore, the sensitivity of the ESI mass spectrum of TEMPO$^{\bullet}$ to i_{ES} could be exploited as a rapid probe of the inherent electrochemistry occurring in a particular ESI source. A fast electrochemical assessment would be useful when constructing or modifying ESI sources, or coupling online capillary electrophoresis with ESI-MS instruments (*228*).

6.0 Conclusions and Suggestions for Future Work

6.1 Chapter 2

The spectroscopic analysis of the heme-pocket and secondary structure conformation of the two commercial sources of HRPC and HRPC-CO revealed that in the absence of added Ca^{2+}, glycosylation plays an important role in the low-pH conformational stability of this class III plant peroxidase. Decreasing the pH promotes loss of stabilizing Ca^{2+} in certain buffers. Thus variation in attached glycans may explain the low-pH activity of class II peroxidases which, apart from relatively weak sequence similarity, possess essentially identical active sites and Ca^{2+} ligands as class III plant peroxidases that function at neutral pH. The results presented in Chapter 2 lead us to hypothesize that the positioning of key glycans determine the acid-base conformational stability, and hence activity, of class II and III plant peroxidases by preventing Ca^{2+} leaching. The discrepancies in the literature in the low-pH stability of HRPC from different sources calls into question all previous work carried out at low pH on this highly researched protein, particularly values of the pK_a of the distal His42, which plays a critical role in acid-base catalysis.

6.2 Chapter 3 and 4

The use of TEMPO$^{\bullet}$ as a scavenger for the mass spectrometric detection of biologically relevant carbon-centered free radicals has been shown in Chapter 3 to be highly effective in two very different radical-generating environments *in vitro*. In both the HRPC-catalyzed peroxidation of aromatic amino-acid derivatives (NAYA, NAWA and NAF) and direct heme-mediated protein peroxidation, TEMPO$^{\bullet}$ significantly outperforms (9 sites in CCP) diamagnetic STs such as MNP in adduct yield (3 sites in CCP). This is consistent with the higher rates expected for spin scavenging *vs* spin trapping. The formation of a diamagnetic adduct rather than a nitroxide spin-adduct greatly diminishes the probability of non-radical side reactions typically associated with STs. Spin scavenging also is expected to be more selective over spin trapping given the high reactivity of stable nitroxide radicals with carbon-centered radicals. Application of the technology described in Chapter 3 should help identify protein-based radicals, elucidate their mechanisms of translocation and hence their roles in redox- and oxidative-stress-signaling pathways.

Exploitation of the well-documented homolysis of the carboxylamine bond at elevated temperatures to confirm spin scavenging by TEMPO$^{\bullet}$ is discussed in Chapter 4. The results reveal that TEMPO-labeling of proteins allows the activation of polypeptide-based radicals as in nitroxide-mediated living free-radical polymerization (LFRP) (*60*). Also, the oxidizing equivalents stored in TEMPO-labeled proteins can be used as selective oxidants as demonstrated here for CCP. These observations offer intriguing possibilities for studies in electron transfer. Furthermore, radical capping may increase

the stability of peroxidases, thereby expanding their utility in industrial applications, which currently include food production, fabric dying and paper-pulp manufacture (*7*).

6.3 Chapter 5

In Chapter 5, the molecular ions present in the ESI mass spectrum of the stable nitroxide radical $TEMPO^{\bullet}$ were shown to be strongly dependent on solution (*i.e.*, solvent and electrolyte) and instrument (*i.e.* spray voltage) parameters. The presence of oxidized ($TEMPO^{+}$), protonated ($TEMPOH^{\bullet+}$) and reduced ($TEMPOH_2^{+}$) ions derived from $TEMPO^{\bullet}$ is attributed to the controlled-current electrolysis that takes place in the ESI source. Furthermore, homogeneous solvent oxidation in an Anelli-like reaction increases $TEMPOH_2^{+}$ production in the source. Thus, care must be taken in interpreting the ESI mass spectra of products from the many reactions involving $TEMPO^{\bullet}$ studied in chemistry and biochemistry. Furthermore, the sensitivity of $TEMPO^{\bullet}$ redox chemistry to source parameters could be exploited as a rapid probe of the variation in electrospray current with ESI-source geometry. Such information would be useful in analyzing compounds with low oxidation potentials ($E < 1.0$V) such as neutral metallocenes, metalloporphyrins and polycyclic aromatic hydrocarbons, and in studying the mechanisms of biological redox reactions or those pertinent to electrochemical organic syntheses.

6.4 Suggestions for Future Work

(1) A pK_a value for His42 in the active site of HRPC in the presence of a non-chelating buffer and exogenous Ca^{2+} should be obtained to clarify the current literature discrepancies.

(2) Spectroscopic comparison of the low-pH secondary and tertiary structures of recombinant HRPC and glycosylation-site mutants from Sf9 and yeast cells, which possess the machinery for protein glycosylation, would indicate the glycosylation sites that play important roles in shielding the protein's Ca^{2+} binding sites from buffer leaching.

(3) Determination of the actual sites of TEMPO-labeling of CCP and selected mutants by MS/MS analysis of the labeled peptides using MALDI-ToF- and ESI-MS would help elucidate the nature and mechanism of radical translocation in CCP. TEMPO-labeled CCP could be isolated by ion-exchange chromatography from the unlabeled protein and digested separately. This would prevent labeled peptides from going undetected in the presence of unlabeled peptides.

(4) The efficiency of spin scavenging in different heme peroxidases, such as lactoperoxidase, should be investigated. Furthermore, the use of nitroxides should be explored in studies of protein-protein radical transfer reactions, such as the transfer of Mb radicals to bovine serum albumin. The mechanisms of radical transfer between proteins are of interest in radical signaling research.

(5) Threshold temperatures for carboxylamine homolysis in smaller TEMPO-labeled aromatics such as NAYA or phenol should be determined. The effects of steric constraints experienced by the TEMPO-labels in intact proteins or peptides on

bond destabilization could then be established. The intriguing possibility of using thermally activatable TEMPO-labeled aromatics as highly controllable oxidants for processes such as hair bleaching could be investigated.

7.0 References

1. Holzbaur, I. E., English, A. M., and Ismail, A. A. (1996) *Biochemistry 35*, 5488-94.
2. Uno, T., Nishimura, Y., Tsuboi, M., Makino, R., Iizuka, T., and Ishimura, Y. (1987) *J Biol Chem 262*, 4549-56.
3. Evangelista-Kirkup, R., Smulevich, G., and Spiro, T. G. (1986) *Biochemistry 25*, 4420-5.
4. Barlow, C. H., Ohlsson, P. I., and Paul, K. G. (1976) *Biochemistry 15*, 2225-9.
5. Smulevich, G., Paoli, M., De Sanctis, G., Mantini, A. R., Ascoli, F., and Coletta, M. (1997) *Biochemistry 36*, 640-9.
6. Feis, A., Rodriguez-Lopez, J. N., Thorneley, R. N. F., and Smulevich, G. (1998) *Biochemistry 37*, 13575-81.
7. Cherry, J. R., Lamsa, M. H., Schneider, P., Vind, J., Svendsen, A., Jones, A., and Pedersen, A. H. (1999) *Nat Biotechnol 17*, 379-84.
8. Smith, A. T., Santama, N., Dacey, S., Edwards, M., Bray, R. C., Thorneley, R. N., and Burke, J. F. (1990) *J Biol Chem 265*, 13335-43.
9. Hartmann, C., and Ortiz de Montellano, P. R. (1992) *Arch Biochem Biophys 297*, 61-72.
10. Harthill, J. E., and Ashford, D. A. (1992) *Biochmical Society Transactions 20*, 113S.
11. Hiner, A. N., Hernandez-Ruiz, J., Garcia-Canovas, F., Smith, A. T., Arnao, M. B., and Acosta, M. (1995) *Eur J Biochem 234*, 506-12.

12. Howes, B. D., Rodriguez-Lopez, J. N., Smith, A. T., and Smulevich, G. (1997) *Biochemistry 36*, 1532-43.

13. Morawski, B., Lin, Z., Cirino, P., Joo, H., Bandara, G., and Arnold, F. H. (2000) *Protein Eng 13*, 377-84.

14. Morawski, B., Quan, S., and Arnold, F. H. (2001) *Biotechnol Bioeng 76*, 99-107.

15. Poulos, T. L. (1993) *Curr Opin Biotechnol 4*, 484-9.

16. Stubbe, J., and van der Donk, W. A. (1998) *Chem Rev 98*, 705-762.

17. English, A. M. (1994) in *Encyclopedia of Inorganic Chemistry: Iron:* (King, R. B., Ed.) pp 1682-1697, John Wiley and Sons, Chichester, England.

18. Fenwick, C. W., and English, A. M. (1996) *J Am Chem Soc 118*, 12236-12237.

19. Filosa, A., and English, A. M. (2001) *J Biol Chem 276*, 21022-7.

20. Dunford, H. B. (1991) in *Peroxidases in Chemistry and Biology* (Everse, I., Everse, K. E. & Grisham, M. B., Ed.) pp 1-24, CRC Press, Boca Raton.

21. Dunford, H. B., and Stillman, J. S. (1976) *Coord. Chem. Rev. 19*, 187-251.

22. English, A. M., and Tsaprailis, G. (1995) *Advances in Inorganic Chemsitry 43*, 79-125.

23. Dunford, H. B. (1999) *Heme Peroxidases*, Wiley-VCH, Toronto.

24. Mylrajan, M., Valli, K., Wariishi, H., Gold, M. H., and Loehr, T. M. (1990) *Biochemistry 29*, 9617-23.

25. Hernandez-Ruiz, J., Arnao, M. B., Hiner, A. N., Garcia-Canovas, F., and Acosta, M. (2001) *Biochem J 354*, 107-14.

26. Erman, J. E., and Yonetani, T. (1975) *Biochim Biophys Acta 393*, 350-7.

27. Sivaraja, M., Goodin, D. B., Smith, M., and Hoffman, B. M. (1989) *Science 245*, 738-40.

28. Fishel, L. A., Villafranca, J. E., Mauro, J. M., and Kraut, J. (1987) *Biochemistry 26*, 351-60.

29. Goodin, D. B., Mauk, A. G., and Smith, M. (1986) *Proc Natl Acad Sci U S A 83*, 1295-9.

30. Goodin, D. B., Mauk, A. G., and Smith, M. (1987) *J Biol Chem 262*, 7719-24.

31. Gajhede, M., Schuller, D. J., Henriksen, A., Smith, A. T., and Poulos, T. L. (1997) *Nat Struct Biol 4*, 1032-8.

32. Patterson, W. R., and Poulos, T. L. (1995) *Biochemistry 34*, 4331-41.

33. Poulos, T. L., Edwards, S. L., Wariishi, H., and Gold, M. H. (1993) *J Biol Chem 268*, 4429-40.

34. Sundaramoorthy, M., Kishi, K., Gold, M. H., and Poulos, T. L. (1994) *J Biol Chem 269*, 32759-67.

35. Poulos, T. L. (1988) *Adv Inorg Biochem 7*, 1-36.

36. Bose-Basu, B., DeRose, E. F., Chen, Y. R., Mason, R. P., and London, R. E. (2001) *Free Radic Biol Med 31*, 383-90.

37. Wright, P. J., and English, A. M. (2003) *J Am Chem Soc 125*, 8655-65.

38. Poulos, T. L., and Fenna, R. E. (1994) *Metalloenzymes Involving Amino Acid-Residue and Related Radicals*, Vol. 30, Marcel Dekker, New York.

39. Smulevich, G., Miller, M. A., Kraut, J., and Spiro, T. G. (1991) *Biochemistry 30*, 9546-58.

40. Erman, J. E., Vitello, L. B., Miller, M. A., Shaw, A., Brown, K. A., and Kraut, J. (1993) *Biochemistry 32*, 9798-806.

41. Vitello, L. B., Erman, J. E., Miller, M. A., Wang, J., and Kraut, J. (1993) *Biochemistry 32*, 9807-18.

42. Charizanis, C., Juhnke, H., Krems, B., and Entian, K. D. (1999) *Mol Gen Genet 261*, 740-52.

43. Lenaz, G. (1998) *Biochim Biophys Acta 1366*, 53-67.

44. Arduini, A., Eddy, L., and Hochstein, P. (1990) *Free Radic Biol Med 9*, 511.

45. Fantone, J., Jester, S., and Loomis, T. (1989) *J. Biol. Chem. 264*, 9408.

46. Giulivi, C., and Cadenas, E. (1998) *Free Radic Biol Med 24*, 269.

47. Gunther, M. R., Tschirret-Guth, R. A., Witkowska, H. E., Fann, Y. C., Barr, D. P., Ortiz De Montellano, P. R., and Mason, R. P. (1998) *Biochem J 330 (Pt 3)*, 1293-9.

48. Gunther, M. R., Sturgeon, B. E., and Mason, R. P. (2000) *Free Radic Biol Med 28*, 709.

49. Catalano, C. E., Choe, Y. S., and Ortiz de Montellano, P. R. (1989) *J Biol Chem 264*, 10534-41.

50. Tsaprailis, G., and English, A. M. (2003) *J Biol Inorg Chem 8*, 248-55.

51. Moad, G., Shipp, D. A., Smith, T. A., and Solomon, D. H. (1999) *J. Phys. Chem. A 103*, 6580-6586.

52. Barr, D. P., Gunther, M. R., Deterding, L. J., and Tomer, K. B. (1996) *J Biol Chem 271*, 15498-15508.

53. Perkins, M. J. (1980) in *Advances in Physical Organic Chemistry* (Gold, V., and Bethell, D., Eds.) pp 1-63, Academic Press, Toronto.

54. Eberson, L. (1998) in *Advances in Physical Organic Chemistry* pp 91-141, Academic Press.

55. Tomasi, A., and Iannone, A. (1993) in *Biological Magnetic Resonance, Volume 13: EMR of Paramagnetic Molecules* (Berliner, L. J., and Reuben, J., Eds.) pp 9-35, Plenum Press, New York.

56. DeGray, J. A., Gunther, M. R., Tschirret-Guth, R., Ortiz de Montellano, P. R., and Mason, R. P. (1997) *J Biol Chem 272*, 2359-62.

57. Lardinois, O. M., Medzihradszky, K. F., and Ortiz de Montellano, P. R. (1999) *J Biol Chem 274*, 35441-8.

58. Qian, S. Y., Chen, Y. R., Deterding, L. J., Fann, Y. C., Chignell, C. F., Tomer, K. B., and Mason, R. P. (2002) *Biochem J 363*, 281-8.

59. McIntire, G. L., Blount, H. N., Stronks, H. J., Shetty, R. V., and Janzen, E. G. (1980) *J Phs Chem 84*, 916-921.

60. Hawker, C. J., Bosman, A. W., and Harth, E. (2001) *Chem Rev 101*, 3661-88.

61. Georges, M. K., Veregin, R. P. N., Kazmaier, P. M., and Hamer, G. K. (1993) *Macromolecules 26*, 2987-2988.

62. Woody, R. W. (1985) in *The Peptides* pp 14-114, Academic Press, New York.

63. Haris, P. I., and Chapman, D. (1992) *Trends Biochem Sci 17*, 328-33.

64. Haris, P. I., and Chapman, D. (1995) *Biopolymers 37*, 251-63.

65. Sage, J. T., Morikis, D., and Champion, P. M. (1991) *Biochemistry 30*, 1227-37.

66. Smulevich, G. (1998) *Biospectroscopy 4*, S3-17.

67. Slichter, C. P. (1963) *Principles of Magnetic Resonance*, 2nd ed., Harper & Row, New York.

68. Smith, C. D., Bartley, J. P., Bottle, S. E., Micallef, A. S., and Reid, D. A. (2000) *J Mass Spectrom 35*, 607-11.

69. Van Berkel, G. J., and Zhou, F. (1995) *Anal. Chem. 67*, 2916-2923.

70. Van Berkel, G. J., and Zhou, F. (1995) *Anal. Chem. 67*, 3958-3964.

71. Blades, A. T., Ikonomou, M. G., and Kebarle, P. (1991) *Anal. Chem. 63*, 2109-2114.

72. Xu, X., Wenzhe, L., and Cole, R. B. (1996) *Anal. Chem. 68*, 4244-4253.

73. Zhou, F., and Van Berkel, G. J. (1995) *Anal. Chem. 67*, 3643-3649.

74. Welinder, K. G., and Mazza, G. (1975) *Eur J Biochem 57*, 415-24.

75. Welinder, K. G., Mauro, J. M., and Norskov-Lauritsen, L. (1992) *Biochem Soc Trans 20*, 337-40.

76. Kirk, T. K., and Farrell, R. L. (1987) *Annu Rev Microbiol 41*, 465-505.

77. Leisola, M. S., Kozulic, B., Meussdoerffer, F., and Fiechter, A. (1987) *J Biol Chem 262*, 419-24.

78. Sitter, A. J., Shifflett, J. R., and Terner, J. (1988) *J Biol Chem 263*, 13032-8.

79. Hashimoto, S., Tatsuno, Y., and Kitagawa, T. (1986) *Proc Natl Acad Sci U S A 83*, 2417-21.

80. Susi, H. (1972) *Methods Enzymol 26*, 455-72.

81. Showen, K. J. B. (1978) *Transition States of Biochemical Processes*, Gandour, R. D.Showen, R. L. ed., Plenum Press.

82. Schonbaum, G. R. (1973) *J Biol Chem 248*, 502-11.

83. Veitch, N. C., Williams, R. J., Bray, R. C., Burke, J. F., Sanders, S. A., Thorneley, R. N., and Smith, A. T. (1992) *Eur J Biochem 207*, 521-31.

84. Susi, H. (1972) *Methods Enzymol 26*, 381-91.

85. Susi, H., Byler, D. M., and Purcell, J. M. (1985) *J Biochem Biophys Methods 11*, 235-40.

86. Hennessey, J. P., Jr., and Johnson, W. C., Jr. (1981) *Biochemistry 20*, 1085-94.

87. Dong, A., Huang, P., and Caughey, W. S. (1990) *Biochemistry 29*, 3303-8.

88. Theorell, H. (1950) *Acta. Chem. Scand. 4*, 22.

89. Keesey, J. (1987) in *Biochemica Information* pp 58, Boehringer Mannheim Biochemicals, Indianapolis, IN.

90. Laemmli, U. K. (1970) *Nature 227*, 680-5.

91. Tsaprailis, G., Chan, D. W., and English, A. M. (1998) *Biochemistry 37*, 2004-16.

92. Strickland, E. H., Kay, E., Shannon, L. M., and Horwitz, J. (1968) *J Biol Chem 243*, 3560-5.

93. Strickland, E. H., Kay, E., Shannon, L. M., and Horwitz, J. (1968) *UCLA Report*, 79-80.

94. Strickland, E. H. (1968) *Biochim Biophys Acta 151*, 70-5.

95. Prestrelski, S. J., Byler, D. M., and Thompson, M. P. (1991) *Int J Pept Protein Res 37*, 508-12.

96. Ismail, A. A., Mantsch, H. H., and Wong, P. T. (1992) *Biochim Biophys Acta 1121*, 183-8.

97. Clark, A. H., Saunderson, D. H., and Suggett, A. (1981) *Int J Pept Protein Res 17*, 353-64.

98. Haschke, R. H., and Friedhoff, J. M. (1978) *Biochem Biophys Res Commun 80*, 1039-42.

99. Morishima, I., Kurono, M., and Shiro, Y. (1986) *J Biol Chem 261*, 9391-9.

100. Shiro, Y., Kurono, M., and Morishima, I. (1986) *J Biol Chem 261*, 9382-90.

101. Chattopadhyay, K., and Mazumdar, S. (2000) *Biochemistry 39*, 263-70.

102. Wyss, D. F., and Wagner, G. (1996) *Curr Opin Biotechnol 7*, 409-16.

103. Kurosaka, A., Yano, A., Itoh, N., Kuroda, Y., Nakagawa, T., and Kawasaki, T. (1991) *J Biol Chem 266*, 4168-72.

104. Li, T., Quillin, M. L., Phillips, G. N., Jr., and Olson, J. S. (1994) *Biochemistry 33*, 1433-46.

105. Morikis, D., Champion, P. M., Springer, B. A., and Sligar, S. G. (1989) *Biochemistry 28*, 4791-800.

106. O'Keefe, D. H., Ebel, R. E., Peterson, J. A., Maxwell, J. C., and Caughey, W. S. (1978) *Biochemistry 17*, 5845-52.

107. Willick, G. E., Schobaum, G. R., and Kay, C. M. (1969) *Biochemistry 8*, 3729-34.

108. Coletta, M., Ascoli, F., Brunori, M., and Traylor, T. G. (1986) *J Biol Chem 261*, 9811-4.

109. Ogawa, S., Shiro, Y., and Morishima, I. (1979) *Biochem Biophys Res Commun 90*, 674-8.

110. Donoso, P., Beltran, M., and Hidalgo, C. (1996) *Biochemistry 35*, 13419-25.

111. George, S. J., Kvaratskhelia, M., Dilworth, M. J., and Thorneley, R. N. (1999) *Biochem J 344 Pt 1*, 237-44.

112. Martell, A. E., and Smith, R. M. (1976) *Critical Stability Constants*, Vol. 4, Plenum Press, New York.

113. Yang, Y., and Orlando, R. (1996) *Rapid Commun Mass Spectrom 10*, 932-6.

114. Tams, J. W., and Welinder, K. G. (1998) *FEBS Lett 421*, 234-6.

115. Dwek, R. A. (1995) *Science 269*, 1234-5.

116. Dwek, R. A. (1995) *Biochem Soc Trans 23*, 1-25.

117. Joao, H. C., and Dwek, R. A. (1993) *Eur J Biochem 218*, 239-44.

118. Takahashi, N., Bok Lee, K., Nakagawa, H., Tsukamoto, Y., Masuda, K., and Lee, Y. C. (1998) *Analytical Biochemistry 255*, 183-187.

119. Goochee, C. F., and Monica, T. (1990) *Biotechnology (N Y) 8*, 421-7.

120. Kay, L. E., and Basile, D. V. (1987) *Plant Physiol 84*, 99.

121. Wobus, U., and Weber, H. (1999) *Biol Chem 380*, 937-44.

122. Kandegedara, A., and Rorabacher, D. B. (1999) *Anal. Chem. 71*, 3140.

123. Renganathan, V., Miki, K., and Gold, M. H. (1985) *Arch Biochem Biophys 241*, 304-14.

124. Nie, G., Reading, N. S., and Aust, S. D. (1999) *Arch Biochem Biophys 365*, 328-34.

125. Welinder, K. G. (1985) *Eur J Biochem 151*, 497-504.

126. Gazarian, I. G., Lagrimini, L. M., George, S. J., and Thorneley, R. N. (1996) *Biochem J 320*, 369-72.

127. Rasmussen, C. B., Hiner, A. N., Smith, A. T., and Welinder, K. G. (1998) *J Biol Chem 273*, 2232-40.

128. McEldoon, J. P., Pokora, A. R., and Dordick, J. S. (1995) *Enzyme Microbiol. Technol. 17*, 359-365.

129. Lai, C.-S., and Piette, L. H. (1979) *Tetrahedron Lett*, 775.

130. Kalyanaraman, B., Perez-Reyes, E., Mason, R. P., Peterson, F. J., and Holtzman, J. L. (1979) *Mol Pharmacol 16*, 1059-64.

131. Timmins, G., Barlow, G., Silvester, J., We, i. X., and Whitwood, A. (1997) *Redox Report 3*, 125-133.

132. Hiramoto, K., Hasegawa, Y., and Kikugawa, K. (1994) *Free Radic Res 21*, 341-9.

133. Zhang, H., He, S., and Mauk, A. G. (2002) *Biochemistry 41*, 13507-13.

134. Gelvan, D., Saltman, P., and Powell, S. R. (1991) *Proc Natl Acad Sci U S A 88*, 4680-4.

135. Gunther, M. R., Kelman, D. J., Corbett, J. T., and Mason, R. P. (1995) *J Biol Chem 270*, 16075-81.

136. Kocherginsky, N., and Swartz, H. M. (1995) *Nitroxide Spin Labels. reactions in Biology and Chemistry*, CRC Press, Boca Raton, FL.

137. Samuni, A. M., DeGraff, W., Krishna, M. C., and Mitchell, J. B. (2001) *Biochim Biophys Acta 1525*, 70-6.

138. Nilsson, U. A., Olsson, L. I., Carlin, G., and Bylund-Fellenius, A. C. (1989) *J Biol Chem 264*, 11131-5.

139. Beckwith, A. L. J., Bowry, V. W., and Ingold, K. U. (1992) *J. Am. Chem. Soc. 114*, 4983-4992.

140. Bowry, V. W., and Ingold, K. U. (1992) *J. Am. Chem. Soc. 114*, 4992.

141. Chateauneuf, J., Lusztyk, J., and Ingold, K. U. (1988) *J. Org. Chem. 53*, 1629.

142. Sobek, J., Martschke, R., and Fischer, H. (2001) *J Am Chem Soc 123*, 2849-57.

143. Davies, M. J. (1991) *Biochim Biophys Acta 1077*, 86-90.

144. Tew, D., and Ortiz de Montellano, P. R. (1988) *J Biol Chem 263*, 17880-6.

145. Newman, E. S., Rice-Evans, C. A., and Davies, M. J. (1991) *Biochem Biophys Res Commun 179*, 1414-9.

146. Skulachev, V. P. (1998) *FEBS Lett 423*, 275-80.

147. Voest, E. E., van Faassen, E., van Asbeck, B. S., Neijt, J. P., and Marx, J. J. (1992) *Biochim Biophys Acta 1136*, 113-8.

148. Quintanilha, A. T., and Packer, L. (1977) *Proc Natl Acad Sci U S A 74*, 570-4.

149. Mitchell, J. B., Samuni, A., Krishna, M. C., DeGraff, W. G., Ahn, M. S., Samuni, U., and Russo, A. (1990) *Biochemistry 29*, 2802-7.

150. Samuni, A., Winkelsberg, D., Pinson, A., Hahn, S. M., Mitchell, J. B., and Russo, A. (1991) *J Clin Invest 87*, 1526-30.

151. Samuni, A., Godinger, D., Aronovitch, J., Russo, A., and Mitchell, J. B. (1991) *Biochemistry 30*, 555-61.

152. Tsaprailis, G., and English, A. M. (1996) *Can. J. Chem. 74*, 2250-2257.

153. Marquez, L. A., and Dunford, H. B. (1995) *J Biol Chem 270*, 30434-40.

154. Ushijima, Y., Nakano, M., Takyu, C., and Inaba, H. (1985) *Biochem Biophys Res Commun 128*, 936-41.

155. Anelli, P., Biffi, C., Montanari, F., and Quici, S. (1987) *J. Org. Chem. 52*, 2559-62.

156. Anelli, P., Banfi, S., and Montanari, F. (1989) *J. Org. Chem. 54*, 2970-2972.

157. Anelli, P., Montanari, F., and Quici, S. (1990) *S. Org Synth. 69*.

158. Perkins, D., Pappin, D., Creasy, D., and Cottrell, J. (1999) *Electrophoresis 20*, 3551-3567.

159. Matthews, J. H., Dinh, T. D., Tivitmahaisoon, P., Ziller, J. W., and Van Vranken, D. L. (2001) *Chem Biol 8*, 1071-9.

160. Yonetani, T., and Schleyer, H. (1967) *J Biol Chem 242*, 1974-9.

161. Jayawardene, D., and Dass, C. (2002) *J Mass Spectrom 37*, 389-94.

162. Bayse, G. S., Michaels, A. W., and Morrison, M. (1972) *Biochim Biophys Acta 284*, 34-42.

163. Amado, R., Aeschbach, R., and Neukom, H. (1984) *Methods Enzymol 107*, 377-88.

164. Giulivi, C., and Davies, K. J. (1993) *J Biol Chem 268*, 8752-9.

165. Giulivi, C., and Davies, K. J. (1994) *Methods Enzymol 233*, 363-71.

166. Harriman, J. (1987) *J. Phys. Chem. 91*, 6102-6104.

167. Ralston, I., and Dunford, H. B. (1978) *Can J Biochem 56*, 1115-9.

168. Ralston, I. M., and Dunford, H. B. (1980) *Can J Biochem 58*, 1270-6.

169. Malencik, D. A., Sprouse, J. F., Swanson, C. A., and Anderson, S. R. (1996) *Anal Biochem 242*, 202-13.

170. Hodges, G. R., Marwaha, J., Paul, T., and Ingold, K. U. (2000) *Chem Res Toxicol 13*, 1287-93.

171. Sharp, R. E., Palmitessa, A., Gibney, B. R., White, J. L., Moser, C. C., Daldal, F., and Dutton, P. L. (1999) *Biochemistry 38*, 3440-6.

172. Osapay, K., Tran, D., Ladokhin, A. S., White, S. H., Henschen, A. H., and Selsted, M. E. (2000) *J Biol Chem 275*, 12017-22.

173. Stachel, S. J., Stockwell, S. A., and Van Vranken, D. L. (1999) *Chem Biol 6*, 531-9.

174. Bosshard, H. R., Anni, H., and Yontetani, T. (1991) *Peroxidases in Chemistry and Biology*, CRC Press, Boca Raton, FL.

175. Pfister, T. D., Gengenbach, A. J., Syn, S., and Lu, Y. (2001) *Biochemistry 40*, 14942-51.

176. Hiner, A. N., Hernandez-Ruiz, J., Rodriguez-Lopez, J. N., Arnao, M. B., Varon, R., Garcia-Canovas, F., and Acosta, M. (2001) *J Biol Inorg Chem 6*, 504-16.

177. Wang, W., Noel, S., Desmadril, M., Gueguen, J., and Michon, T. (1999) *Biochem J 340*, 329-36.

178. Everse, J., Everse, K., and Grisham, M. B. (1991), CRC Press, Boca Raton, FL.

179. Yamashita, M., and Fenn, J. B. (1984) *J. Phys. Chem. 88*, 4451-4459.

180. Skene, W. G., Belt, S. T., Connolly, T. J., Hahn, P., and Scaiano, J. C. (1998) *Macromolecules 31*, 9103-9105.

181. Veregin, R. P. N., Georges, M. K., Hamer, G. K., and Kazmaier, P. M. (1995) *Macromolecules 28*, 4391-4398.

182. Lide, D. R. (1996) *CRC Handbook of Chemistry and Physics*, Vol. 77th, CRC, Boca Raton, Fl.

183. Finzel, B. C., Poulos, T. L., and Kraut, J. (1984) *J Biol Chem 259*, 13027-36.

184. Wright, P. J., and English, A. M. (2003) *J Am Chem Soc 125*, 8655-65.

185. Rychnovsky, S. D., Vaidyanathan, R., Beauchamp, T., Lin, R., and Farmer, P. J. (1999) *J Org Chem 64*, 6745-6749.

186. Coenjarts, C., Garcia, O., Llauger, L., Palfreyman, J., Vinette, A. L., and Scaiano, J. C. (2003) *J Am Chem Soc 125*, 620-1.

187. Skene, W., Scaiano, J., Listigovers, N., Kazmaier, P., and Georges, M. (2000) *Macromolecules 33*, 5065-5072.

188. Georges, M. K., Veregin, R. P. N., Kazmaier, P. M., Hamer, G. K., and Saban, M. (1994) *Macromolecules 27*, 7228-7229.

189. Zweier, J. L., Chzhan, M., Samouilov, A., and Kuppusamy, P. (1998) *Phys Med Biol 43*, 1823-35.

190. Mitchell, J. B., Xavier, S., DeLuca, A. M., Sowers, A. L., Cook, J. A., Krishna, M. C., Hahn, S. M., and Russo, A. (2003) *Free Radic Biol Med 34*, 93-102.

191. Egawa, T., Shimada, H., and Ishimura, Y. (2000) *J Biol Chem 275*, 34858-66.

192. Hanan, T., and Shaklai, N. (1995) *Free Radic Res 22*, 215-27.

193. Ortiz de Montellano, P. R., and Catalano, C. E. (1985) *J Biol Chem 260*, 9265-71.

194. Evans, S. V., and Brayer, G. D. (1990) *J Mol Biol 213*, 885-97.

195. Goodin, D. B., and McRee, D. E. (1993) *Biochemistry 32*, 3313-24.

196. Briere, R., Lemaire, H., and Rassat, A. (1965) *Bull. Soc. Chem. Fr.*, 3273-3283.

197. Margoliash, E., and Frohwirt, N. (1959) *Biochem. J. 71*, 570-572.

198. Kang, D. S., and Erman, J. E. (1982) *J Biol Chem 257*, 12775-9.

199. Hunter, C. L., Mauk, A. G., and Douglas, D. J. (1997) *Biochemistry 36*, 1018-25.

200. Wan, L., Twitchett, M. B., Eltis, L. D., Mauk, A. G., and Smith, M. (1998) *Proc Natl Acad Sci U S A 95*, 12825-31.

201. Giulivi, C., and Cadenas, E. (1994) *Methods Enzymol 233*, 189-202.

202. Dawson, J. H. (1988) *Science 240*, 433-9.

203. Aitken, S. M., Turnbull, J. L., Percival, M. D., and English, A. M. (2001) *Biochemistry 40*, 13980-9.

204. Kato, M., Kamigaito, M., Sawamoto, M., and Higashimura, T. (1995) *Macromolecules 28*, 1721-1723.

205. Moad, F., Rizzardo, E., and Solomon, D. (1982) *Macromolecules 15*, 909-14.

206. Samuni, A., Min, A., Krishna, C. M., Mitchell, J. B., and Russo, A. (1990) *Adv Exp Med Biol 264*, 85-92.

207. Samuni, A., Krishna, C. M., Mitchell, J. B., Collins, C. R., and Russo, A. (1990) *Free Radic Res Commun 9*, 241-9.

208. Rosen, G. M., Cohen, M. S., Britigan, B. E., and Pou, S. (1990) *Free Radic Res Commun 9*, 187-95.

209. Anderson, D. R., Deute, J. S., Koch, T. H., and Mosley, R. H. (1977) *J. Am. Chem. Soc. 99*, 6332.

210. Borbat, P. P., Costa-Filho, A. J., Earle, K. A., Moscicki, J. K., and Freed, J. H. (2001) *Science 291*, 266-9.

211. Blough, N. V., and Simpson, D. J. (1988) *J. Am. Chem. Soc. 110*, 1915.

212. Li, B., Gutierrez, P. L., and Blough, N. V. (1999) *Methods Enzymol 300*, 202-16.

213. Herbelin, S. E., and Blough, N. V. (1998) *J. Phys. Chem. 102*, 8170.

214. Deng, H., and Van Berkel, G. J. (1999) *Anal Chem 71*, 4284-4293.

215. Van Berkel, G. J., Giles, G. E., Bullock, J. S., and Gray, L. J. (1999) *Anal Chem 71*, 5288-5296.

216. Van Berkel, G. J., and Zhou, F. (1999) *Anal Chem 64*, 1586.

217. Van Berkel, G. J. (1997) in *Electrospray Ionization Mass Spectrometry* (Cole, R. B., Ed.) pp 65-105, Wiley, New York.

218. Fenn, J. B., Mann, M., Meng, C. K., Wong, S. F., and Whitehouse, C. M. (1989) *Science 246*, 64-71.

219. Van Berkel, G. J., and Kertesz, V. (2001) *J Mass Spectrom 36*, 1125-32.

220. Johnson, K. A., Shira, B. A., Anderson, J. L., and Amster, I. J. (2001) *Anal Chem 73*, 803-8.

221. Fish, J., Swarts, S., Sevilla, M., and Malinski, T. (1988) *J. Phys. Chem. 92*, 3745-3751.

222. Smith, C. D., Bartley, J. P., and Bottle, S. E. (2002) *J Mass Spectrom 37*, 897-902.

223. Moini, M., Cao, P., and Bard, A. J. (1999) *Anal Chem 71*, 1658-61.

224. Rieger, P. H. (1994) *Electrochemistry*, 2nd ed., Chapman & Hall, New York.

225. Weissberger, A., Proskaner, E. S., Riddick, J. A., and Tops, E. E. (1955) *Jr. Organic Solvents*, 2nd ed., Wiley (Interscience), New York.

226. Kebarle, P. (2000) *J. Mass Spectrom. 35*, 804-17.

227. Fenn, J. B. (1993) *J. Am. Soc. Mass Spectrom. 4*, 524-535.

228. Bateman, K. P. (1999) *J. Am. Soc. Mass Spectrom. 10*, 309–317.